Strength and Life Prediction of FRP Composite Bridge Deck

Prasun Kanti Majumdar

Dissertation submitted to the faculty of the Virginia Polytechnic Institute and State University in partial fulfillment of the requirements for the degree of

Doctor of Philosophy

in

(Engineering Mechanics)

Dr. John J. Lesko (Committee Chair)

Dr. Thomas E. Cousins

Dr. Scott W. Case

Dr. Scott L. Hendricks

Dr. Muhammad R. Hajj

(April 23, 2008)

(Blacksburg, Virginia)

Keywords: FRP bridge deck, Adhesive joint, Tire patch loading, Performance evaluation, Strength and failure mode, Fatigue life, Pultrusion

Strength and Life Prediction of FRP Composite Bridge Deck

Prasun Kanti Majumdar

ABSTRACT

Fiber reinforced polymer (FRP) composites are considered very promising for infrastructure applications such as repair, rehabilitation and replacement of deteriorated bridge decks. However, there is lack of proper understanding of the structural behavior of FRP decks. For example, due to the localization of load under a truck tire, the conventionally used uniform patch loading is not suitable for performance evaluation of FRP composite deck systems with cellular geometry and relatively low modulus (compared to concrete decks). In this current study, a simulated tire patch loading profile has been proposed for testing and analysis of FRP deck. The tire patch produced significantly different failure mode (local transverse failure under the tire patch) compared to the punching-shear mode obtained using the conventional rectangular steel plate. The local response of a cellular FRP composite deck has been analyzed using finite element simulation and results are compared with full scale laboratory experiment of bridge deck and structure. Parametric studies show that design criteria based on global deck displacement is inadequate for cellular FRP deck and local deformation behavior must be considered.

The adhesive bonding method is implemented for joining of bridge deck panels and response of structural joint analyzed experimentally. Strength, failure mode and fatigue life prediction methodologies for a cellular FRP bridge deck are presented in this dissertation.

Acknowledgement

I would like to express my sincere gratitude to my advisor and committee-chair Dr. Lesko for his support over the entire course of my studies at Virginia Tech. No word is enough to explain how great a person you are and how cordial an advisor can be while guiding a graduate student. I think it is the greatest experience in my life to meet a person like you and feel fortunate to work closely under your supervision. Your suggestions and support in difficult times helped me a lot to overcome the reality. Your persistent faith on my ability to succeed has helped build my confidence. I thank you for providing me such an exceptional work environment and you will remain as an idol for me in my future endeavors.

Dr. Cousins is another excellent person I am fortunate to work with. I enjoyed the great time while we all used to sit together and discuss bridge rehabilitation project. I am very grateful that you and Jack had supported me through that project. I had no idea about bridge decks and was not sure how could I contribute to bridge deck with my background in composite materials until in touch with you. I never heard of "L/800", "HS-20" and "Load distribution factor" until you mentioned it in one of our group meeting. Your expertise in the field of bridge decks brought a great deal to my research.

I would also like to thank my committee member Dr. Case for providing fundamental knowledge on composite strength and life prediction. You are probably the best teacher I ever had. You are also an amazing person and an integral part of MRG life. You are always very organized and quick to give the best answer to any question I might have. Your expertise in the life prediction methodologies is invaluable in my dissertation work.

Dr. Hendricks, you are a wonderful teacher and I learned the basics of dynamics from your "Intermediate dynamics" course. I feel proud to have a great scholar like you in my committee.

Dr. Hajj, I am thankful to you for serving as an honorable committee member and dedicating your valuable time. You have been very cordial and helpful to me and all students I know, and always with a nice smile that we miss from many.

I special thanks to Zihong Liu, my friend and co-worker of last four years. You worked with me in dusty conditions in the lab, helped me drill 1800 hundred holes, do sanding on

Table of Contents

List of Figures:

List of Tables:

Dedication

To My Father

Chapter 1: Introduction

Steel reinforced concrete bridges have been an integral part of civil infrastructure for many years. Fiber reinforced polymer (FRP) composites were first introduced in civil infrastructure applications in the early 1950s as alternative measures for reinforcing concrete. However, FRP composites were not perceived as materials likely to make an impact on infrastructure applications such as bridges. There was no significant progress in this area until mid-1990s when civil engineers started to look for materials which are lightweight and resistant to environmental degradation. At the beginning of new millennium, deterioration of concrete structures has become an important issue in the civil engineering community. Nearly 15% of the 600,000 bridges in USA suffer from loss of material properties due to environmental degradation and age, and additional 14% are experiencing more traffic than originally intended (FHWA/USDOT 2005). The annual direct cost of corrosion for highway bridges is $8.3 billion and life-cycle analysis estimates indirect costs (due to traffic delays and lost productivity) to be 10 times the direct cost (FHWA). There is an urgent need for cost-effective and durable technologies for repair, or retrofit the aging structures to meet the increased traffic demands.

1.1 Prospects of FRP Composites for Bridge Deck

Due to high specific strength and better environmental durability, fiber reinforced polymer (FRP) composite materials can provide significant advantages over conventional materials for infrastructure application such as construction of bridges. Some of the possible benefits are reduction in dead load and subsequent increase in live load rating, rehabilitation of historic structures, widening of bridges without imposing additional dead load, faster installation reducing cost and traffic congestion, and enhanced service life even under harsh environment. Two major types of FRP composite bridge decks are currently in use: sandwich type construction and cellular or stiffened structure. Each type can be manufactured using cost-effective processes (such as pultrusion and VARTM) in modular forms to be joined on-site for faster installation.

1.2 Challenges of Implementing FRP Composites for Bridge Deck

However, there are significant challenges involved to implement a FRP bridge deck. Some of the major challenges are higher initial material cost, difficulties in developing efficient designs of

panel-to-panel and deck-to-stringer connections, lack of comprehensive standards and design guidelines, and uncertain durability characteristics under combined mechanical and environmental loads.

Although low cost manufacturing processes like VARTM and pultrusion are being used, the higher cost of reinforcing fibers (carbon and glass) and resins (vinyl ester, epoxy and polyester) limit the potential benefits of using FRP decks. The lower bound cost estimate of GFRP bridge decks is approximately \$65/ft^2 which is more than twice the cost of conventional steel reinforced concrete (RC) decks (\$30/ft^2). In order to be competitive with RC decks, the initial costs of FRP decks should be approximately \$ 40/ft^2. There is lack of reliable data on durability of FRP bridge decks to justify its use based on life cycle cost analysis.

For civil infrastructure applications, joining multi-part assemblies presents additional challenges. Joining of composite structural components can be achieved using either mechanical fasteners or the adhesive bonding method. The adhesive bonding method is gaining more attention as there are potential advantages of weight saving by eliminating fasteners, introducing more uniform load transfer and providing better long term performance. However, there is little existing research on efficient design, performance evaluation and reliability of adhesive joint in FRP composite bridge decks.

Most researchers over the last decade have focused primarily on performance evaluation and characterization of FRP composite deck systems on a case study basis. There is little or no effort has been made to develop test methods and design guidelines for FRP composite deck. In absence of a structured and coordinated research, there is lack of proper understanding of the structural behavior of FRP deck. This can lead to either over design or poor design leading to premature failure and unexpected failure modes being reported in the literature. This eventually hinders understanding the long term degradation mechanism and prediction of realistic service life of the structure.

1.3 Synopsis of the Issues Addressed in the Dissertation

We will first present a review of the research efforts (**Chapter 2**) conducted by different researchers on FRP composite bridge deck to address the challenges outlined in previous section. Based on the knowledge of the state of the art research efforts on FRP bridge decks, the possible

scope of contribution will be identified. The entire premise of the dissertation will revolve around a case study of rehabilitation of Hawthorne Street Bridge utilizing FRP composite bridge deck. Different aspects of the research work will be categorized into manuscripts which will also constitute individual chapters in this dissertation. The first paper will discuss a new proposed simulated tire patch loading for characterizing FRP composite bridge deck (**Chapter 3**). The second paper (**Chapter 4**) will describe implementation adhesive bonding of FRP composite bridge deck panels while the third paper (**Chapter 5**) will focus on global response of deck and bridge super structure considering for local effects. Finally, the strength and life prediction approaches will be presented in a separate paper (**Chapter 6**). At the end of this dissertation, overall conclusions and recommendations will be presented (**Chapter 7**).

Chapter 2: Literature Review

FRP materials have received considerable attention as both internal and external reinforcing materials primarily for deteriorating concrete structures. There has been significant increase in research on FRP composites for bridge application since mid-1990s (Hollaway 2003). Many researchers reported implementation of FRP composites in infrastructure as promising while others expressed concerns about is high initial cost and construction issues (such as lack of unfamiliarity and learning curve for the industry) (Ballinger 1992; Busel and Lockwood 2000; Anon 2001; Bakis et al. 2002; Busel 2002; Karbhari 2004; Reising et al. 2004; Bank 2005; Iyer and Bharil 2005; Harries 2006; Hong and Hastak 2007). A number of case studies and fundamental research related to FRP composite bridge deck will be discussed in the following sections with emphasis on some important areas of interest.

2.1 Joining of FRP Deck Panels

Mechanical fastening had been the primary method of joining structural components made of conventional materials for long time. However, alternative methods such adhesive bonding is now getting much attention because of the introduction of new material systems in infrastructure. Adhesive bonding is a technology that is well suited to FRP composite structures because their relatively poor transverse properties and brittleness limits the efficiency of bolted and riveted joints. There have been a number of success stories of implementation of adhesive bonding in primary structural components especially in the aerospace industry. Hart-Smith discussed some important factors to be considered during design and analysis of bonded composite joints in aircraft structures (Hart-Smith 2002) . He emphasized the basic design rule for adhesive joint that undamaged bonded joints must always be stronger than the structure tying them together, regardless of the nominal design loads. The reason for this is that bonds are continuous and any initial damage or defect could propagate catastrophically if even a perfect bond were allowed to become a weak-link fuse. In analyzing adhesively bonded joints, one must account for the fact that failure can occur by more than one mechanism such as shear and peel stresses (Goland and Reissner 1943; Volkersen 1965). In well-designed bonded composite joints, none of these phenomena should be allowed to govern and adherend should fail first at such high load utilizing high strength of fibers.

Over the years, a number of joint configurations have been developed and used in joining different structural components. A significant amount of research efforts have been dedicated towards analyzing most common idealized joint configurations such as single lap, double lap, scarf, and stepped joint.

Many researchers have proposed failure criteria for adhesively bonded joints; for the most part they fall into three distinct categories (Du et al. 2004). The simplest method is based on the strength of materials in which the joint failure is assumed to occur when the maximum stress or strain predicted exceeds the measured stress or strain. The second method is based on linear-elastic fracture mechanics where the applied strain-energy release rate in an adhesive joint is evaluated, and the joint failure is assumed to occur when the predicted crack-growth driving force exceeds the measured fracture resistance. The third method is the cohesive zone approach. In the cohesive zone models, the microscopic fracture processes of the adhesive and the macroscopic non-linear deformations of the adherends are analyzed independently and then linked together through a traction–separation law for the local de-cohesion processes to express the overall behavior. The core of all these methods is appropriate analysis of joints and most researchers had to reply on numerical methods due to complexity in analysis.

For isotropic adherends, the design and analysis of adhesively bonded joints is now a relatively matured discipline (Adams RD 1997). There is also a wealth of well developed research on stresses analysis and design of simple lap joints with composite adherends (Renton and Vinson 1975; Pickett and Hollaway 1985; Pickett and Hollaway 1985; Hildebrand 1994; Bogdanovich and Kizhakkethara 1999; Bogdanovich and Yushanov 1999; Quaresimin and Ricotta 2006; Quaresimin and Ricotta 2006). It is observed that the peel and shear stresses can vary significantly along the bond line of an adhesive lap joint (Matthews et al. 1982). Scarf joints are believed to provide more uniform load transfer compared to simple butt and lap joints. However, a scarf joint in a composite structure is more complex because, unlike lap or stepped-lap joints, the stiffness of the bonded surface varies along the bond line. Material nonlinearities of adhesive layer and orthotropy of FRP composite further add to the complexity of obtaining a closed form solution for stress distribution in scarf joint. Simple methods for the design of such joints have been proposed, however, they typically assume that the stresses along the bond line can be approximated as constant.

One of the very few analytical expressions for shear and peel stress in an adhesively bonded scarf joint with the assumption of similar isotropic adherends has been developed by Gleich (Gleich et al. 2000). The analysis adopted a modified version of scarf joint which includes finite adherend tip thickness and assumed constant stress across the adhesive layer. The shear stress distribution was in close agreement with finite element results, but the peel stresses were overestimated. Subsequent research gave a solution of the problem for adherends having differing elastic constants and also under pure bending (Wah 1976; Chen and Cheng 1989). The theoretical threshold of the first micro cracks in the scarf joint was proposed by Objois (Objois et al. 2005). This threshold is particularly important because it marks the end of the elastic behavior of the bonded structure. The model accurately predicted the micro cracking of the joint provided that the scarf-angle value is more than 10°. When it is smaller than 10°, the theoretical model can no longer predict the very complex micromechanical behavior at the extremities of the joint. The model was again limited to isotropic material properties. Gunnion and Herszberg reported a broad study on the effect of various parameters on the performance of a scarf joint using parametric finite element model (Gunnion and Herszberg 2006). The stress distribution along the bond-line has been investigated, and the sensitivity of peak stresses determined with respect to changes in scarf angle, adhesive thickness, ply thickness, laminate thickness, over-laminate thickness and lay-up sequence. The results of this investigation provide further insight into the stresses that develop in scarf repairs of composite structures under load. This insight may lead to improved design and analysis techniques of scarf joints in composite structures.

It is far more challenging to implement joint at a large structural level than any idealized coupon joint configuration. It appears that there has been relatively little research in the area of adhesively bonded structural joints in pultruded FRP composite. Zetterberg investigated both bolted and adhesive joint between composite profiles for bridge deck applications (Zetterberg et al. 2001). He pointed difficulties in implementing scarf and stepped joints and eventually used single lap joint between bridge deck profiles. Instead of analyzing the structure, an idealized lap joint configuration was analyzed using finite element method. Results showed adhesively bonded joint provided better safety margin for design.

Boyd investigated finger joint in pultruded composite and found that the performance is only comparable to double strap joint although finger joint had four times less bond area (Boyd et al. 2004). The most surprising finding from the tests on the finger joints was that the failure occurred nearly entirely cohesively. This implies that such a joint is dependent on the strength of the adhesive, and refinement of the geometry may improve the joint strength. Thermo-elastic stress analysis (TSA) is used to provide the full field stress distribution over the joint. It is shown that by increasing finger tip angle there is a decrease in load carrying capacity, a decrease in shear stress and an increase in stress concentration factor at the finger joint tip (Boyd et al. 2006). Zhou and Keller pointed out that in a lap joint through-thickness tensile and shear stresses have peaks at the edges. They proposed a quadratic stress failure criterion for bonded joints in pultruded GFRP laminate (Zhou and Keller 2005). A performance comparison of four different FRP deck panels installed in a five span bridge has been reported by Reising (Reising et al. 2004). Two deck panels implemented tongue and groove type joint while other used splice plate joint. The research found pultruded deck panel had better dimensional accuracy in joint.

Keller and co-workers performed quasi-static axial tension experiments on double-lap joints composed of pultruded GFRP flat profiles and investigated effect of the overlap, the adhesive layer thickness and the degree of chamfering of the adherends (Keller and Vallee 2005; Keller and Vallee 2005; Keller and Vallee 2006). Chamfering reduced through-thickness tensile and shear stress peaks towards the chamfered joint edges. However, joint strength was not significantly improved by chamfering. The adhesive layer thickness had an insignificant influence on the stress–strain distributions along the overlaps and joint strength.

For adhesively bonded fiber reinforced plastic (FRP) structures, durability prediction is a much more complicated process. As Hart-Smith points out for adhesively bonded structures, information from small laboratory coupons cannot be effectively translated into prototype structure performance (Brinson and Grant 1986).

A methodology for the life prediction of bonded joints in composite materials has been presented by Quaresimin and Ricotta (Quaresimin and Ricotta 2006). The model describes the crack nucleation phase by a generalized stress intensity factor approach, whereas for the subsequent propagation phase the crack growth rate is correlated to the strain energy release rate. With the aim to provide a reliable tool for the fatigue design of bonded connections, the

model provides life estimations at different probabilities of survival. Wahab proposed a generalized technique for the prediction of fatigue crack propagation lifetime in bonded structures using finite element analysis (Abdel Wahab et al. 2004). The method is based on numerical integration of the fatigue crack growth law from an initial to a final crack size. The technique has been applied to carbon fiber composite joints bonded with an epoxy adhesive. A crack growth law was determined experimentally using double cantilever beam (DCB) samples. Experimental load-life data were then generated for single and lap joints. The crack growth law determined from the DCB samples was used to predict the load-life response of the single and double lap joints.

Keller studied quasi-static and fatigue performance of a cellular FRP bridge deck adhesively bonded to steel girders (Keller and Gurtler 2005). This is one of the few works that reported testing of joints at a structural component level. The results of the investigation showed that the well-established design method for steel–concrete composite girders with shear stud connections can be extended to be used for the design of such FRP-steel girders.

Experimental and numerical investigations were carried out on adhesively bonded full-scale double lap joints composed of pultruded GFRP profiles with relatively thick adhesive layers (Vallee et al. 2006). Thick adhesive layers are often used in infrastructure applications in order to compensate for geometrical tolerances. The influence of different geometric parameters on the joint strength was investigated: the thickness of the adhesive layer (5–35 mm), the fillet radius (2–10 mm) and the overlap length (100–300 mm). It was found that the joint strength (i) decreases with the adhesive layer thickness, (ii) is almost independent of the fillet radius and (iii) increases with overlap length. It was concluded that the shape of through-thickness tensile and shear stress distributions influences joint strength and that joint strength is therefore influenced by a statistical size effect. A probabilistic method has been developed for the strength prediction of balanced adhesively bonded double lap joints composed of pultruded GFRP adherends(Vallee et al. 2006). The failure criterion applied considers the interaction of through-thickness tensile and shear stresses at the location of failure inside the mat layer of the inner adherend at a depth varying from 0.5 to 1.5 mm. Results showed that the statistical approach to predicting joint strength provides reasonable results for brittle joint failure where statistical size effects occur. The method is not appropriate for quasi-brittle or pseudo-ductile failure behavior.

Summary on FRP deck joint literature:

Research work on stress analysis of basic joint configuration such as simple lap joint is well developed for both isotropic and FRP composite adherends. However, more complex joint configurations like scarf joints, common approaches are still numerical solution using finite element method or analytical formulation based on simplified assumptions. Most of the analytical work was found to be focused on joints typical in aerospace structures. There are only few experimental work on adhesive joints in infrastructure application but still limited to representative coupon or component level. Most of these analyses assumed simple loading cases such as tensile load. However, bending load is applied in bridge deck applications which in turn induces shear and peel stresses in the adhesive joint. A full scale structural investigation of joints in bridge deck application is necessary to fully understand the response and predict durability. Also, there is no established link between well developed coupon joint analysis and structural joints for possible simplified analysis or design criteria.

2.2 Performance Evaluation and Failure Mechanisms in FRP Composite Bridge Decks

Characterization studies of the demonstration projects have recognized that FRP bridge systems are highly stiffness driven. The development of deck systems with high flexural stiffness-to-weight has received a great deal of attention. To date, a number of research groups proposed several novel FRP deck systems. These can be categorized into two types such as cellular structure and sandwich construction.

The structural behavior of a fiber reinforced polymer (FRP) web core skew bridge superstructure was studied by Aref (Aref et al. 2005). The structural response was investigated using finite element plate model and compared with field test results. The failure was observed at the shear-key joint combining both panels(Aref et al. 2005). Optimization design procedures has also been developed to overcome the challenge of high initial construction costs associated with the fiber reinforced polymer (FRP) sandwich deck systems (He and Aref 2003). The first fiber reinforced polymer deck, installed on a truss bridge in New York State was load tested to study its behavior (Alampalli and Kunin 2002; Alampalli and Kunin 2003; Alampalli 2006). The sandwich deck panels were bonded using epoxy adhesive. The test data indicated that localized bending effects may play a role in the strain distribution of FRP decks and should be appropriately considered.

Several other researchers looked at modeling and characterization of fiber-reinforced plastic honeycomb sandwich panels for highway bridge applications (Davalos et al. 2001).

Most of the research on cellular FRP deck panels at an early stage considered deck panels as beam and tested under three point bend loading (Harik et al. 1999). Punching shear and edge delamination were reported as failure mode.

Debonding of the pultruded components surrounding the loaded region and punching at the loading point was reported as failure mode for the same deck system by other researchers (Alagusundaramoorthy et al. 2006). Structural performance of FRP deck with very unusual geometry was reported by Kumar (Kumar et al. 2004) and the shape of the deck was made look like several I-beam joined together. There was no clear advantage of using such deck system. All of those research works were simply limited to checking the deflections against existing design criteria.

Park tried to optimize the material property and geometry of a cellular deck based on simple one-way bending tests in longitudinal and transverse direction (Park et al. 2005). However, he later used a simply supported plate like test setup to investigated structural response of deck panel. The failure locations were identified as near joint between flange and web mostly due to stress concentration along the steel loading patch edges.

Wan studied the structural behavior of a GFRP bridge deck system and conducted parametric studies to investigate the effects of diaphragms, girder stiffness, girder spacing and composite action on the characteristics of the system (Wan et al. 2005). FEA results were validated with laboratory experiment and field testing data.

Another type of cellular FRP deck made of adhesively bonded pultruded box shapes has been under investigation for a number of years at Virginia Tech and several researchers contributed to this study (Hayes et al. 2000; Zhou et al. 2005). In the laboratory tests, the AASHTO steel patch was compared to the simulated tire patch made from a truck tire reinforced with silicon rubber. The simulated tire loading developed greater global displacement at the same static load. The failure mode is localized and dominated by transverse bending failure of the composites under the simulated tire loading as opposed to punching shear for the AASHTO recommended patch load.

Qiao and Davalos presented a systematic analysis and design approach for single-span FRP deck-stringer bridges (Qiao et al. 2000). This design approach includes analyses using ply micromechanics, panel macro-mechanics, laminated beam theory, elastic equivalent deck model, and finally combined deck-stringer system (series approximation technique). Other research efforts also attempted finite element and approximate series solution method for analyzing FRP composite deck based on the assumption of orthotropic plate behavior (Salim et al. 1997; Shen et al. 2002; Atadero et al. 2005; Mu et al. 2006; Salim et al. 2006; Prachasaree et al. 2007).

A number research works also explored dynamic response of a bridge with FRP composite deck (Alampalli 2000; Aluri et al. 2005; Zhang et al. 2006; Zhang et al. 2006; Chiewanichakorn et al. 2007; Zhang and Cai 2007). Wu reported an interesting computational study on strategic sensor locations of FRP bridge decks (Wu et al. 2003). However, the analysis is only limited to equivalent isotropic deck and suitable for global response.

A gap analysis study was undertaken under the aegis of the Civil Engineering Research Foundation and the Federal Highway Administration to identify and prioritize critical gaps in durability data (Karbhari et al. 2000; Karbhari et al. 2003). The study focuses on the use of FRP in internal reinforcement, external strengthening, seismic retrofit, bridge decks, structural profiles, and panels. Environments of interest are moisture/solution, alkalinity, creep/relaxation, fatigue, fire, thermal effects (including freeze-thaw), and ultraviolet exposure.

Deterioration of reinforced concrete bridges is not only a problem in United States but also throughout the world. To this end, project ASSET (a four-year EC-funded research program) was initiated to develop an optimized FRP bridge deck system for deck replacement. The detailed analysis and optimization of the ASSET profile together with the design and practical issues for a case study is reported by Luke (Luke et al. 2002). The Friedberg Bridge, to be constructed during 2006-07, will be the first major FRP road bridge in Germany. The innovative technology, its economical aspects and the design of the bridge are highlighted by Knippers (Knippers and Gabler 2006). Besides pultruded cellular deck and VARTM manufactured sandwich decks, there are other types of bridge decks are also proposed by many researchers. Filament-wound glass fiber reinforced polymer bridge deck modules was reported by Williams (Williams et al. 2003) and Davey proposed an innovative PVC molded resin core deck (Davey et al. 2001).

There are significant amount of reports on field tests of installed FRP composite deck system and those are not cited in this literature review. Most of these field performance studies are limited to service load tests with AASHTO design truck and durability data is not yet available since such FRP deck systems are relatively new.

Summary of literature on performance evaluation and case studies:

Different types of deck systems have been proposed by many researchers over the past years. Most of the research works were carried out on structural component level at the laboratory. There is no full scale laboratory investigation of FRP deck on a bridge structure. This limits the understanding the performance of FRP deck at a structural level. Also, analytical works using finite elements methods and theoretical plate solutions considered FRP decks as orthotropic plates. Such analyses yielded satisfactory results for studying the global response but the local effects remain unknown. Current test methods and guidelines were followed in all experimental and FEA simulations. Effectiveness of uniform steel patch loading and corresponding analyses of deck response may be inadequate to capture true long term degradation mechanism. Although most research validated the design against deflection criteria on the structure, none of them considered possibility of limiting criteria based on relative deflection of the deck itself.

2.3 Fatigue Life of Composite Bridge Decks

Because of the relatively large number of possible failure mechanisms in FRP composite materials, the prediction of fatigue life in a component is not simple. In a composite material, fatigue damage can take the form of any or all of the following: delamination, matrix cracking, fiber failure, matrix crazing, fiber-matrix debonding and void growth. It is dependent on variables associated with the testing conditions and the construction and composition of the material. The S-N curve appears still to be the most popular method of characterizing the fatigue behavior of composite materials. Several empirical equations exist for describing S-N curves. Most are based on the classical power law that gives a straight line in a log-log plot of the fatigue data. Other theories are essentially three types: theories based on the degradation of residual strength, theories based on changes in modulus and theories based on actual damage mechanisms.

Philippidis discussed state-of-the-art phenomenological residual strength models and reviewed on probabilistic and deterministic theories that predict strength degradation under various

loading conditions (Philippidis and Passipoularidis). He concluded that the use of complicated phenomenological models requiring large experimental data sets does not necessarily pay back in terms of accurate predictions and consequently simple models requiring limited experimental effort should be preferred.

Huston reviewed existing fatigue life prediction models and reported tension fatigue test data on unidirectional carbon fiber reinforced epoxy fitted to residual strength and residual stiffness models (Reifsnider 1986; Reifsnider and Gao 1991; Huston 1994; Reifsnider et al. 2000). Further fatigue tests were carried out under spectrum loading so that the results could be correlated with the cumulative damage predicted by the residual strength model. A limiting property governing the thermo-mechanical behavior of composites is the strength transverse to the fibers. A number of researchers have focused on off-axis fatigue in unidirectional and cross-ply composites (Reifsnider and Gao 1991; Berbinau et al. 1999; Philippidis and Vassilopoulos 1999; Plumtree and Cheng 1999; Kawai et al. 2001; Kawai et al. 2001; Pandita et al. 2001; Plumtree and Shi 2002; Kawai 2004; Kawai and Taniguchi 2006; Shokrieh and Taheri-Behrooz 2006; Liu and Mahadevan 2007; Varvani-Farahani et al. 2007). Several researchers looked at durability characteristics of FRP bridge decks under environmental conditions such as temperature (Datta et al. 2002; Shahrooz et al. 2007). Liao studied glass-fiber-reinforced vinyl ester composite coupons aged in water or in salt solutions and subjected to four-point-bend fatigue (Liao et al. 1999). The tolerance of composites to damage induced by cyclic loading and moisture ingress is of utmost importance. McBagonluri highlighted the effects of short-term cyclic moisture aging on the strength and fatigue performance of a glass/vinyl ester pultruded composite system (McBagonluri et al. 2000). The exposure to moisture caused permanent damage in the material system. A methodology and strategy has been proposed for fatigue damage assessment and life prediction of bridge-deck sections with online structural health monitoring data (Chan et al. 2001; Li et al. 2001). A fatigue damage model based on the continuum damage mechanics (CDM) is developed for evaluating accumulative fatigue damage of existing bridges. For accurate estimation of fatigue life, the nonlinear fatigue model based on CDM may be better than Miner's rule. However, this needs further verification on structural fatigue tests although it has been verified by material fatigue tests.

When an FRP deck is used in rehabilitation of a bridge, a system level approach should be used to evaluate the dynamic and fatigue response of the bridge. Chiewanichakorn studied the

behavior of a FRP deck in truss bridge using finite element models (Chiewanichakorn et al. 2007). FE models were employed to conduct dynamic time-history analyses with a moving AASHTO fatigue truck over the bridge. Fatigue life was evaluated based on fatigue resistance formulae specified in AASHTO-LRFD design specifications. Axial tension–tension fatigue experiments were performed by Keller on pultruded glass fiber reinforced polymer (GFRP) plates in a laboratory environment (Keller et al. 2005). A loading range dependant loss of stiffness up to 50% could be observed, which can only be explained by considerable fiber failures during the fatigue loading. This result is consistent with Mandell's postulate that fatigue failure of composites is basically fiber dominated. Other methods of fatigue life estimation include acoustic emission analysis and CG method (Djiauw and Fesko 1979; Momenkhani and Sarkani 2006).

Summary of fatigue analysis literature:

Fatigue life prediction methodologies are mostly well developed based coupon level experimental data and there is lack of system or structural level work. There is even less research on pultruded FRP composites and their structural components such as bridge decks. Some researchers have only performed some fatigue tests on structural components up to a certain number of cycles at service load level and verified structural integrity (no failure). However, there is no research reported in the literature that employed nonlinear damage models (residual strength or stiffness) to predict life of FRP composite bridge deck.

2.4   FRP Composite Bridge Deck Test Methods and Design Guidelines

Design guidelines and codes developed for conventional materials still being used for FRP composites without any consideration for the differences in their response. Little or no effort has been made to emphasize the need for guideline for testing and characterizing FRP composite bridge deck systems. As a result, years of research on FRP composite deck systems still remain difficult to compare and varies on each case. Lack of proper loading method is perhaps one of the most important issues left unaddressed for long time. Unrealistic loading methods often provide premature failures at unexpected locations and predicting the long term behavior becomes much more difficult. Truck tire induces much localized stresses on to the pavement and the distribution is highly non-uniform (Pottinger 1992; de Beer 1996; Pottinger and McIntyre 1999; Soon et al. 2004; De Beer et al. 2005; Wang and Machemehl 2006). Current guidelines for

conventional decks assume a uniform distribution of patch loading for characterizing FRP deck. Experimental determination of contact pressure distribution between bridge decks and truck tires have revealed that increase in inflation pressure increases the peak values of the contact pressure distribution profile and maximum contact pressure is found to be about 2.5 times the average pressure computed from the current AASHTO specifications for highway bridges (GangaRao and Vali 1990). From the tire footprint of different truck tires it is clear that commercial truck tire causes heavy concentration of stress near the center and the distribution is far from uniform.

A realistic loading method is needed for both experimental characterization and as a design tool for analytical investigation.

2.5   Scope of Contribution

Based on the literature review, it can be concluded that there is lack of adequate research in the following areas of potential interest. (a) Lack of guidelines for characterizing FRP composite deck systems (b) Implementation and analysis of adhesive joints in Bridge decks (c) Performance evaluation of FRP deck systems through full scale laboratory experiments utilizing tire patch loading and FEA simulation to investigate local effects (d) Strength and Fatigue life prediction of FRP deck systems

This dissertation will therefore attempt to address some of the critical issues in those areas. The following chapters will therefore focus on each of these areas and the chapter sections are organized such that it facilitates contribution as individual paper.

Chapter 3:   Conformable Pressure Analysis of Proposed Simulated Tire Patch for Loading on Cellular FRP Deck

Conformable Tire Patch Loading for FRP Composite Bridge Deck

[1] Prasun K. Majumdar, [2]John J. Lesko, [3]Zihong Liu, , [4]Thomas E. Cousins

Abstract

Fiber reinforced polymer (FRP) composites are increasingly being used in bridge deck applications. However, there are currently only fledgling standards to design and characterize FRP deck systems. One of the areas that should be addressed is the loading method for the FRP composite deck. It has been observed that the type of loading patch greatly influences the failure mode of cellular FRP deck. The contact pressure distribution of real truck loading is non-uniform with more concentration near the center of the contact area as a result of the conformable contact mechanics. Conversely, conventional rectangular steel patch on FRP decks act like a rigid flat punch and produces stress concentration near the edges. A proposed simulated tire patch has been examined for loading cellular FRP deck with the load distribution characterized by a pressure sensitive film sensor and 3D contact analysis using ANSYS 11.0. A loading profile is proposed as a design tool for analyzing FRP deck systems for strength and durability. Local top surface strains and displacements of a cellular FRP deck are found to be higher with proposed loading profile compared to those for the conventional uniformly distributed loading. Parametric studies on deck geometry show that the global displacement criteria used for characterizing bridge deck is inadequate for cellular FRP deck and that the local effects must be considered.

CE Database subject headings: Fiber reinforced polymers, Bridge decks, Finite element method, Composite structures, Load transfer, Failure modes, Standards and codes, Tires

[1]Corresponding author. Graduate Student, Department of Engineering Science & Mechanics, 120 Patton Hall, Virginia Tech, Blacksburg, VA 24061, USA. Tel.:540-449-2282; Fax: 540-231-9187 Email: pkm2004@vt.edu
[2]Professor, Department of Engineering Science & Mechanics, 120 Patton Hall , Virginia Tech, Blacksburg, VA 24061, USA. Email: jlesko@vt.edu
[3] Graduate Student, Department of Civil & Environmental Engineering, 200 Patton Hall, Virginia Tech, Blacksburg, VA 24061, USA. Email: lzh@vt.edu
[4]Professor, Department of Civil & Environmental Engineering, Virginia Tech, Blacksburg, VA 24061, USA. Email: tcousins@vt.edu

3.1 Introduction

There is a growing concern for the deterioration of reinforced concrete bridges and their decks all over the world. Therefore, cost-effective and durable technologies are needed for bridge repair, rehabilitation and replacement (ASCE; FHWA). Fiber reinforced polymer (FRP) composite can be a viable alternative for construction of bridge decks. FRP composite can provide significant advantages over conventional materials for construction of bridges, such as reduction in dead load and subsequent increase in live load rating, rehabilitation of historic structure, faster installation, and enhanced service life even under harsh environment. However, higher initial cost of materials is a concern.

To be cost-effective, FRP composite deck systems should be designed to meet a relatively long service life (usually 50-75 years). Lack of proper understanding of the structural behavior of FRP deck can lead to either over design or poor design leading to premature failure and unexpected failure modes. The key element in investigating the response of a deck is to apply proper loading in critical locations to produce the maximum load effect consistent with its application. The current practice is to apply design wheel load uniformly distributed over a finite surface area (tire contact area) of the deck specified by the American Association of State Highway and Transportation Officials (AASHTO) and AASHTO LRFD specifications (AASHTO 1996; AASHTO-LRFD 1998) and characterize the response. This is known as "Patch loading" and usually applied through a rectangular steel plate. However, this effort for achieving uniform distribution of stress may not be realistic in bridge deck application as it did not consider actual distribution of stresses induced by a truck tire.

There has been extensive research on tire induced stress profiles and tire-pavement interaction mechanisms over the last 10 years (Marshek et al. 1986; Tielking and Roberts 1987; Kim et al. 1989; Sebaaly and Tabatabaee 1989; Pottinger 1992; Sebaaly 1992; Tielking and Abraham 1994; Yue and Svec 1995; Myers 1999; Pottinger and McIntyre 1999; Al-Qadi et al. 2002; Soon et al. 2004; Prozzi and Luo 2005; Wang and Machemehl 2005; Fernando et al. 2006; Wang and Machemehl 2006; Wang and Machemehl 2006). Traditional design guidelines assumed that contact stress is uniformly distributed over a rectangular or circular area and stress value is equal to tire inflation pressure. However, a number of studies

including tire footprint analysis by Pottinger (Pottinger 1992; Pottinger and McIntyre 1999), and Stress-in-Motion (SIM) sensor analysis by de Beer (De Beer 1996; De Beer et al. 2005) have demonstrated that tire induced normal contact stress is far from uniform. Maximum contact pressure can be as high as 2.5 times the average pressure depending on tire inflation pressure, tire load, and tire type (GangaRao and Vali 1990; De Beer 1996). A typical truck tire contact pressure profile by Pottinger (Pottinger and McIntyre 1999) is considered as reference in subsequent analysis. The effect of non-uniform contact pressure profile of actual truck tire on FRP composite deck systems should be investigated further.

Moreover, the current loading method was originally developed for bridge decks made of conventional materials (steel and concrete). Many researchers have used these specifications to analyze and test FRP decks over the past years without any consideration for the differences between FRP decks and conventional bridge decks. The important distinctions between FRP deck and conventional decks are the differences in stiffness and geometry. The response of the deck will be different depending on contact interactions of the specific loading patch and deck itself. As a result, the load transfer mechanisms can be quite different for a particular loading patch on FRP deck compared to conventional decks. Principles of contact mechanics can be applied to better understand the load transfer mechanisms for different loading patches acting on a FRP composite deck.

3.1.1 Review of Contact Problems

Based on configuration of contact zone, contact problems can be classified into three types; **advancing**, **conforming**, and **receding** (Faraji 2005). Indentation of an elastic half-space by a rigid flat punch (Fig. 1) is the most commonly discussed conforming contact problems in the literature (Gladwell 1980; Johnson 1985; Fischer-Cripps 2000; Laursen 2002; Faraji 2005; Wriggers 2006). Analytical solution for this two dimensional rigid punch contact problem predicts stress concentration (theoretically infinite stress with small deformation assumption) at the edge of the contact for isotropic materials (dotted line in Fig. 3.1 represents contact pressure profile).
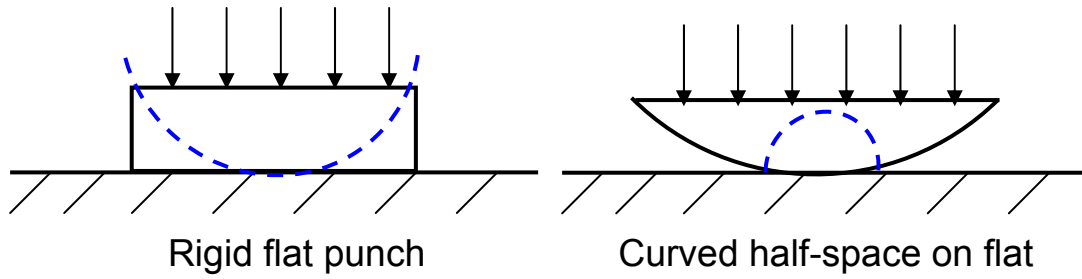
Figure 3.1 Rigid flat punch and curved indenter contact problem

Another important class of contact problem is advancing contact of curved surface (quadratic in case of Hertzian) pressed on to flat surface as shown in Fig. 1 (right sketch). The two dimensional problem with polynomial approximation of the conforming surface has been solved by Johnson (Johnson 1985). The contact pressure is highest at the center of contact and diminishes to zero at the end of the contact path.

3.1.2   Thought experiment to study contact interaction involving FRP composite

A slight variant of the 2D rigid flat punch problem is of interest in this discussion. We consider a three dimensional non-Hertzian contact problem involving a 50 mm thick rectangular block (228.6 mm by 457.2 mm) in contact with a simply supported orthotropic laminated composite plate (1830 mm x1830 mm x171 mm) under bending load (Fig. 3.2). The problem constitutes a flexible-flexible contact pair of dissimilar materials having different elastic modulus and Poisson's ratio.
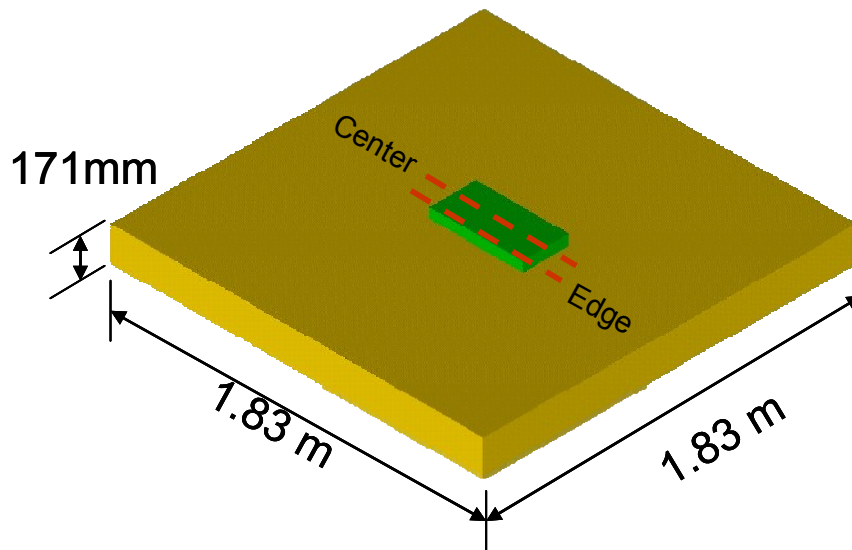
Figure 3.2 Solid FRP deck with flat punch of variable stiffness

19
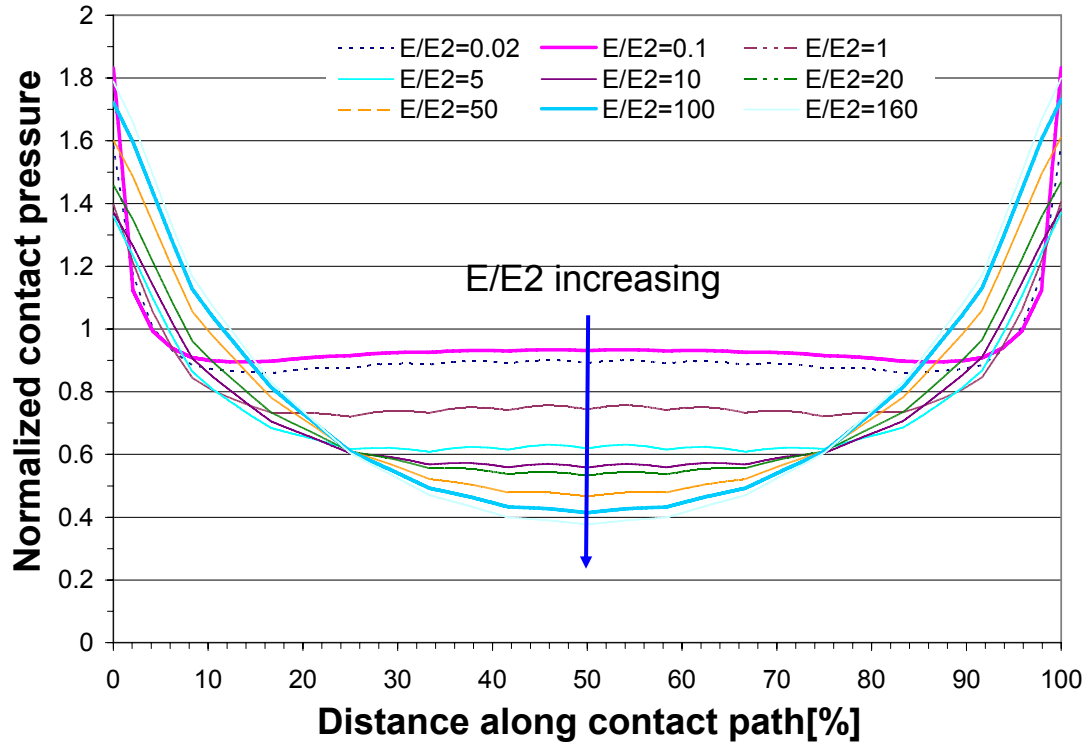
Figure 3.3 Effect of stiffness on contact pressure for flat flexible contact pair

A 3D finite element model has been developed using ANSYS to study the effect of relative stiffness of contacting bodies. When the block is much stiffer than the plate material, contact pressure is heavily concentrated along edge of the contact and well below the average near the center as shown in Fig. 3. In this plot, the modulus of indenter is denoted by E and E2 is the transverse (lowest) modulus of orthotropic plate. On the other hand, for softer punching block, the contact pressure rises towards average at the central zone but edge stresses still remain very high. This demonstrates that it is not possible to achieve a uniform distribution of contact pressure for a flexible contact pair such as solid rectangular block on laminated orthotropic surface.

These two contact problems provide insight to a number of practical applications and the interaction of loading patch with bridge deck surface is one of them. As stated earlier, current practice for performance evaluation of FRP deck uses a rectangular steel patch for loading on all types of deck systems. The stress distribution profile for conventional steel loading patch will be explored using contact mechanics and its applicability in FRP deck systems will be examined. Research work on the development of suitable loading method for performance evaluation of FRP composite bridge deck will be discussed in the following sections.

3.2 Conventional Loading Method and its Applicability for FRP Deck Systems

3.2.1 Relative Stiffness Effect

It is commonly perceived that steel patch loading provides uniform stress distribution in FRP deck and the possible effect of relative stiffness (between deck and loading patch material) is often neglected. However, a number of researchers have reported severe localized stress concentrations along the edges of the steel loading plate and a local punching shear identified as typical mode of failure (Temeles 2001; Zhou et al. 2005). This is very consistent with our contact analysis result which predicts significant stress concentrations near edges for a rectangular block on a flat surface for a wide range of relative stiffness ratio (Fig. 3.3).
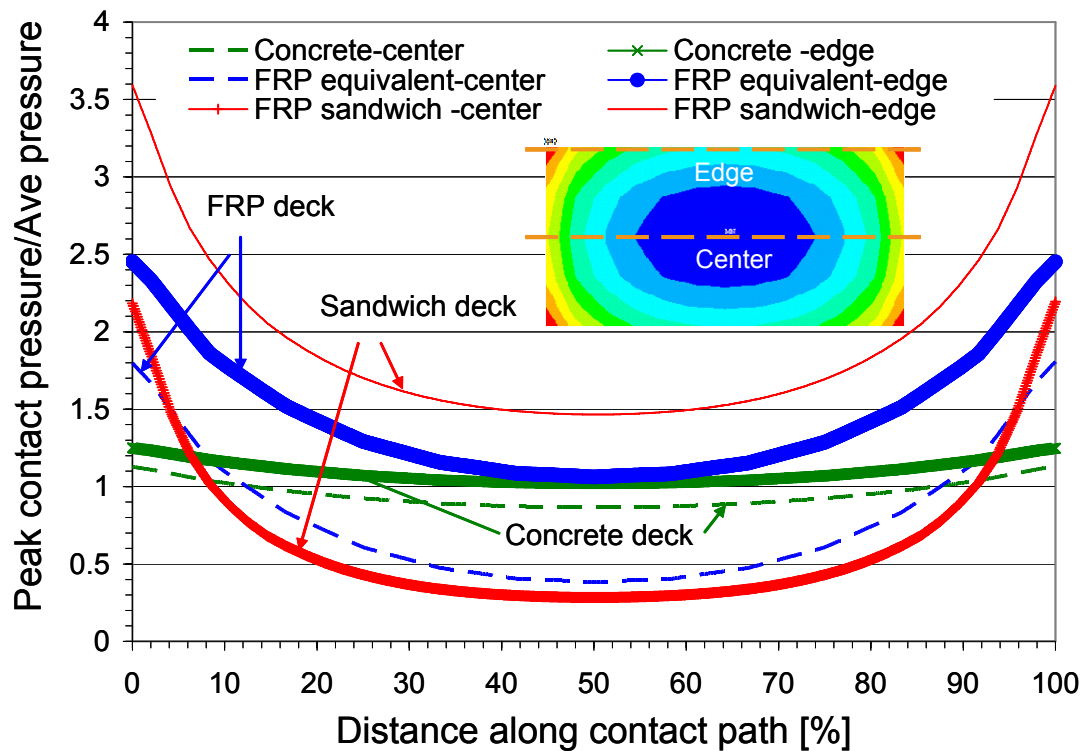
Figure 3.4 Contact pressure profile for Steel patch loading on different decks

To further explore the effect of relative stiffness specific to bridge deck application, a 3D contact model has been developed for steel patch in contact with a typical elastic equivalent solid FRP deck (E = 6.894 GPa for Strongwell deck), equivalent sandwich deck with E= 3.81 GPa (Davalos et al. 2001), concrete deck (E=27.57 GPa) and steel deck (E =207 GPa).

The contact stress values along center and edge lines are normalized by average pressure, and the distribution is shown in Fig. 3.4. Steel loading patch on thick steel deck constitutes a rigid contact pair with nearly uniform load distribution. However, for elastic equivalent solid FRP deck and sandwich deck, the pressure distribution shows higher edge stresses and below average stress near the center.

It is clear that the steel patch loading could not provide a uniform stress distribution in solid FRP deck (approximated elastic equivalent deck) and sandwich deck due to relative stiffness effect. It will be interesting to know what the contact pressure distribution might be if the cellular geometry of the FRP deck system is considered instead of solid deck.

3.2.2   Geometry Effect

In a separate 3D finite element contact model with steel patch on a representative cellular FRP deck, it is observed that conformable contact pressure profile is far from uniform. Moreover, there are localized peaks at the locations of vertical stiffeners in addition to high stresses near the edges (Fig. 3.5). From the principles of mechanics, it is known that stresses always go through the stiffest path and the higher stresses are therefore expected at vertical stiffener location compared to center span.
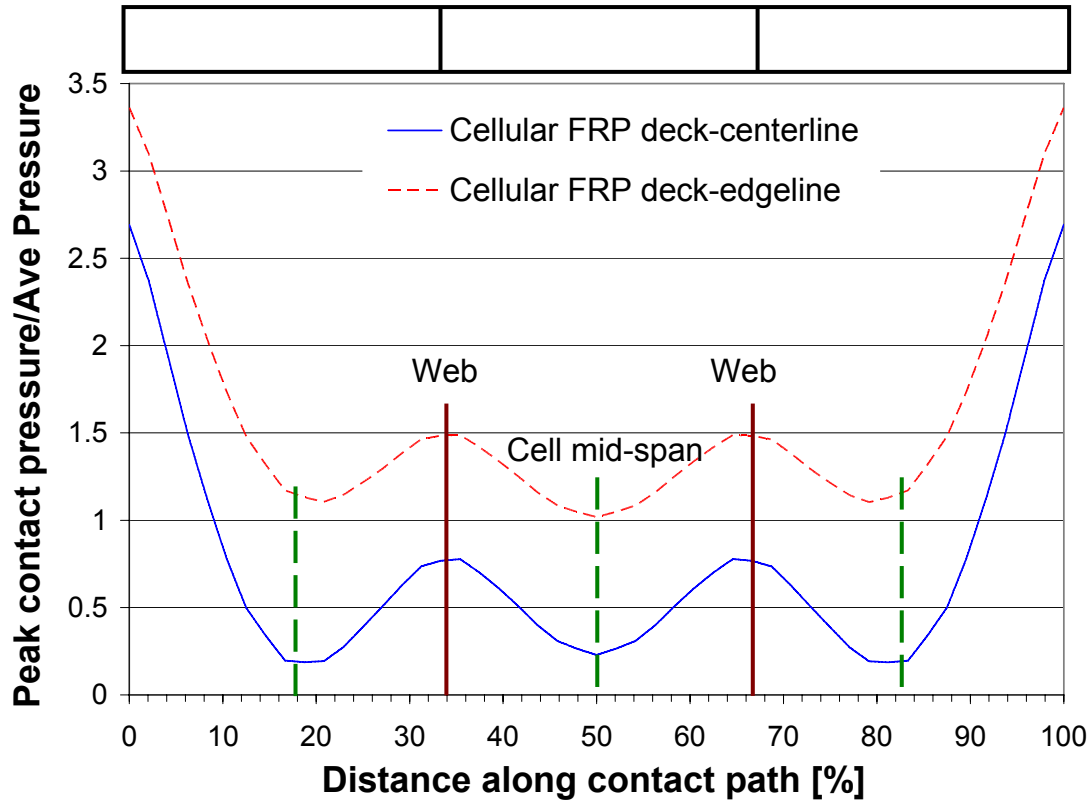
Figure 3.5 Contact pressure profile for steel patch loading on cellular FRP deck

At this point it is evident that conventional steel patch loading can not provide uniform stress distribution for solid, sandwich or cellular deck system if there is significant difference in stiffness (for example FRP composite deck).

3.3 Proposed Simulated Tire Patch (STP)

This has led to the development of a proposed simulated tire patch (STP) for loading on FRP composite decks. The simulated tire patch consists of a quarter section of a truck tire half-filled with hyper-elastic silicone rubber as shown in Fig. 3.6. Maximum height of silicone is 76 mm at central location and the rest of the height of tire section is filled with steel plate (203 mm by 457 mm). When load is applied on this STP, it deforms and develops conformable pressure, and transfers load on to the FRP deck. The proposed STP is similar to curved elastic contact surface and is expected to provide maximum stress near center of contact zone.

3.3.1   Characterizing Proposed STP: Experiment

For the proposed STP to be used in evaluating performance of FRP deck systems, the behavior of this tire patch needs to be characterized to understand the parameters of interest, i.e. contact area and contact pressure as a function of applied load.

3.3.1.1 Experimental Procedure
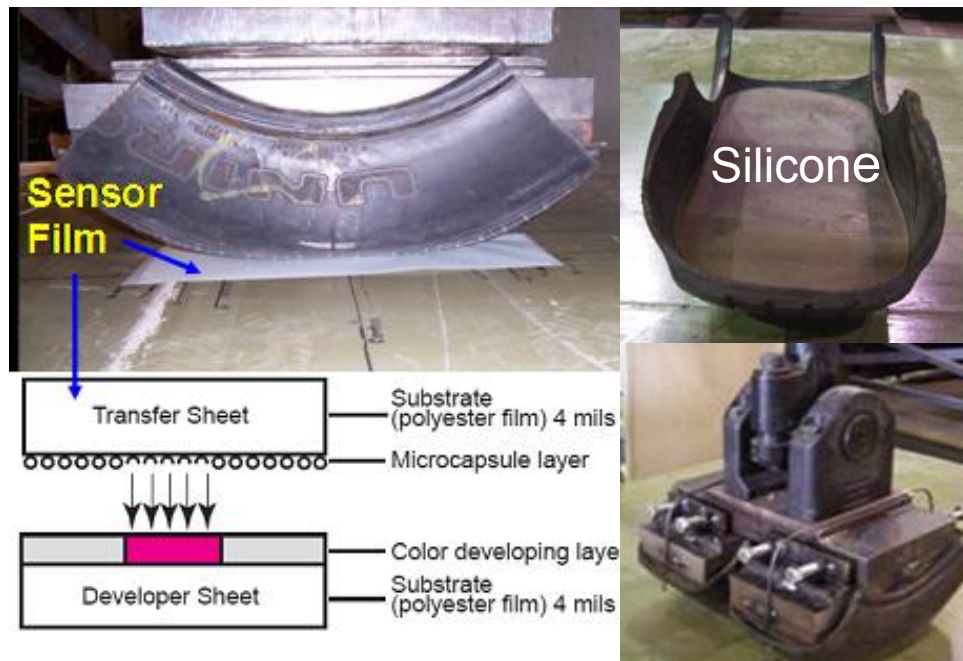
Figure 3.6 Tire patch contact test setup with Pressurex sensor

A series of tire contact tests are conducted at different load levels (22, 44, 66, 98, and 133 kN) on a 1.83m by 1.83m FRP composite deck panel manufactured by Strongwell Corporation (Strongwell). The FRP deck is made of pultruded box shapes (152.4mm inch by 152.4mm) adhesively bonded together to form cellular structure. There are also 9.5 mm thick top and bottom plates bonded to the square tube assembly. Load is applied through simulated tire patch and a pressure sensitive film named Pressurex (SPI) is placed between tire and deck surface to measure contact pressure (Fig. 3.6). Contact area can be measured from the footprints obtained from pressure film sensor. In addition, the color intensity of the Pressurex film is directly related to the amount of pressure applied to it. The greater the pressure, the more intense is the color.
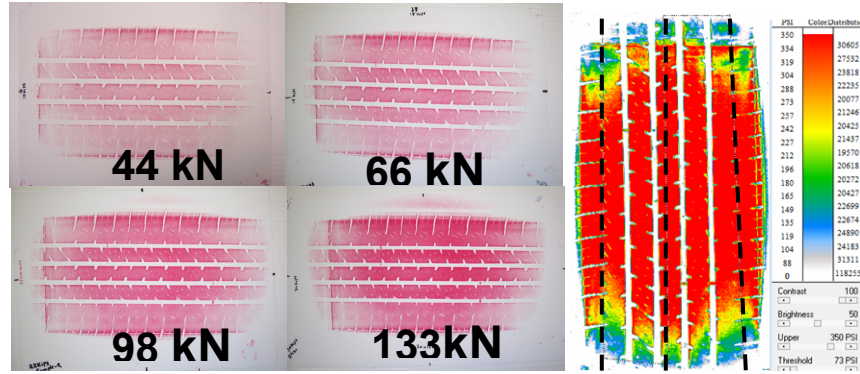
Figure 3.7 Contact surface image and contour plot using TOPAQ analyzer

3.3.1.2 Pressure Sensitive Sensor and Image Analysis

A representative set of tire patch footprint images are shown in Fig. 3.7 and these images were analyzed by pixel based image processing software to map the color intensity contour. The footprint of the STP produces a non-uniform contact pressure profile similar to the actual truck tire. The images from Pressurex sensor films were further developed into complete pressure contour maps using TOPAQ pressure analysis system (SPI). The TOPAQ system provided color coded mapping of pressure profile and magnitude between two surfaces that come into contact as shown in Fig. 7. At each applied load level, contact pressure distribution is calculated along three lines (along two edges and center) and the average of these is taken as pressure profile at that particular load level. Conformable contact pressure plots for the proposed STP at different load levels along the traffic direction are shown in Fig. 3.8. From experimental data it is observed that contact pressure does not vary significantly in the width (transverse to traffic) direction.
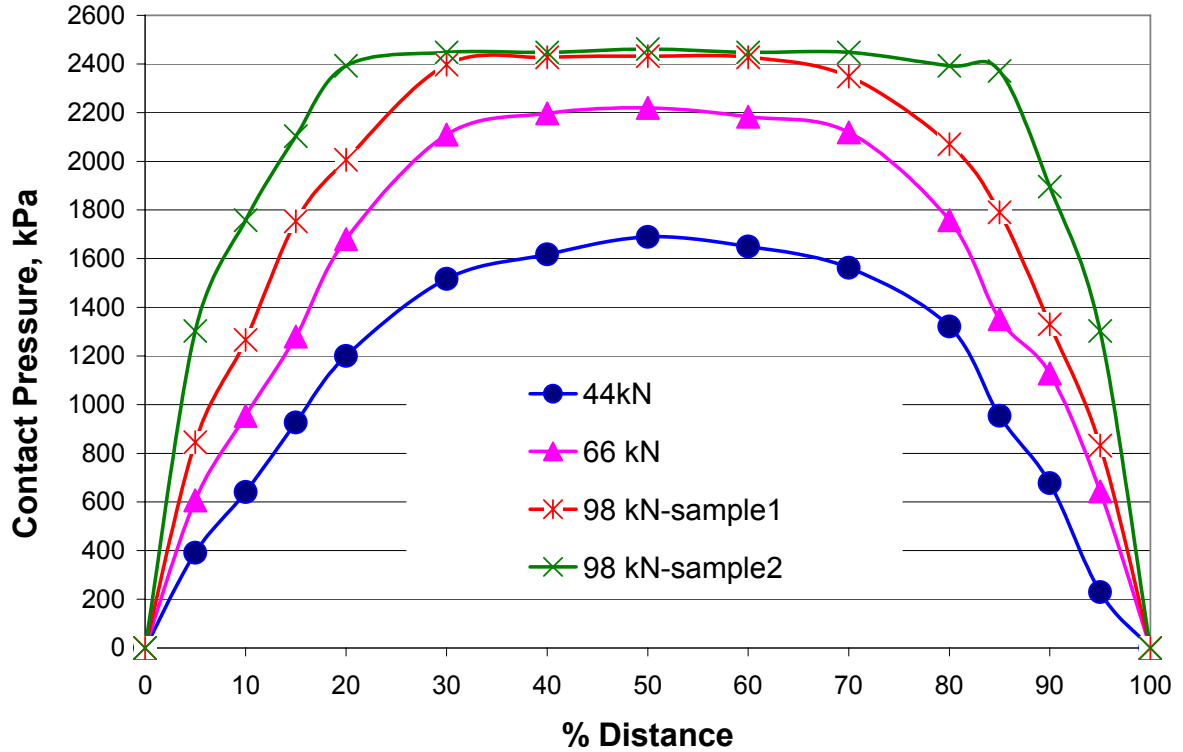
Figure 3.8 Contact pressure distribution at different load levels from experiment

3.3.2 Characterizing Proposed STP: Finite Element Contact Analysis

A three dimensional finite element model utilizing the contact theory has been developed to simulate the contact behavior of proposed tire patch loading. The deck is modeled using solid elements with quadratic shape functions (Solid95 in ANSYS) and orthotropic material properties are used (Fig. 3.9). A simplified tire patch model used higher order 18X series of solid elements (Solid186) in ANSYS 11.0 capable of hyper elasticity, large strain and mixed u-p formulation. The surface-to-surface contact algorithm using augmented Lagrange method (Laursen 2002; Wriggers 2006)) was chosen and Neo-Hookian hyper elastic model was used to describe nonlinear material response. The details of finite element contact theory are not discussed here as it is well documented in ANSYS theory reference and advanced analysis guide (ANSYS).

26
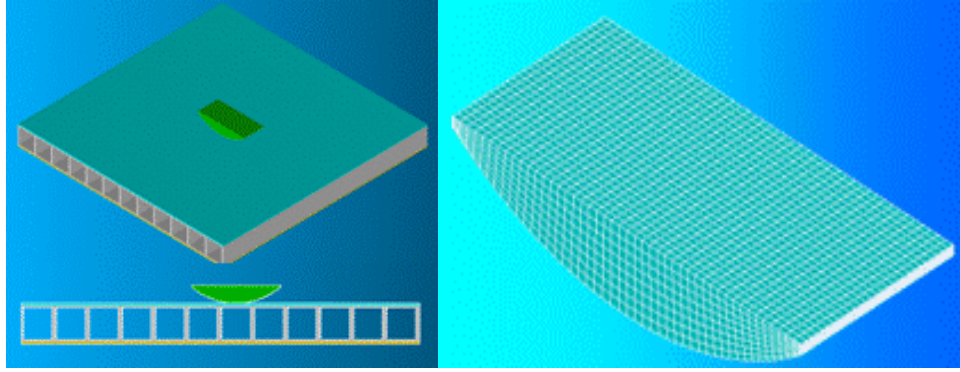
Figure 3.9 FEA model of the proposed tire patch contact with FRP composite deck

3.3.2.1 Calculation of tire contact pressure

For the simulated tire patch, it is observed that highest stresses occur at the central part of the contacting area. However, no concentration was observed at the contacting edges for the simulated tire patch. The contact pressure distribution is normalized with average contact pressure and compared with experimental results (Fig. 3.10). It is observed that both experimental data and finite element predictions fall within a small range of values compared to actual tire profile. Such collapse of normalized data in a reasonably narrow band allow for a curve fit to obtain pressure profile which can account for variation of tire size, inflation pressure and applied loading.
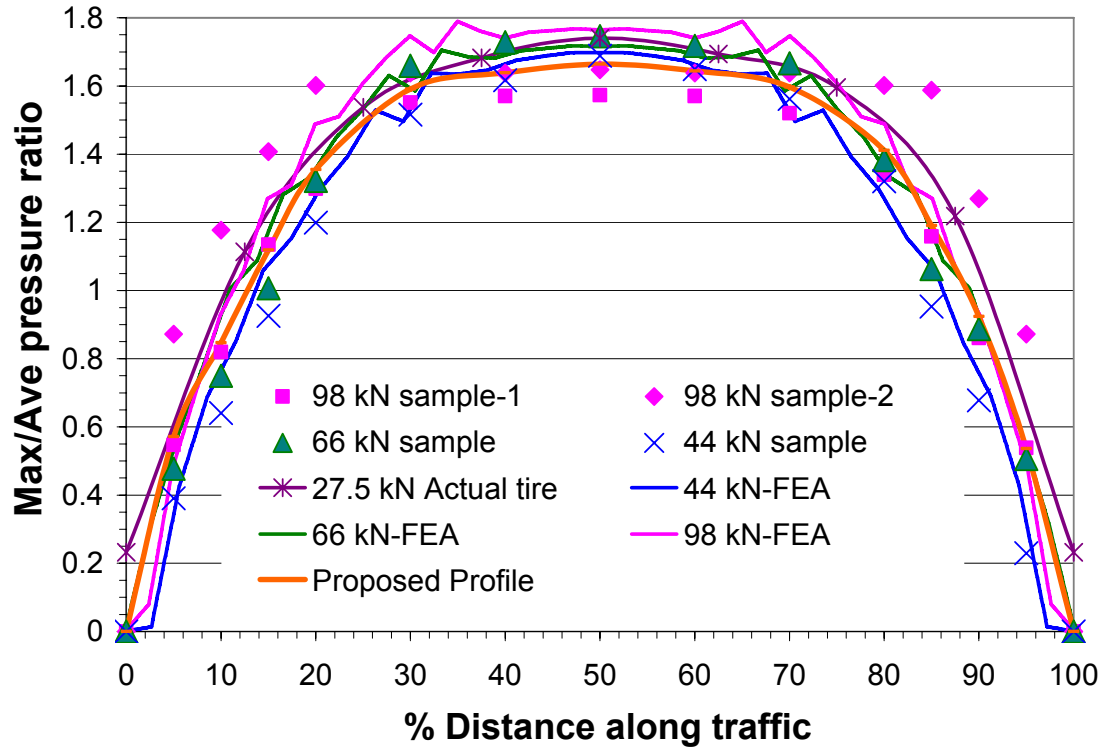
Figure 3.10 Normalized contact pressure distribution- Experiment vs. FEA

The maximum contact pressure in actual truck tire varies widely from 1.3 to 2.5 times the inflation pressure and with increasingly higher inflation pressure of modern truck tires, the peak stresses between 1.7 to 1.9 times the inflation is frequently reported in the literature (GangaRao and Vali 1990; Tielking and Abraham 1994; De Beer 1996; BLAB 1999). The maximum contact stress achieved using simulated tire patch also fits well within that range of peak stresses. The proposed STP pressure profile and contact area will be discussed in later sections.

3.3.2.2 Calculation of tire contact area

Tire contact area is defined as length of contact path along length of tire patch (rolling direction) multiplied by path distance in the tire patch width direction. Tire contact length was measured from tire footprint images obtained from sensor film analysis and also from 3D contact model using finite element method. Tire contact length is plotted as a function of applied load in Fig. 3.11 and the plot shows gradual increase in tire contact length with increase in applied load. Form experimental data it has been found that tire contact in the width direction is relatively constant up to ~133kN (30kips) and therefore, the tire contact width is considered to be equal to tire width.
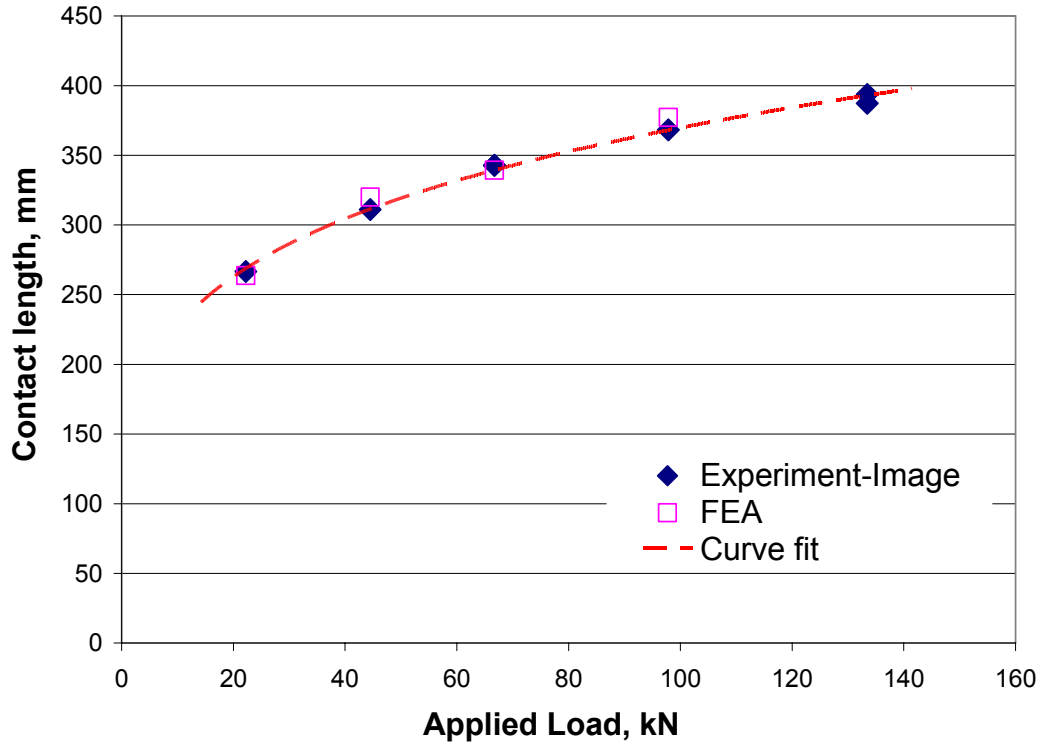
Figure 3.11 Contact length (traffic direction) as a function of applied load

3.3.3 Proposed Model for Tire Contact Area and Contact Pressure Profile

Based on tire contact data, a power law type curve fitting has been done to express tire contact length as a function of applied load. With constant width assumption, tire contact area is expressed as

$$Contact\ area, A = C * P^{0.212} * W$$

here, P = applied load on single tire and W = width of tire patch. If load is in kN (kips) and width in mm (inch), the constant C is equal to 139.2 (7.52). For applied load above 133 kN (30 kips), a 10% increase in width may be used as an approximation.

Average contact pressure can be easily calculated from applied load and contact area.

$$Average\ contact\ pressure, p_{ave} = 1000 * \left(\frac{P}{A} \right)$$

Normalized contact pressure profile from experimental data and finite element simulation were plotted in Fig. 3.10. A curve fit to those data can provide an expression of approximate

contact pressure profile for the proposed simulated tire patch. The contact pressure profile can be expressed by a polynomial approximation as follows:

$$p = p_0 + 0.1 \; x^6 - 0.14 \; x^5 - 1.46 \; x^4 + 0.11 \; x^3 - 0.29 \; x^2 + 0.02 \; x$$

Where, p_0 is the intensity factor defined as max pressure divided by average pressure and in this current study p_0 is equal to 1.66. The variable x is the normalized distance defined as path distance (length direction) divided by half of the total contact length and it varies from -1 to 1. The variation of contact pressure in the tire width direction is much less compared to rolling direction. Therefore, a conservative approximation would be to consider the above profile loading to be constant across the width during local loading analysis.

3.4   Proposed STP: Application to Cellular FRP Deck

3.4.1   STP as an Experimental Tool

The proposed simulated tire patch has been used in performance evaluation of FRP composite deck manufactured by Strongwell Corporation and this deck system was installed at Hawthorne Street Bridge, Covington, VA. Extensive lab testing of full scale bridge sections are conducted using the simulated tire patch (Majumdar 2007). From laboratory test results it has been observed that the response of the deck is substantially different under tire patch loading compared to the case when a conventional steel patch or bearing pad was used. Previous research at Virginia Tech has also reported punching shear failure mode while using steel patch (Temeles 2001; Coleman 2002). However, using the simulated tire patch, a transverse tension failure was observed at the top flange of the tube of the cellular deck (Majumdar 2007). This difference in failure mode can be attributed to the fact that the load transfer path with STP is completely different than rectangular steel patch loading. The simulated tire patch provides more localized effects on the deck. This difference in failure mode indicates completely different damage modes and areas on the deck that will affect long-term performance of the deck. A separate fatigue test with STP provided identical damage in the form of transverse tension crack (Fig. 3.12). Thus the proposed STP provides valuable information about possible damage areas and this knowledge can help efficient design.
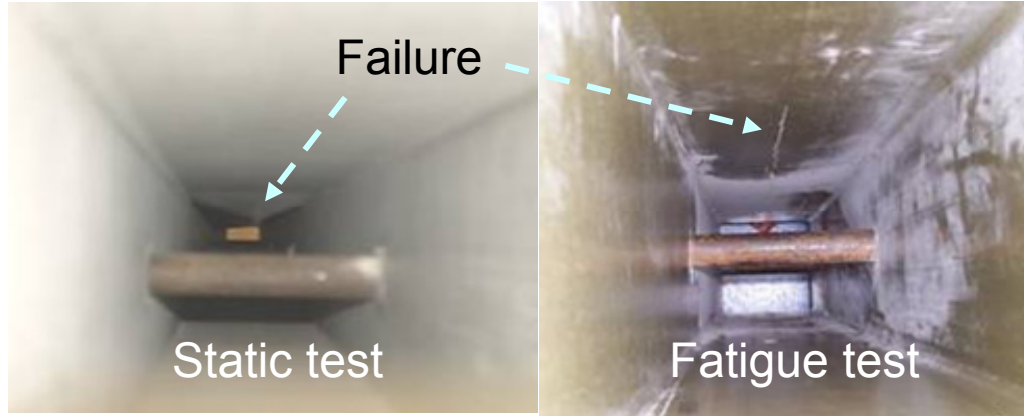
Figure 3.12 Failure mode at static and fatigue using STP

3.4.2 STP as Modeling and Analysis Tool
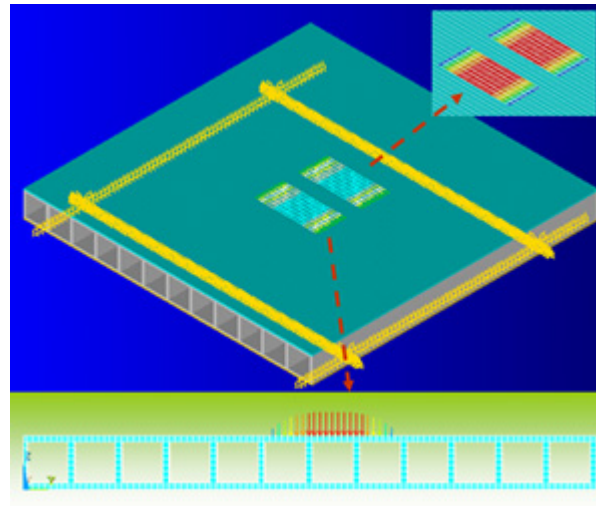
Figure 3.13 Proposed contact pressure profile applied to cellular FRP composite deck

In this current study, the proposed pressure profile has been used as input to finite element model of a 1.83m by 1.83m (6 ft by 6 ft) cellular FRP composite deck panel (Fig. 3.13). The deck is modeled using solid95 in ANSYS 11.0 and the conformable pressure profile applied though user defined programming feature using ANSYS Parametric Design Language (APDL). The response of the deck panel from finite element simulation is compared with experimental results obtained using proposed tire patch. It is observed from both experimental and FEA results that displacement at top flange and bottom of the deck were initially identical until 33.33 kN (7.5kips). However, as the load increases, the difference gradually increases and the displacement of the top flange is found to be 15-17% higher than displacement at the bottom of

31

the deck at 209 kN (47kips) load. Higher transverse strain and displacement at top flange again demonstrates local conformable deformation characteristics of the cellular FRP deck. This local effect can not be predicted by uniform patch loading.

3.4.3 Parametric Study on Behavior of Cellular FRP Deck

Parametric studies have been carried out to investigate the effect of cellular FRP deck geometry (plate thickness and web spacing) on displacement-strain behavior. For five cases, the same normalized displacement can be achieved at the bottom of the deck (BC in Fig. 3.14) by varying thickness and web spacing. However, the transverse strain at the top flange of the tube (TC in Fig. 3.14) can be very different for each of those cases (Fig. 3.14). From this parametric study it is observed that the concept of global deflection (displacement to span ratio) may be inadequate for design criteria of cellular FRP composite deck. This demonstrates that local effects should be considered during design of cellular FRP composite deck.
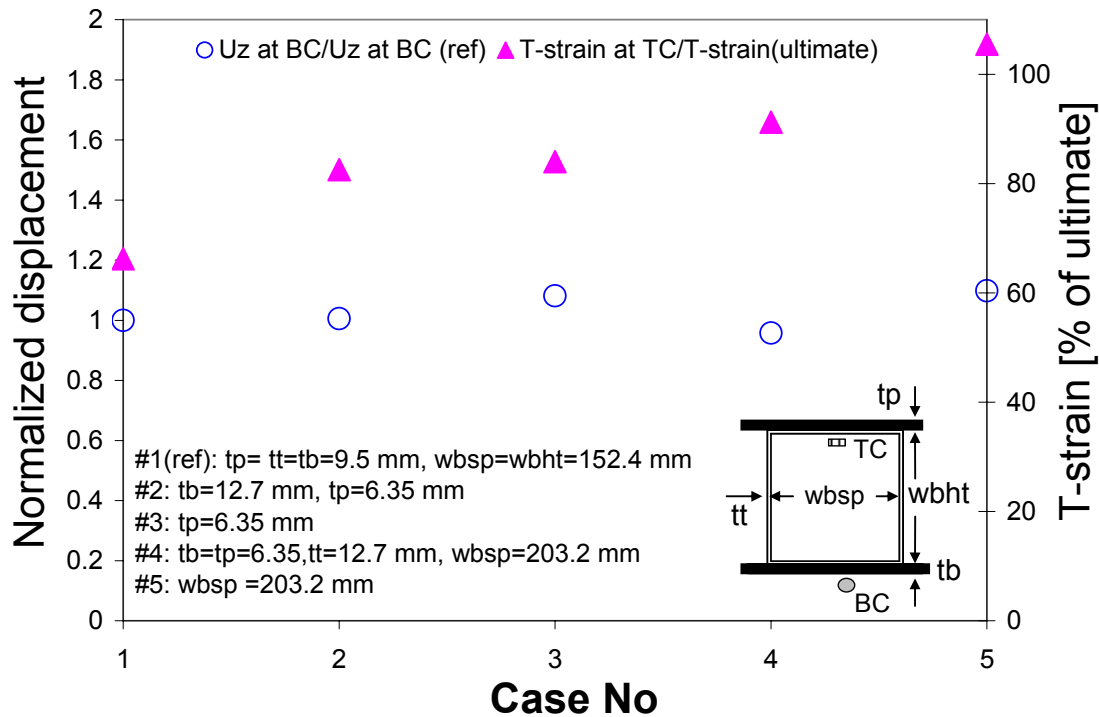
Figure 3.14 Effect of geometry on global displacement and local strain

32

3.5 Conclusion

The contact pressure distribution of real truck loading is non-uniform with more concentration near the center of the contact area, in direct contrast to the conventional steel patch loading that produces stress concentration near edges. Due to the localization of load under the tire, conventional uniform patch loading is not suitable for performance evaluation of FRP composite deck systems with cellular geometry and relatively low modulus as compare to concrete decks. A new simulated tire patch is proposed for loading on FRP deck and the load distribution are characterized by contact area studies using pressure sensitive sensors and 3D contact analysis using finite element method. The proposed profile can be a useful design tool for performance evaluation of cellular FRP deck.

The conformable pressure profile obtained from experimental observations is applied in FEA simulation of a cellular FRP deck.

- A simulated tire patch yielded larger local maximum deflection and strain than the rectangular uniform patch loading.

- The tire patch produced significantly different failure mode (local transverse failure under the tire patch) compared to the punching-shear mode using the rectangular steel plate. Such difference in damage mode and areas will contribute to long-term behavior of the FRP deck.

- Parametric studies show that design criteria based on global deck displacement is inadequate for cellular FRP deck and local deformation behavior needs to be considered.

In summary the authors conclude that due to the local effects of a real tire load and relative stiffness effect, a simulated tire loading patch would be more appropriate for performance testing of FRP deck accounting for the conformable contact between the tire and the FRP deck.

Chapter 4:   Implementation of Adhesive Joints in Bridge Decks

Part-I: Development and Evaluation of an Adhesively-bonded Panel-to-panel Joint for a FRP Bridge Deck System

Zihong Liu[5]; Prasun K. Majumdar[6]; Tommy Cousins[7]; and Jack Lesko[8]

Abstract

A fiber-reinforced polymer FRP composite cellular deck system was used to rehabilitate a historical cast iron thru-truss structure (Hawthorne St. Bridge in Covington, VA). The most important characteristic of this application is reduction in self-weight, which raises the live load carrying capacity of the bridge by replacing the existing concrete deck with a FRP deck. This bridge is designed to HL-93 load and has a 22.86 m clear span with a roadway width of 6.71 m. The panel-to-panel connections were accomplished using full width, adhesively   structural urethane adhesive   bonded tongue and groove splices with scarfed edges. To ensure proper construction, serviceability, and strength of the splice, a full-scale two-bay section of the bridge with three adhesively bonded panel-to-panel connections was constructed and tested in the Structures Laboratory at Virginia Tech. Test results showed that no crack initiated in the joints under service load and no significant change in stiffness or strength of the joint occurred after 3,000,000 cycles of fatigue loading. The proposed adhesive bonding technique was installed in the bridge in August 2006.

CE Database subject headings: Rehabilitation; Fiber reinforced polymers; Bridge decks; Fatigue; Joints; Bonding.

4.1 Introduction

The deteriorating state of transportation infrastructure system is a serious concern worldwide. In the United States, nearly 180,000 of the 600,000 bridges are either structurally deficient or functionally obsolete (FHWA/USDOT 2005). There is a growing interest in finding

---

[5] Graduate Research Assistant, Dept. of Civil and Environmental Engineering, Virginia Tech, Blacksburg, VA, 24061. Phone: (540)231-3974; Email: lzh@vt.edu.
[6] Graduate Research Assistant, Dept. of Engineering Science and Mechanics, Virginia Tech, Blacksburg, VA, 24061. Phone: (540)231-3139; Email: pkm2004@vt.edu.
[7] Professor, Dept. of Civil and Environmental Engineering, Virginia Tech, Blacksburg, VA, 24061. Phone: (540)231-6753; Email: tcousins@vt.edu.
[8] Professor, Dept. of Engineering Science and Mechanics, Virginia Tech, Blacksburg, VA 24061. Phone: (540)231-5259; Email: jlesko@vt.edu.

cost-effective and durable technologies for bridge repair, rehabilitation, and replacement. In recent years high-performance fiber reinforced polymer (FRP) composite materials have been identified as an excellent candidate for rehabilitating deteriorated bridges. One of the most promising applications for this high-performance material is bridge decking. Since 1996 approximately 83 vehicular bridges in the United States have been constructed or rehabilitated using FRP decks. Although many demonstration projects are based on new bridges, FRP decks hold greatest promise as a method of deck replacement on older structures (Moses 2006).

The minimum installation time, high strength-to-weight ratio, high fatigue resistance, and excellent corrosion resistance are desirable characteristics for bridge deck application. Their low self-weight (480-1440 N/m^2) compared to conventional concrete decks (about 5300 N/m^2) is particularly attractive for rehabilitating posted bridges because the live load-carrying capacity of existing bridges can be increased by replacing an existing concrete deck with an FRP deck.

Figure 4.1 The Hawthorne St. Bridge in Covington, VA

The Hawthorne St. Bridge in Covington, Virginia (Figure 4.1) is one of many candidates for rehabilitation or replacement in Virginia. The thru-truss bridge has a 22.86 m (75 ft.) clear span 5-bay Pratt-truss structure, with a roadway width of 6.71 m (22 ft.), running over three rail-lines. It also serves as the only lifeline to parts of downtown Covington during periods of high water, and thus must support emergency vehicles. The historical significance of its cast iron thru-truss has ruled out bridge replacement. Virginia Department of Transportation (VDOT) plans to rehabilitate the bridge superstructure with a new deck/stringer/floor-beam system and

keep the historical thru-truss. VDOT plans to replace the existing, deteriorating reinforced concrete deck with an FRP composite bridge deck system. The most important characteristic of the deck/beam/girder replacement is the reduction in self-weight of the bridge, which will increase the posting (current posted at a maximum load of 7 tons) to 20 tons and allow for use by emergency vehicles.

One critical challenge in this application is the development of the panel-to-panel connection, accomplished using a full length, adhesively bonded tongue and groove splice. The development and evolution of the panel-to-panel connection is briefly reported herein. Evaluation of the developed connection by testing on a full-scale two-bay section of the bridge is discussed in detail in this paper.

4.2 Development and Evolution of the Panel-To-Panel Connection at Virginia Tech

Generally, FRP decks are made as wide and as long as is practical to transport. Because of the size limitations, manufacturers typically provide FRP bridge decks in modular panel forms and almost all decks are joined in the field by panel-to-panel connections to create a seamless final installation.

Panel-to-panel connections are designed to efficiently transfer bending moments and shear forces between joined modular panels; to ensure deformation compatibility due to thermal effects; and to simplify on-site installation. Several techniques have been developed for panel-to-panel connections, including adhesively bonded splicing tongue-groove connection and shear key or clip-joint mechanical fixing connection (Zhou and Keller 2005).

Researchers at Virginia Polytechnic Institute and State University (Virginia Tech) began developing the Strongwell Tube-and-Plate deck system since 1997. Both field and laboratory tests showed that the strength capability of this deck system exceeded what was mandated by design codes (Hayes et al. 2000; Temeles 2001; Coleman 2002; Zhou et al. 2005). Recent research has focused on panel-to-panel connections to ensure their satisfactory performance in field applications. A four-stage research plan was conducted on panel-to-panel connections at Virginia Tech.

The research began with a project conducted by Christopher T. Link (Link 2003) and is referred to as Stage I. Two panel-to-panel connections were developed and tested, as shown in Figure 4.2. One was a bolted connection and the other was an adhesive shear-key joint. Results

showed that the bolted joint could carry the design load, but was susceptible to fatigue damage. The adhesive shear-key connection showed less capacity than bolted connection. However, it showed more promise than a bolted connection because of better fatigue performance and a linear behavior up to failure with a progressive, nearly "ductile" failure mode.

The findings from Stage I research showed that although mechanical connections have the advantage of easy disassembly for repair, adhesively-bonded connections are more efficient in load transfer and fatigue resistance and are easier and cheaper to construct, which was in agreement with published research (Zetterberg et al. 2001). Thus Stages II through IV research focused on developing and evaluating a redesigned adhesively-bonded tongue and groove joint.

Stage-I: Bolted and Adhesive bonded shear key connection

Stage II: Adhesively-bonded with I-connector

Butt joint

Scarfed joint

Scarfed with I-connector

Stage III: Adhesively bonded scarfed tongue and groove connection.

Stage IV: Adhesively bonded scarfed tongue and groove connection.
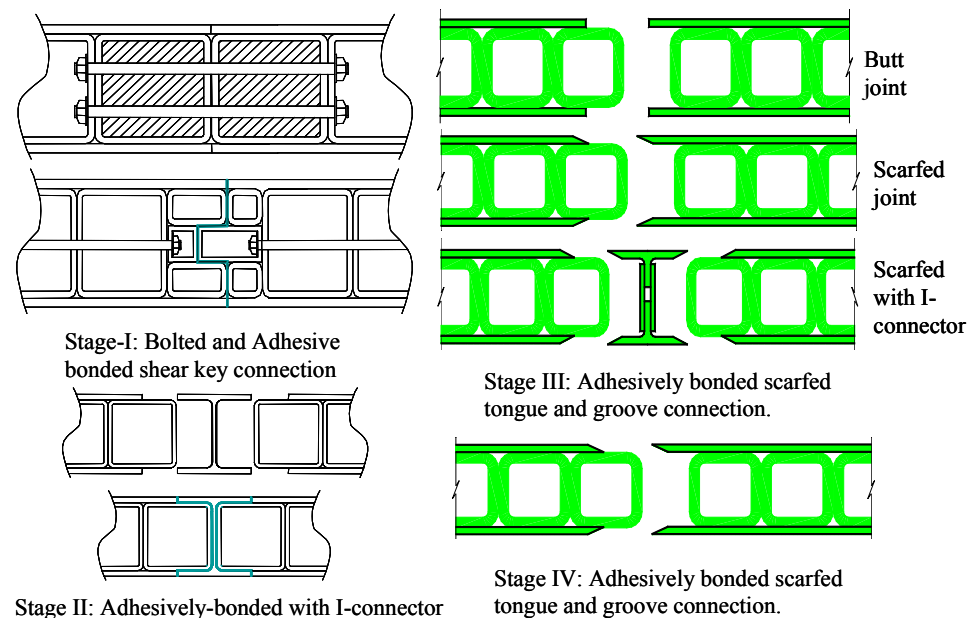
Figure 4.2 Evolution of panel-to-panel connections at Virginia Tech

In Stage II, a full-length, a simplified adhesively-bonded tongue and groove panel-to-panel connection was tested under a weak-direction (beam) bending configuration. The testing showed some promising aspects: linear behavior up to failure stage; crack initiation after design service load strain was reached; and a factor of safety of 2.4 with respect to the anticipated service strain. Testing results indicated the adhesive bonding was a viable technique in using with panel-to-panel joint for FRP decks. Stage III research was aimed to further optimize this design.

In Stage III, different connection geometries (scarfed vs. butt joint behavior) were investigated. The joining effectiveness of simple butt joint geometry was tested as shown in

Figure 4.2. Premature cracking was observed in the butt joint area. To eliminate this tendency the joints in Stage III panels were sloped or scarfed. Figure 4.3(a) shows the testing setup and the mimic part of the FRP deck system. Figure 4.3(b) shows that under a four-point bending configuration, FRP samples with a scarfed edge have better performance than those having a butt joint (90°). The critical load and displacement (at crack initiation) increased as scarf angle decreased. But for FRP deck panels, sharper scarf angles (smaller than 27°) are difficult to manufacture and can be easily damaged during transportation and installation. Therefore, scarf joints with an angle of 27° were used on the test specimens and recommended for future field application.
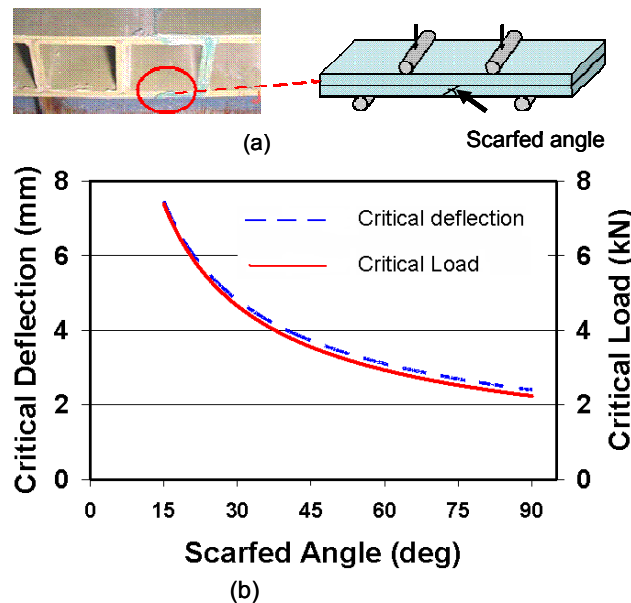
Figure 4.3 Critical load and displacement vs. scarf angle behavior for joint sample

Two types of adhesively-bonded panel-to-panel connections with scarfed joints were tested in Stage III: one single seam connection and one double seam connection, as shown in Figure 4.2(d). A plate bending setup with three sides simply supported and one side free (which approximates the support condition near an abutment) was used to better represent the on-site situation instead of one-way bending setup in Stage II.

Testing indicated that both types of connections exceeded service load without cracking. Crack initiation in all adhesive joints tested occurred at a load level at least 30% greater than the HL-93 design truck loads as specified in AASHTO LRFD Bridge Design Specifications (AASHTO-LRFD 1998). It corresponds to a service tire load of 71.2 kN (16 kips), with a dynamic load allowance of 33%, which yields a load of 94.8 kN (21.3 kips). The observed

failure occurred not in the adhesive joints, but was localized in the top plate and tube section at a very high load and strain level. Failure loads were at least two times the design service load. No significant advantage or difference in behavior was found using double seam connection (using I-connectors) compared to single seam connection for the deck joints tested. Since the double seam connection involves developing a new, special pultruded shape (I-connector), the single seam connection [Figure 4.2(e)] was used in the Stage IV study: a two-bay mock-up test of the Hawthorne St. Bridge.

Finally in Stage IV, a full-scale two-bay section of the bridge was constructed and tested in the Structures Laboratory at Virginia Tech. Static, fatigue, and failure tests were conducted on the adhesive panel-to-panel connections to evaluate their performances.

4.2.1   Objective of Testing Program

In order to evaluate the structural behavior and constructability of the proposed panel-to-panel connection, a 10.06 m by 6.71 m. (33 ft. by 22 ft.) FRP deck supported by a two-span mock-up of the Hawthorne St. Bridge superstructure was built in the Structures and Materials Laboratory at Virginia Tech. The mock-up was built and tested to address the following concerns: (a) constructability of the system; (b) global and local behavior of the structure; and (c) performance of the panel-to-panel connections and deck-to-stringer connections.

This paper investigated the constructability and performance of an adhesively-bonded, panel-to-panel connection. The objectives of this study are four-fold: (1) investigate connection behavior under simulated pseudo-static service load; (2) examine flexural strength and failure mode of connections and deck; (3) explore fatigue behavior during simulated cyclic wheel loading and residual strength after fatigue loading; and (4) develop installation protocol of panel-to-panel connection in Hawthorne St. Bridge.

4.2.2   FRP Bridge Deck System

The FRP Deck System developed for the Hawthorne St. Bridge was based on previous research projects conducted at Virginia Tech, and was fabricated from standard EXTREN® structural shapes and plate manufactured by Strongwell Corp. of Bristol, VA. These components are made of E-glass roving and continuous strand mat embedded in polyester resin. Figure 4.4 shows the typical cross section of a deck panel. The significant components include: 152.4 mm. x 152.4 mm. x 9.5 mm. (6 in. x 6 in. x 3/8 in.) pultruded EXTREN® tubes, 9.5 mm. (3/8 in.)

pultruded Extern top and bottom plates as well as 25.4 mm. (1 in.) diameter steel thru-rods. The tubes, top and bottom plate are adhesively bonded to form FRP bridge deck panels. The steel thru-rods are used to provide necessary binding forces when the deck panels are in curing. Bonding is accomplished in a vacuum bag to produce uniform pressure and continuous bonding.
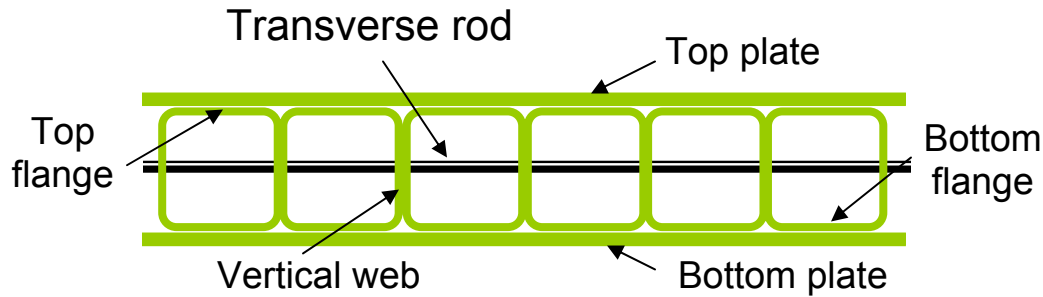
Figure 4.4 Cross section of the Strongwell FRP Deck System

The material properties of Strongwell's deck components are listed in Table 4.1 (tube and plates). The given material properties are taking from Extren Design Manual (Strongwell Inc. 2002), which are minimum ultimate coupon properties.

Table 4.1 Material Properties of Strongwell's Deck Components

Mechanical Properties	Top/Bottom Plate	Tube
Ultimate flexural stress, LW[1] (Mpa)	207	207
Ultimate flexural stress, CW[2] (Mpa)	124	69
Flexural modulus of elasticity, LW[1] (Gpa)	13.8	11
Flexural modulus of elasticity, CW[2] (Gpa)	9.7	5.5
Estimated ultimate strain[3], LW[1] ($\mu\varepsilon$)	15000	18800
Estimated ultimate strain[3], CW[2] ($\mu\varepsilon$)	12800	12500

[1: LW – lengthwise (longitudinal); 2 CW – crosswise (transverse); 3: Ultimate strain approximated by dividing ultimate stress by elastic moduli]

Figure 4.5 shows a plan view of deck panels, panel-to-panel connections, and supporting steel superstructure. The FRP deck specimen consisted of five individual modular deck panels that were jointed together using three adhesive panel-to-panel connections (Seam #1 through #3) and one dowel joint. The dowel joint was developed as an expansion joint for future applications, and will not be discussed here. Each individual panel was 6.71m. by 2.29 m. (22 by 7.5 ft.), with the exception of the two end panels which measured 6.71m. by 1.68 m.(22 by 5.5 ft.), and 6.71m. by 1.52 m.(22 by 5 ft.). These individual panels were connected to form a full width 6.71 m. (22 ft.) panel that was about 10.058 m. (33-ft.) long in the direction of traffic.
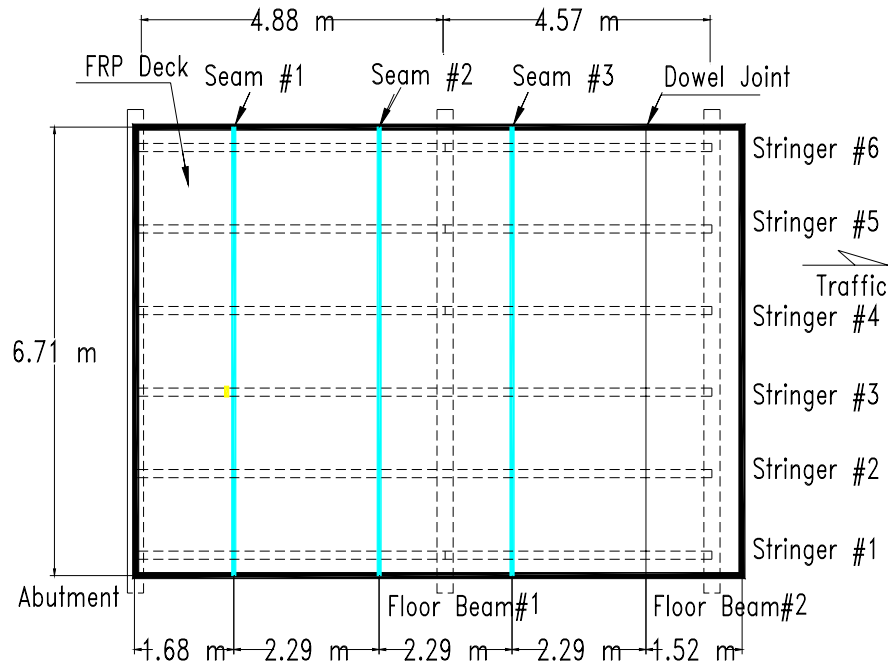
Figure 4.5 FRP deck panels and joints of the Hawthorne St. Bridge mock-up

The FRP deck specimen was connected to stringers by deck-to-stringer connections; these connections were not intended to develop composite action. Neoprene rubber pads (6.4 mm thickness) were used to cover all contact areas between the deck panels and the steel superstructures.

4.3   Construction of Adhesively-bonded Panel-to-Panel Connections

The accuracy of panel dimensions of the mating parts has a significant impact on the ease of installation and quality of the adhesive panel-to-panel connections. Therefore, the first step was to dry-fit every panel-to-panel connection to ensure the best fit. Specifically, the scarfed edges should match and side walls of the tube bonding surface should match as well [Figure 4.6(a)]. The gap distance between two bonding surfaces should be controlled to less than 3 mm. any circumstance.

During dry-fitting of three panel-to-panel connections, it was found that the sweep of the tubes was not well controlled during pultrusion. Figure 4.6(b) shows the curved panels resulting from the use of curved tubes. Each panel had a pre-existent sweep with a midway deflection about 12.7 mm. (0.5 in.) [Figure 4.6(c)]. The worst case was Seam #1 with two opposite curvatures at the side walls of the tube bonding surface. Although Seam #2 and #3 also had similar curvatures, however mating tubes were bent in the same direction. The deck panels

were autopsied after testing was completed to further investigate the bonding quality. Figure 4.6(d) shows that the gap distance between two bonding tube surfaces of Seam #1 was about 25.4 mm. (1 in.). The gap distances of Seam #2 and #3 were less than 3 mm. and all scarfed edges matched well. Figure 4.6(e) shows the bonding quality of Seam #2.
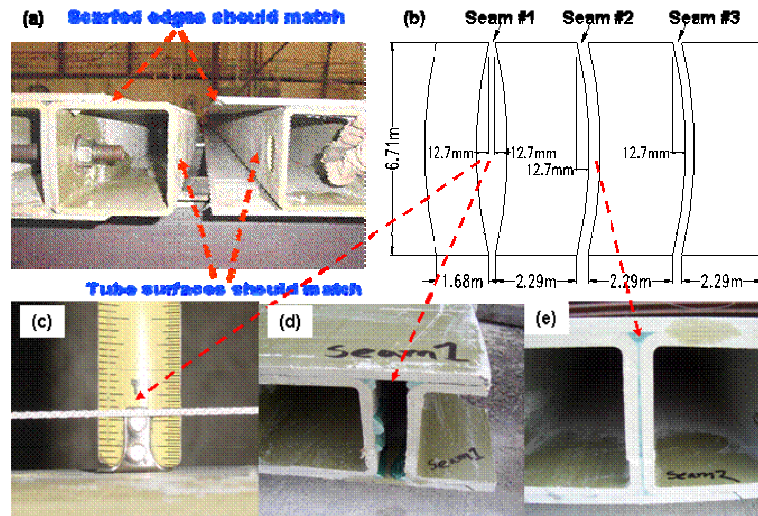
Figure 4.6 Fitting of the adhesively-bonded panel-to-panel connection

Quality control procedures should be adopted to prevent such out-of-straightness of panels in future application. The manufacture quickly improved the panel quality by using more precise cutting machine and stricter quality control procedures during pultrusion and bonding of tubes. The quality of the panels used in the actual bridge was much improved. The gap distance reported above for Seam #2 and Seam #3 were typical of what was seen in the field.

The fabrication protocol developed for construction of the adhesively-bonded panel-to-panel connections included:

(1) Sanding the bonding surfaces to remove the non-stick film remaining from pultrusion. This typically involved removing about 2 mm. from the top surface so that traces of fibers could be visible; then the surface looked dull instead of a polished greenish color.

(2) Bolting down the deck panel with the grooved end (the right side of the connection in Figure 4.6(a)) to the stringers with deck-to-stringer connectors.

(3) Flushing of all the bonding surfaces with acetone to remove any loose dirt that could hinder the bonding quality. Note that the surface must be allowed to dry before adhesive application.

42

(4) Trial application of adhesive on flat surface to make sure the correct mixing proportions of the adhesive.

(5) Appling structural urethane adhesive on the bonding surfaces with a special pneumatic gun from a bulk dispensing unit, shown in Figure 4.7(a). The adhesive layout pattern will be discussed later in this section.

(6) Aligning the tongue-end panel (the left side of the connection in Figure 4.6(a)) so that the tongue fits in the groove.

(7) Joining deck panels by equal jacking pressure from six hydraulic jacks with a manifold system, shown in Figure 4.7(b). Enough pressure must be applied to close the joint and ensure that adequate adhesive squeezes out.

(8) Maintaining the jack pressure for about 12 hours, until the adhesive cured.

(9) Bolting down the deck panel to the stringers with deck-to-stringer connectors.

(10) Going through steps (3) through (9) for another adhesive connection.
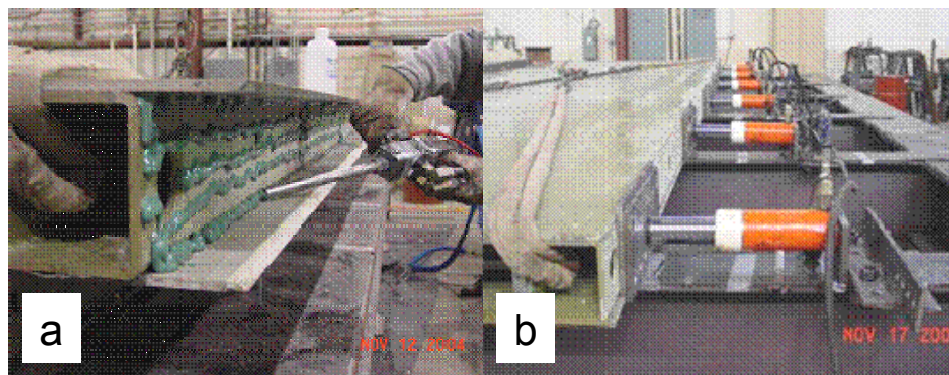
Figure 4.7 Panel-to-panel connection (a) Adhesive application b) Jacking system

The performance of adhesive bonding is not only dependent on the matching condition of mating parts, surface preparation, and joint geometry as discussed above, but also the amount of adhesive applied. Adequate adhesive squeezing out is a sign that plenty of adhesive was applied and is recommended as the quality control check-point in field construction. Increasing amount of adhesive was applied to three seams during construction from Seam #1 to Seam #3 in order to compare performances of seams with different amount of adhesive. Seam #3 was thought to be the best joint with the best fit and plenty of adhesive squeezing out. Figure 4.8 shows Seam #3 after adhesive was applied and plenty of adhesive squeezed out from the top, side and bottom of the joint. Although Seams #1 and #2 performed well during static tests

43

(discussed in a later section), the amount of adhesive used for Seam #3 was selected as enough to ensure adequate strength and life of the panel-to-panel connection.
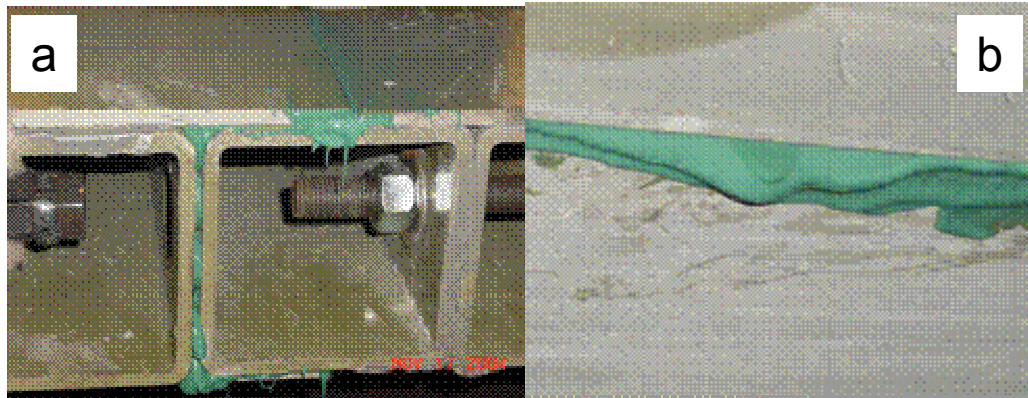
Figure 4.8 Adhesive squeezing out from joints (a) Side view (b) Bottom view

The Pliogrip 8000/6660 two-component, structural urethane adhesive system from Ashland Chemicals Inc. was used in this application for its superior adhesion property, UV resistance and proper glass transition temperature. Figure 4.9 shows how the adhesive beads were applied on the tongue and groove parts. Each bead had a width of about 10-15 mm. and a thickness of about 6-12 mm. One bead of adhesive applied on each scarfed edges. The amount of adhesive applied per connection is about 14.2 Liters of Pliogrip 8000 and 6.3 Liters of Pliogrip 6660.
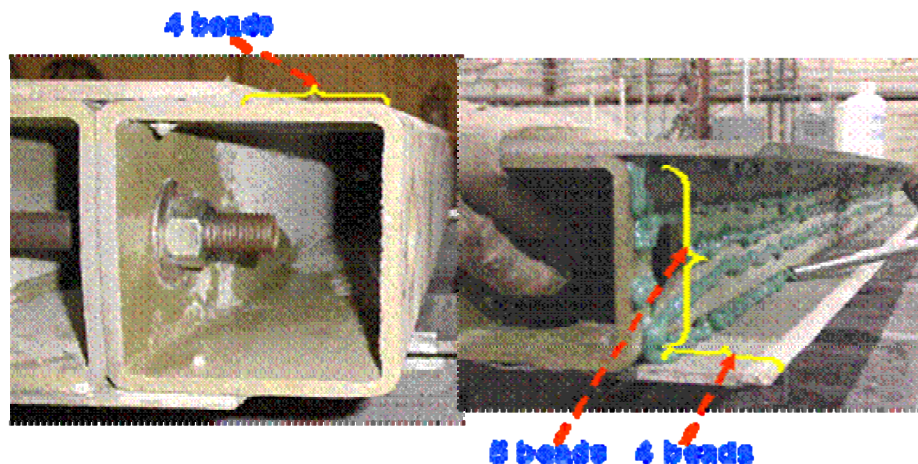
Figure 4.9 Adhesive laid out pattern (a)Adhesive on tongue part (b) Adhesive on groove part

The available working time for the adhesive is 45 minutes at 73°F and 35 minutes at 99°F (Ashland Pliogrip 8000/6660 Urethane Adhesive System Work Sheet). Application of adhesive and joining of deck panels took approximately 25 minutes and was performed at an

ambient temperature of 75°F. This yielded a safety factor before adhesive set of about 2 and was deemed acceptable for this application.

4.4   Test Setup and Instrumentation

4.4.1   Test Setup

The steel frame mock-up of the Hawthorne St. Bridge superstructure consisted of two bays, which were 4.877 m. (16 ft.) and 4.572 m. (15 ft.) in length in the direction of traffic. Figure 4.10 shows a framing plan of the steel superstructure. Each bay had six wide-flange W14x34 stringers, having a transverse spacing of 1219 mm (4 ft) on-center. Diaphragm members, consisting of C10x15.3 steel sections, were bolted to connector plates, which were in turn welded to the stringers. Two W14x120 floor beams were supported by four pedestals that simulated the hangers in the through-truss bridge. All steel member sizes and dimensions mimic the actual ones in the Hawthorne St. Bridge superstructure. Neoprene pads were used between floor beams and pedestals to avoid direct contact of steel and to allow some movement at floor beam ends. Stringers and floor beams were jointed together using moment resisting connections. A W21x132 beam was used to simulate the concrete abutment in situ, and five end diaphragms (C10x30) were flush with the top stringer to avoid free edge effect of the FRP deck. All Stringers at the abutment rested on the bearings anchored on the abutment.

Figure 4.10 Steel superstructure of the Hawthorne St. Bridge mock-up

Although the rehabilitated bridge will be still posted to 20 tons, a higher load level (HL-93 design truck loads as specified in AASHTO LRFD Bridge Design Specifications) was used for evaluating the performance of the adhesive panel-to-panel connections. The purpose was to gain some insight into the applicability of this deck system to the typical highway bridge deck which is designed for the HL-93 design truck. This is a service tire load of 71.2 kN (16 kips) with a dynamic load allowance of 33%, which yields a load of 94.8 kN (21.3 kips). Therefore, a load limit of 97.9 kN (22 kips) was chosen because it was slightly higher than the required 94.8 kN (21.3 kips).

Figure 4.11 Load Cases for service load test

Figure 4.11 shows five Load Cases used for service load tests. All Load Cases followed HL-93 truck weights and dimensions to apply the worst-case load scenario to the FRP deck and superstructure. Load Cases 1–4 were single truck cases. Load Cases 1, 2 and 4 were the critical cases for flexure of an FRP deck transverse to the traffic, with a wheel located at mid-span between two stringers. Load Case 3 represented a truck straddling on Stringer 3. Load Case 5 is the symmetric case, with double trucks representing the full lane Load Case.

The double truck service load test (case 5) was simulated by two single-truck setups, as shown in Figure 4.12. A special loading patch which consisted of a quarter tire internally reinforced with silicone rubber was used to mimic the cushioning effect of a pneumatic tire. This was done to minimize the local stress concentrations of a standard rectangular steel patch because of the relative local flexibility of the FRP composite cellular decks, as compared to the steel plate (Zhou et al. 2005).
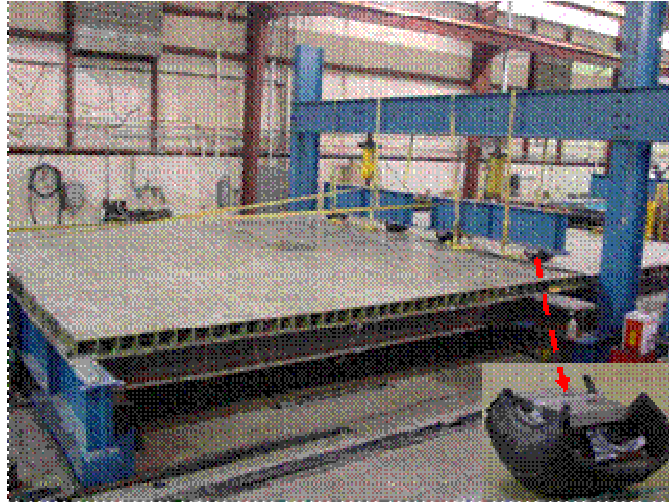
Figure 4.12 Experimental Setup for service load test (Load Case 5) on Seam #3

In strength tests, the same hydraulic actuator and tire patch pair was used to apply load to the deck directly between two adjacent stringers, to simulate one wheel load. A number of steel plates were inserted in between the loading ram and the tire patches to ensure a nearly uniform distribution of load from the actuator to the two tire patches. For fatigue tests, load was applied using a servo-controlled hydraulic actuator mounted on the same load frame. Because of concern about stability of the actuator and load patch assembly, a neoprene rubber patch was used instead of tire patch to transfer load from the actuator to the top surface of the deck on top of the adhesive joint. The neoprene rubber pad can also prevent the steel plate connected to the actuator from locally damaging the deck and joint during testing. The base neoprene rubber pad was 457 mm. (18 in.) by 229 mm. (9 in.) and. The base neoprene rubber pad is a little smaller than the "tire contact area" of 510 mm by 250 mm defined in AASHTO LRFD Specifications (AASHTO 2004).

4.4.2   Instrumentation

Figure 4.13 shows a schematic of the instrumentation plan used to investigate the performance of adhesively-bonded joints. The stringers and floor-beams are referred to as "Stringer #1" through "Stringer #6" and "Floor Beam #1" and "Floor Beam #2." For consistency throughout the discussion, all references to "longitudinal" and "transverse" are given with respect to the bridge deck orientation; thus, "longitudinal" implies parallel to the pultruded tube direction of the FRP deck system, and the "transverse" direction refers to the traffic flow direction (perpendicular to the tube axis).
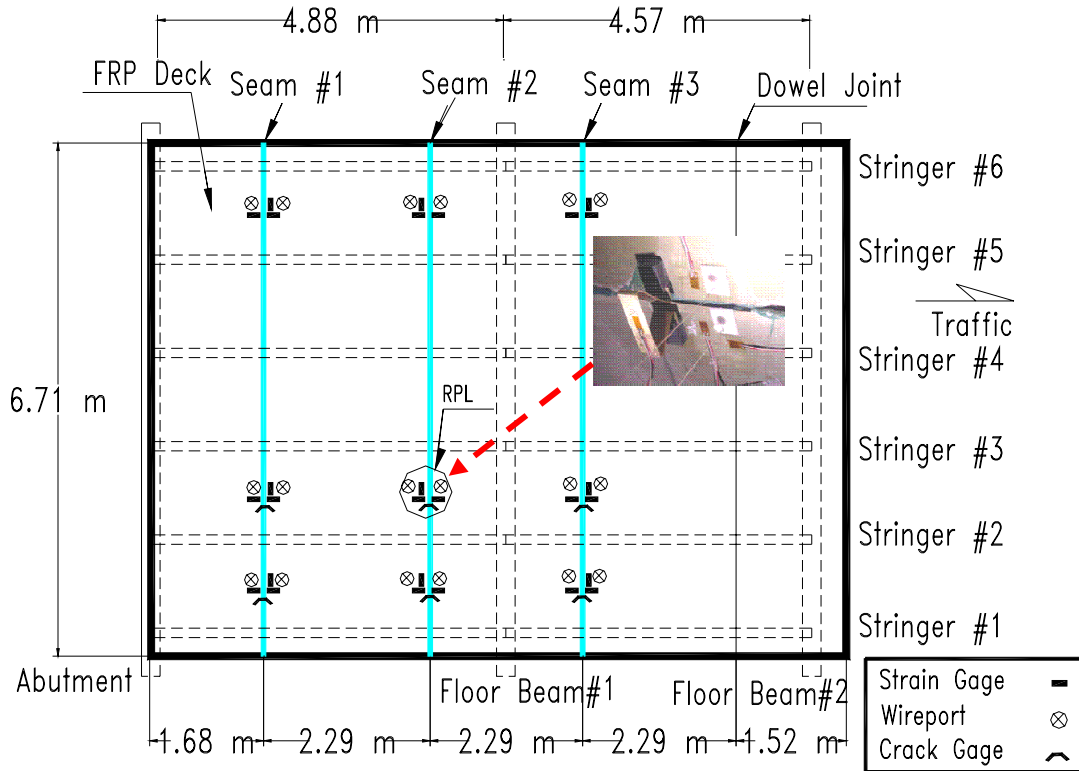
Figure 4.13 Instrumentations for three adhesive joints (underneath the deck)

As shown in Figure 4.13, at the bottom surface of the deck, two strain gauges and two wire pots (displacement transducers) were used to measure transverse strains and displacements, respectively, at both sides of the joint. Another strain gauge was placed to measure longitudinal strain at the side of the adhesive joint adjacent to the load. A specially-designed crack detection gauge was installed across each joint to monitor crack opening, if any. This instrumentation pattern was repeated for each loading location while testing near a joint. Load, deflection, and strain were continuously recorded during testing using a high-speed data acquisition system.

4.5 Experimental Procedure and Results

4.5.1 Service Load Test

The purpose of these tests was to observe the behavior and assess the serviceability and performance of the adhesively-bonded, panel-to-panel joint up to a wheel load of 97.9 kN (22 kips) (a 195.7 kN axle load).

Figure 4.14 shows representative span deflection and crack gauge responses at one location, location RPL [Shown in Figure 4.13] under Load Case 4. The load vs. strain and load

vs. deflection behaviors were observed to be fairly linear elastic up to the design service load. The absolute deflection at the mid-span of the deck was 8.5 mm, as shown in Figure 14(a), and the relative deflection at this point with respect to supporting stringers was 1.9 mm. at the design service load, which indicated an L/649 response.
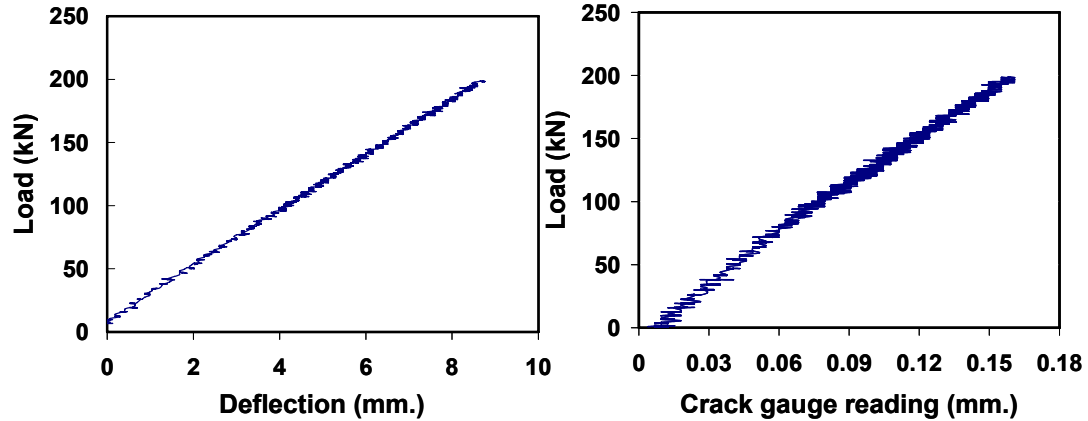
Figure 4.14 Span deflection and crack gage reading in service load tests

At location RPL under Load Case 4, the longitudinal strain on the bottom plate right under the load patch was 1090 με, which is only 6% of the estimated ultimate strain of the bottom plate. Transverse strain at one side of the seam close to the loading patch was 492 με at the design service load, which was about 45% of the longitudinal strain at this load. However, transverse strain at the other side of the seam was -290 με at the design service load, which was in compression; this indicated that this region experienced double curvature due to an applied load at one side of the seam. Figure 4.14(b) shows the linear response of crack gauge, indicating that no crack was initiated up to design service load.

For all loading cases, deflection and longitudinal strain were reasonably consistent. This consistency of measured responses from both continuous deck sections and adhesive joints indicated effective performance of the adhesively-bonded, panel-to-panel connections. However, transverse strains were found to be very sensitive to the exact location of both the gauge and the applied loads, and more difficult to interpret. This agreed with published findings (Turner 2004; Coogler K 2005). Due to their variability, such measurements are less suitable for performance assessment and will not be used in strength and fatigue performance evaluation.

All the adhesive connections were able to resist the service tire patch load without any indication of cracking. Table 4.2 summarizes data of service load tests performed on Seams #1 to #3. In each of these tests, Load Cases 1, 4 and 5 were followed.

Table 4.2 Data from Service Load Tests

	Load case	Maximum longitudinal strain ($\mu\varepsilon$)	Mid-span relative deflection, (mm)	Deflection index (span length / relative deflection)
Seam #1	1	839	2.1	596
	4	549	2.3	537
	5	852	1.6	785
Seam #2	1	804	1.7	714
	4	1085	1.9	649
	5	802	1.8	679
Seam #3	1	680	2.1	583
	4	535	1.6	770
	5	688	1.8	663
Average		759	1.9	664

4.5.2 Strength Test

Two strength tests were conducted at mid-span between Stringers #4 and #5 on Seams #2 and #3. These tests were designed to evaluate the safety factors of the adhesive joints and investigate the failure mode.

The strength test included several static load cycles of increasing intensity. Load was increased at 111.2 kN (25 kips) increments until failure was detected. The results from the last one of these cycles in the strength test at mid-spans between Stringers #4 and #5 on Seam #2 will be discussed below.

In order of progression, the load cycle up to 333.6 kN (75 kips) preceded the load cycle up to 444.8 kN (100 kips). For the cycle up to 444.8 kN (100 kips), both the deflection and strain data indicate fairly linear and consistent response. The local deformation on top of the deck near the tire patch could be easily perceived by visual inspection because of high compressive strain levels in the contact area. Slight cracking noises were first heard at about 413.7 kN (93 kips); small strain and deflection drops could also be observed at this load, which will be referred to as the "crack initiation" load. Then the deck was continuously loaded up to 427.0 kN (96 kips),

with increasing cracking sounds. Because visible cracks on the top plate of the deck could be easily observed at the load of 427.0 kN (96 kips), the deck was unloaded and two rubber patches were removed to inspect the failure mode. No further cycles were performed because of significant failure in the top plate and the tops of the tubes.

Strength tests were also conducted on as-received deck at a location 510 mm away from Floor Beam #2. This will also create a benchmark for evaluating the strength and failure mode at adhesively-bonded panel-to-panel connections. All testing data from strength tests are included in Table 3 for comparison. Test results show that average first failure load for two joints was 444.8 kN (100 kips), which is close to the first failure load (lowest of all strength test on virgin deck) found in strength test of as-received deck (418.1 kN). This indicates the adhesive joint did not influence the strength of the deck.

Table 4.3 Strength test data

Location		Load at initiation of crack (kN)	Mid-span relative deflection (mm)	Safety Factor
Mid-span between Stringer #4 and #5	Seam #2	413.7	11.2	4.4
	Seam #3	476.0	11.6	5.0
Mid-span between Stringer #1 and #2	As received deck	418.1	12.1	4.4
Residual strength after fatigue	Seam #3	418.1	10.2	4.4

4.5.3   Fatigue Performance and Residual Strength

At mid-span between Stringers #1 and #2 on Seam #3, the deck was subjected to fatigue loading for 3,000,000 cycles, then tested to failure under a static loading. It should be note that the number of cycles (3 million) is not indicative of the service life of the Hawthorne Street Bridge. This bridge will be still posted to 20 tons after rehabilitation, therefore, no heavy vehicles such as HS-93 design trucks will across the bridge during the bridge's service life.

The fatigue test was conducted in load control at a minimum/maximum load ratio of R=10, with a maximum load of 97.9 kN (22 kips) and a minimum load of 8.9 kN (2.2 kips). The deck cycled through a maximum deflection range of about 4.8 mm. (0.19 in.) at the load point and through a maximum bottom plate longitudinal strain (along the tube direction) of about 600 $\mu\varepsilon$ underneath the loading patch. The fatigue cycles were interrupted periodically for static service load tests, and the deck panel was inspected for signs of deterioration at this time as well.
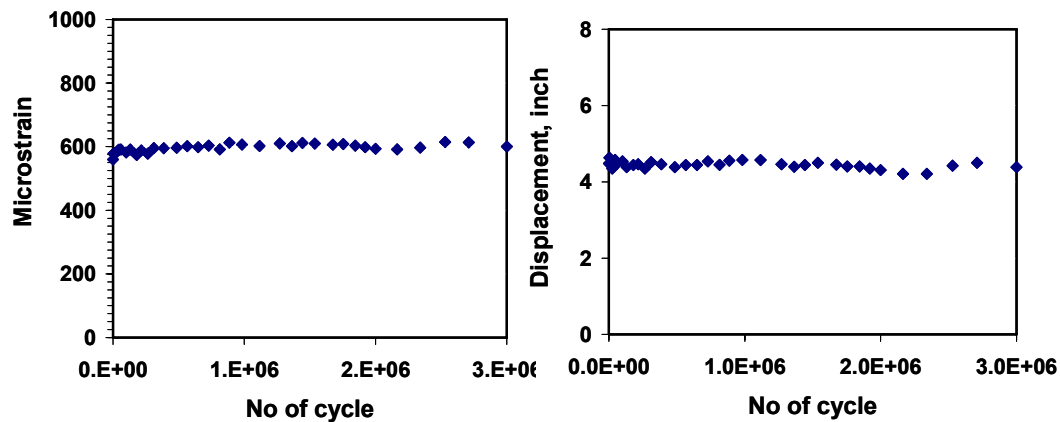
Figure 4.15 Maximum strain and deflection at service load after interrupted fatigue loading

The maximum deflection and strain measurements at the service load (97.9 kN) taken during each static test can be seen in Figure 4.15. The deflection and strain responses remained fairly constant for all of the static service load tests, and the deck demonstrated no apparent loss in stiffness near the adhesive joint. The crack gauge measurements taken during the static test after 3,000,000 cycles show linearly response indicating no crack was initiated after 3,000,000 cycles. Similar deflection measurements at two sides of the adhesive joints during the static test after 3,000,000 cycles also demonstrated that no crack was initiated inside the joint.

Inspection of the deck at the time of each static service load test also revealed no visible signs of damage to the plate or adhesive bonding due to fatigue loading. In addition, a careful inspection the area of deck-to-stringer connections near loading patch was conducted after 3,000,000 cycles, and no damage to the deck panel and no slack in the connection were observed.

The fatigue test was followed by a residual strength test at the same location. Figure 4.17(a) shows the load versus deflection plot and Figure 4.17(b) shows the load versus crack gauge plot. Both responses showed fairly linear-elastic behavior up to the crack initiation of the adhesive joint after 3,000,000 fatigue cycles. The first failure (crack initiation in the joint)

occurred at 419.9 kN (94.4 kips). At the crack initiation point, both plots showed a significant drop due to stiffness loss caused by cracking in the adhesive joint. Figure 4.17(b) also shows a clear crack propagation stage after crack initiation.
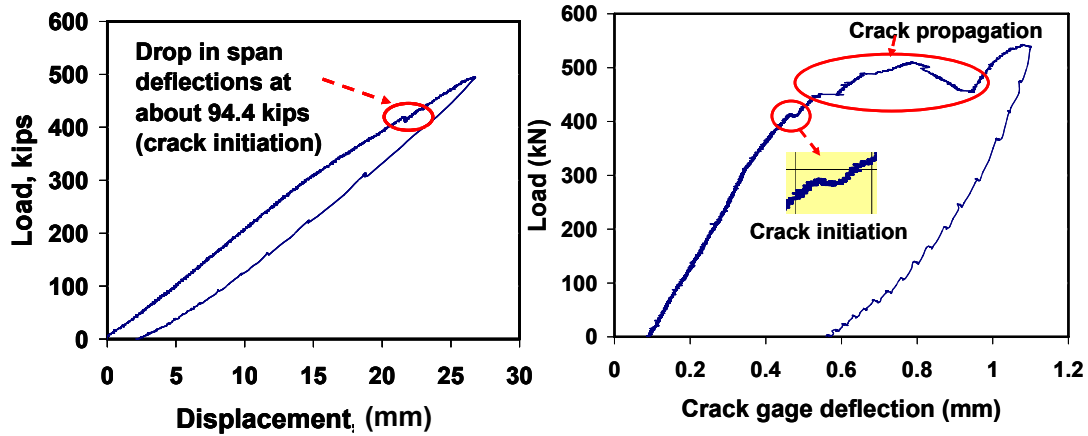
Figure 4.16 Crack gauge and deck deflection results in residual strength test after 3,000,000

The strength test data shown in Table 2 indicate no significant loss in strength after fatigue loading. The residual strength mode of failure observed on the fatigued seam is typical of those observed in the two strength tests discussed above. This observation, when combined with the observed retention of stiffness after fatigue loading, demonstrates the good durability of the adhesive joint under repetitive loadings.

4.6 Failure Mode of Deck Panel loaded on Adhesive Joint

The failure mode observed on the seam that was fatigued to 3,000,000 cycles and then tested to failure is very consistent with that observed on two adhesive seams tested to failure without being fatigued. For all seams in the ultimate test, the failure areas were highly localized and right under the tire patches, as seen in Figure 4.18(a). Failure mode was flexural failure of the top plate and top flange of the tube. Three cracks could be seen [Figure 4.18(b)]. Two cracks developed along two webs of the tube under the loading tire patch, and one crack was at about the center of the 152.4 mm. (6 in.) span between two webs of the tube. Figure 4.18(c) shows a side view of the top surface flexural failure; no crack was observed on the tube webs. Also, no visible crack was observed at the bottom side of the deck near the adhesive joint after the top surface failed. From these results, it was concluded that the top plate and the top flange of the tube failed in weak-axis bending, with cracking parallel to the tube webs.

54
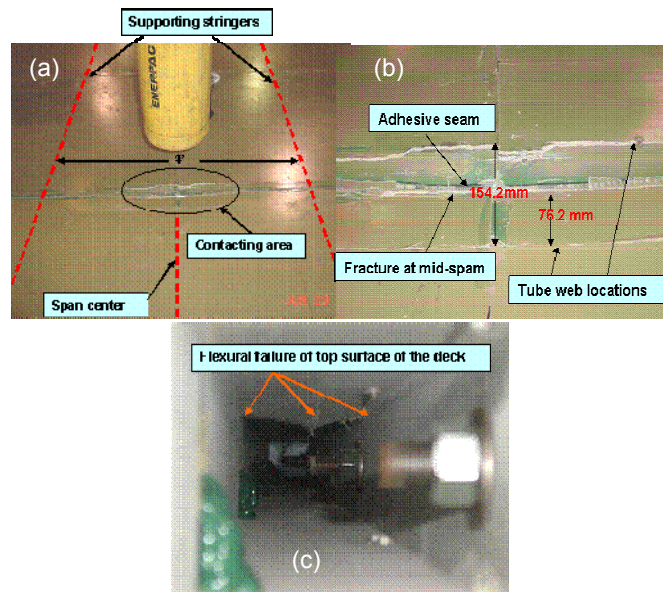
Figure 4.17 Failure mode (a) localized failure (b) Failure detail on top surface (c) failure inside tube

Another important observation from Figure 4.18(b) is that although the fracture at mid-span of two webs of the tube was near the adhesively-bonded line, no failure was observed in the adhesive layer or in the joint interface. This suggests the adhesive layer and adhesive-substrate interface are stronger than the FRP components and that adhesive bonding is a viable technique for the panel-to-panel connections in FRP bridge deck system.

The tests demonstrated localized ductile failure rather than a total collapse, which provide plenty of time for evacuation and maybe considered as another advantage of this FRP deck system.

4.7 Bridge Installation

The FRP bridge deck was installed at the Hawthorne St. Bridge on August 29th, 2006. Figure 4.19 shows the adhesive bonding process of the panel-to-panel connections during deck installation. The accuracy of panel dimensions of the mating parts was well controlled and installation protocols were strictly followed during the field installation. The bridge is scheduled for a controlled live load test and the response of the adhesively bonded panel-to-panel connection will be monitored.

Figure 4.18 Field installation of the FRP bridge deck (a) Dry fit (b) Adhesive application (c) Seam curing (d) Jacking system

4.8 Conclusion

The following conclusions can be drawn from the static and fatigue tests conducted on the adhesively-bonded, panel-to-panel connections of an FRP bridge deck system.

1. The proposed full-length, adhesively-bonded tongue and groove panel-to-panel joints can meet the necessary strength performance criteria. No failure was observed in the adhesive layer or in the joint interface, which indicates the adhesive layer and adhesive-substrate interface are stronger than the FRP components. Thus adhesive bonding will not control the design strength of this FRP deck system.

2. The average first failure load was 444.8 kN (100 kips) in the strength tests on the adhesive joints, about five times the design service load of 97.9 kN (22 kips). This value is close to the first failure load found in strength tests of as-received decks. This indicates the adhesive joint will not influence the strength of the deck.

3. The failure in the top plate and the top flange of the tube was characterized by weak-axis bending, with cracking parallel to the tube webs. This is also consistent with the failure mode in strength tests of as-received decks.

4. The strain and displacement showed linear elastic behavior up to design service load. The test results revealed an average deflection of span/664, which is slightly larger than the span/800 criteria in the AASHTO LRFD Bridge Design Specifications (AASHTO 2004). It should be noted that this limit is not intended for application to FRP composite bridge decks. However, no appropriate design limit is presently available.

5. No significant change in stiffness or strength of the deck after 3,000,000 cycles of a fatigue load at a minimum/maximum load ratio of R=0.1, with the maximum load of 97.9 kN (22 kips) and the minimum load of 8.9 kN (2 kips). This demonstrated the durability of the adhesive joint under repetitive loading.

6. The mock-up test in the laboratory provided valuable insights into the constructability of the adhesive panel-to-panel connections. These results will help develop a protocol for adhesive construction during the future bridge installation. Furthermore, the data collected during the test will be used to compare with later test data from an in-situ bridge test.

Based on the results of this four-stage study, it was concluded that this adhesive bonding technique is suitable for use with Strongwell's FRP deck system to replace the deteriorated RC deck in the Hawthorne St. Bridge.

Acknowledgement

Part-II: Analysis of Adhesive joint in Bridge deck

Research work on stress analysis of basic joint configuration such as simple lap joint is well developed for both isotropic and FRP composite adherend. However, more complex joint configuration like scarf joint is still analyzed numerically using finite element method or theoretically based on very simplified assumptions (yielding little practical significance). Most of the analytical work was found to be focused on joints typical in aerospace structures. There are only few experimental work on adhesive joints in infrastructure application but still limited to representative coupon or component level. Most of these analyses assumed simple loading cases such as tensile load. However, bending load is applied in bridge deck applications which in turn induces shear and peel stresses in the adhesive joint. Therefore, sample joint configuration and applied loading are not well linked to structural joint application.

A full scale structural investigation of joints in bridge deck application is necessary to fully understand the response and predict durability. Analysis of bridge deck on supporting structure (using analytical and finite element method) generally requires great amount structural detail to be included to get meaningful results. This makes analysis and simulation model quite large. It would be even more difficult to implement detail about any structural joint (such as adhesive joint) and investigate behavior of the joint exclusively. On the other hand, analysis of idealized joints (such as simple lap joint under tension load) provides very little information about actual joint in the structure. Therefore, a connection between simplified joint and the structure is needed such that analysis on the "representative joint" is indicative of the performance of the structural joint. Such approximation is never exact but might provide some information for design and analysis of structural joint. In this study, a simple framework is presented to characterize bridge deck joint from analysis of a "representative joint". The proposed framework utilizes single span analysis of FRP deck as equivalent orthotropic plate, determination of maximum transverse stress (at joint location) and applying this to analysis of representative joint. The representative joint is taken as a beam specimen containing joint section and analyzed under bending load.

4.9 A proposed Framework for Representative Joint Analysis in FRP bridge deck

Bridge decks are usually treated as continuous plates in practical bridge design and construction. An alternative method to investigate the behavior of continuous bridge decks is to subdivide the continuous deck into several single-span deck section, find the proper boundary conditions for each single-span, and conduct the analysis of the continuous deck using single span analysis methods (Salim and Davalos et al [1997, 1999], Brown [1998], and Qiao et al [2000].)

Popular method of performing single span analysis is to represent FRP deck as equivalent orthotropic plate and apply plate theories to get deformation behavior (stress, strain and displacement) under bending load. We can use the same approach to analyze deck panel with joint as orthotropic plate under patch loading (common for bridge deck application).

4.9.1 Plate Theory Formulation under Conformable Pressure Loading
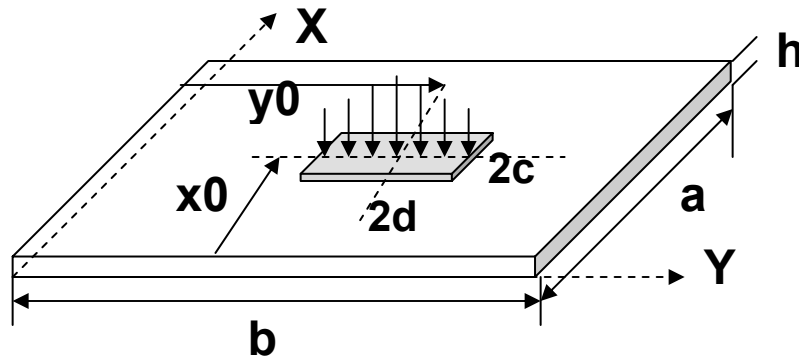
Figure 4.19 Schematic of patch loading on FRP composite plate

Plate theories (CLPT and higher order) and their solution using infinite series (Navier and Levy solution) are well developed for different boundary conditions (Reddy 1997; Reddy 1999) and loading (uniformly distributed and point load). There is limited solution available for uniform patch loading and mostly available for CLPT (Zhou 2002). However, we need to incorporate tire patch loading profile into plate theories. Also, we need to use higher order theories as elastic equivalent plates are thick and shear deformation need to be accounted for. Let us consider plate with length, a, width, b and thickness, h. The plate is loaded with simulated tire patch having contact area 2c by 2d. We will consider simply supported boundary condition to demonstrate the approach and the formulation can be extended for other boundary conditions.

Also, the deck will be treated as a single layer and specially orthotropic plate. Assumed displacement field for higher order plate theories are given below (Reddy 1997):

First-order Shear Deformable Theory (FSDT):

$$u = u_0 + z\phi_x$$

$$v = v_0 + z\phi_y$$

$$w = w_0$$

Third-order Shear Deformable Theory (TSDT):

$$u(x,y) = u_0(x,y) + z\phi_x - \frac{4}{3h^2}z^3\left(\phi_x + \frac{\partial w_0}{\partial x}\right)$$

$$v(x,y) = v_0(x,y) + z\phi_y - \frac{4}{3h^2}z^3\left(\phi_y + \frac{\partial w_0}{\partial y}\right)$$

$$w(x,y) = w_0(x,y)$$

For Navier solution, assumed displacements are

$$u_0(x,y) = \sum_n \sum_{m=1}^{\infty} U_{mn} \cos\alpha x \sin\beta y, \quad v_0(x,y) = \sum_n \sum_{m=1}^{\infty} U_{mn} \sin\alpha x \cos\beta y$$

$$w_0(x,y) = \sum_n \sum_{m=1}^{\infty} W_{mn} \sin\alpha x \sin\beta y, \quad \phi_x(x,y) = \sum_n \sum_{m=1}^{\infty} X_{mn} \cos\alpha x \sin\beta y$$

$$\phi_y(x,y) = \sum_n \sum_{m=1}^{\infty} Y_{mn} \sin\alpha x \cos\beta y \qquad \alpha = \frac{m\pi}{a} \text{ and } \beta = \frac{m\pi}{b}$$

Governing equation in terms of displacement becomes:

$$\left[\tilde{S}\right]\{\Delta\} = \{F\}, \text{ where } \left[\tilde{S}\right] = \begin{Bmatrix} U_{mn} \\ V_{mn} \\ W_{mn} \\ X_{mn} \\ Y_{mn} \end{Bmatrix} \text{ and } \{F\} = \begin{Bmatrix} 0 \\ 0 \\ Q_{mn} \\ 0 \\ 0 \end{Bmatrix}$$

In Navier method, the force is also expressed in terms of series.

$$q(x,y) = \sum_n \sum_{m=1}^{\infty} Q_{mn} \sin\alpha x \sin\beta y$$

For our case of patch loading, we can write,

$$Q_{mn} = \frac{4}{ab} \int_{x0-c}^{x0+c} \int_{y0-d}^{y0+d} q(x,y) \sin \alpha x \sin \beta y$$

Applied load q(x,y) is expressed as,

$$q(x,y) = q0 * P(x,y) = \frac{Q0(applied\ load\ per\ tire\ in\ kips) * 1000}{2c * 2d\,(contact\ area)} * P[y]$$

$$Contactlength(inch) = 2d = 7.52 * Q_0^{0.212} \quad and \quad 2c = Tirewidth(inch)$$

$$P[y] = 1.66 + C1[(y-y0)/d] + C2[(y-y0)/d] + C3[(y-y0)/d] +$$
$$C4[(y-y0)/d] + C5[(y-y0)/d] + C6[(y-y0)/d]$$

$$C6[y] = 0.1 * y^6 \quad C5[y] = -0.14 * y^5 \quad C4[y] = -1.46 * y^4$$

$$C3[y] = 0.11 * y^3 \quad C2[y] = -0.29 * y^2 \quad C1[y] = 0.02 * y$$

Now, following standard procedure outlined in text book, solution can be obtained for displacement, stress, strain and moments. Since the applied load is a nonlinear function of position (not constant), explicit expression can't be obtained for Q_{mn} and one can use programming packages like Mathematica to do the calculation.

4.9.2 Link from Structure to Representative Joint

Using plate theory (convenient) or FEA (expensive), we can get transverse stress(y-direction) at the bottom of the equivalent plate. Now, we consider a representative joint as shown in Figure 4.19 which retains the same joint configuration as in actual structure but now can be analyzed more like a simple beam (Figure 4.20). Bending analysis can be performed on this representative joint under 4-point bend load. The applied load can be found such that it generates same transverse stress as in the deck joint. Then, detail analysis of adhesive scarf joint with pultruded adherends can be conducted.
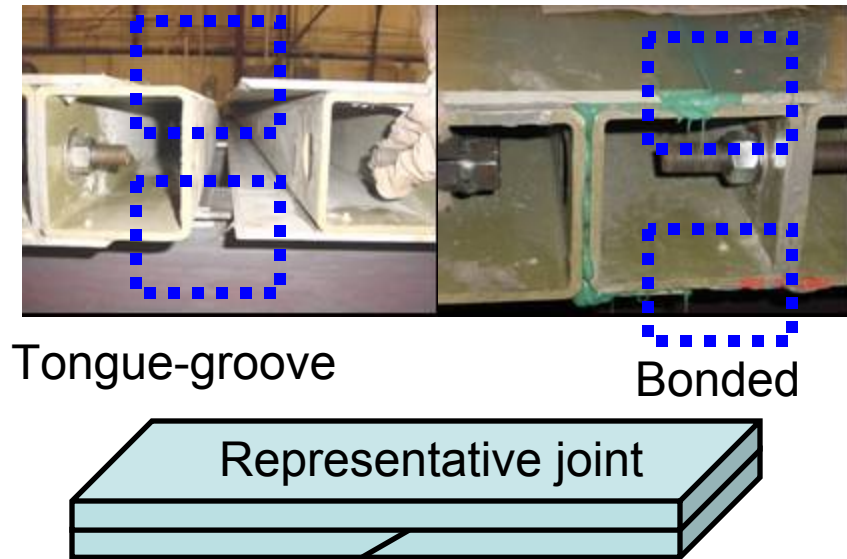
Figure 4.20 Representative joint for a FRP bridge deck
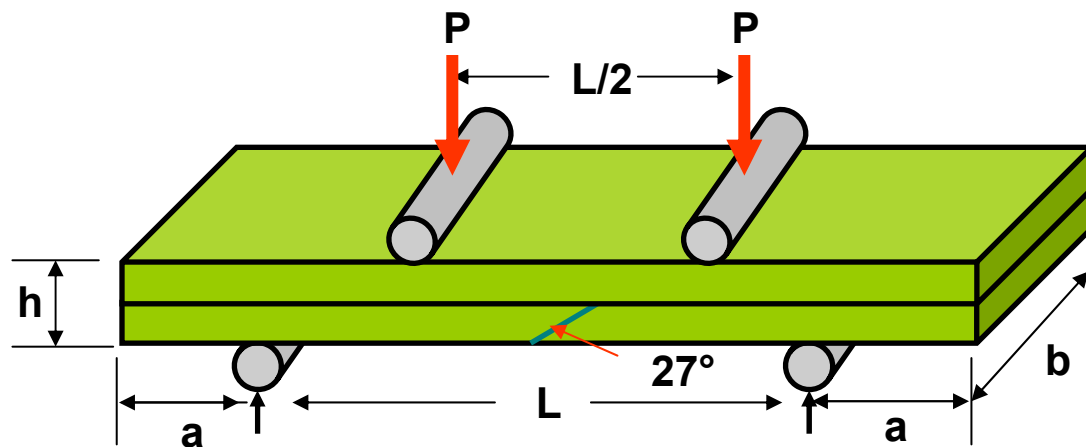
Figure 4.21 Test configuration for representative joint

The applied load for bending configuration can be obtained from beam formula:

$$P = \frac{2 * \sigma^{jo\,int} * bh^2}{3L} \; where, \; \sigma^{jo\,int} = \sigma_{yy}^{deck}$$

4.10 Summary

Plate theories are extended to include conformable pressure profile of simulated tire patch loading and applied to single span analysis of bridge deck. A simplified approach is presented to

analyze structure adhesive joint in bridge deck by using a "representative joint". A schematic of the proposed framework is given below:

```
┌──────────────────┐      ┌──────────────────┐      ┌──────────────────┐
│  Deck Properties │  →   │ FRP deck Analysis│  →   │   Cellular deck  │
└──────────────────┘      └──────────────────┘      └──────────────────┘
         │                         │                          │
         │                         ▼                          ▼
         │                ┌──────────────────┐      ┌──────────────────┐
         │                │ Orthotropic Plate│ ───→ │       FEA        │
         │                └──────────────────┘      └──────────────────┘
         │                         │                          │
         ▼                         ▼                          ▼
┌──────────────────┐      ┌──────────────────┐   ┌─────────┐   ┌──────────────────┐
│ Equivalent plate │  →   │   Plate Theory   │→  │ Stress  │ → │  Representative  │
│    Properties    │      │                  │   │ Results │   │  Joint Analysis  │
└──────────────────┘      └──────────────────┘   └─────────┘   │   (FEA or EXP)   │
                                                                └──────────────────┘
```
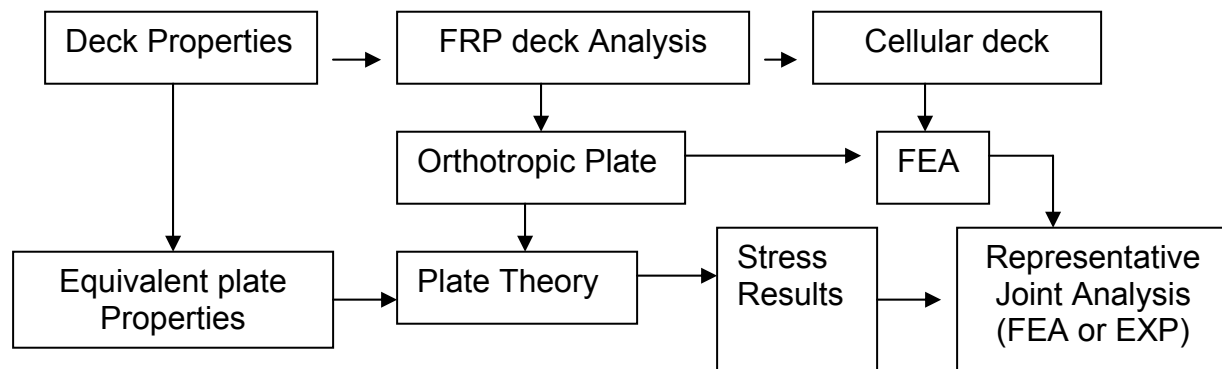
Figure 4.22 Proposed Framework to analyze bridge deck joint

Analysis of such representative joint can be done using FEA to obtain useful information (such as parametric study on joint configuration, adhesive properties and durability, and joint quality analysis using element birth and death approach) for design and characterization of structural joint. For example, a study on influence of scarf angle is presented in Chapter-4 and it had helped redesign the structure joint in FRP deck.

Chapter 5:   Performance Evaluation of FRP Deck

Performance Evaluation of FRP Composite Deck for Rehabilitation of the Hawthorne Street Bridge

[9] P. K. Majumdar, [10] Z. Liu, [11] J.J. Lesko, [12] T.E. Cousins

Abstract

Deterioration of bridges over time has become an important issue in the civil engineering community and there is urgent need of repairing or replacement as well as upgrading to meet the increased traffic of modern days. However, complete replacement is not welcomed readily due to cost of replacement and in some cases desire to preserve historically important structures. One way to address the problem is to rehabilitate the structure utilizing state of the art technology and advanced material systems such as fiber reinforced polymer (FRP) composites. In this context, a case study of rehabilitation of the structurally deficient Hawthorne Street Bridge at Covington, Virginia has been presented. The objective of this research is to implement a cost competitive lightweight FRP bridge deck system in the Hawthorne St. Bridge to increase its current load rating. Major challenges to implement such rehabilitation are to ensure construction feasibility, serviceability, and durability of the proposed deck system. To explore those issues, a two-bay section of the bridge has been constructed in the Structures Laboratory at Virginia Tech. An extensive experimental scheme has been put into place to evaluate structural performance of the proposed FRP composite deck under different probable loading scenarios at service load level and also investigate the strength of the deck system. From the experimental observations it has been found that the response of the deck is linear elastic and there is no evidence of deterioration at service load level (HS-20). The lowest failure load (93.6 kips or 418.1kN) was approximately 4.5 times the design load (21.3 kips or 94kN) which includes dynamic allowance to HS-20 load

---

[9] Graduate Student, Department of Engineering Science & Mechanics, Virginia Tech, Blacksburg, Virginia 24061, USA. Email: pkm2004@vt.edu

[10] Graduate Student,   Department of Civil & Environmental Engineering, Virginia Tech, Blacksburg, Virginia 24061, USA. Email: lzh@vt.edu

[11] Professor, Department of Engineering Science & Mechanics, Virginia Tech, Blacksburg, Virginia 24061, USA. Email: jlesko@vt.edu

[12] Professor,   Department of Civil & Environmental Engineering, Virginia Tech, Blacksburg, Virginia 24061, USA. Email: tcousins@vt.edu

level. The failure mode was consistent in all loading conditions and was observed to be confined within a localized region. Global behavior of the bridge superstructure was also linear within elastic limit and the study verified that there was no composite action consistent with initial design assumption. This research found proposed FRP composite deck system to be promising candidate for rehabilitation of bridge application. In addition to global performance, local deformation behavior is also investigated using finite element simulation. Local analysis suggests that local effects are significant and should be incorporated in design criteria. This paper reports the results of the construction, testing and finite element simulation of the FRP bridge deck system.

CE Database subject headings: Rehabilitation; Fiber-reinforced polymer (FRP); Bridge deck; Adhesively-bonded; Full-scale Tests; Failure modes; Composite structures.

5.1 Introduction and Background

Reinforced concrete bridges have been an integral part of civil construction for many years. However, there is a growing concern of deterioration of such structures with time. According to the 2005 Transportation Statistics Annual Report (FHWA/USDOT 2005), nearly thirty percent of 600000 US bridges are either structurally deficient (15%) or functionally obsolete (14%). To be structurally deficient and functionally obsolete means these bridges suffer from loss of material properties due to degradation and age, and are experiencing more traffic than they were originally intended for.

The annual direct cost of corrosion for highway bridges is $8.3 billion and life-cycle analysis estimates indirect costs to the user due to traffic delays and lost productivity at more than 10 times the direct cost of corrosion (FHWA). The state and federal agencies are looking for cost-effective and durable technologies for bridge repair, rehabilitation and replacement.

Figure 5.1 Hawthorne Street Bridge, Covington, Virginia

The Hawthorne Street Bridge in Covington, Virginia is one of the 1161 bridges in Virginia considered structurally deficient. The through truss bridge has a 22.86 m (75 ft) clear span Pratt-truss structure with a roadway width of 6.7 m (22 ft), running over three rail-lines as shown in Figure 5.1. Due to the use of the Phoenix Column in the truss, the bridge is considered historically significant. The Hawthorne Street Bridge is an integral part of lifeline access for emergency vehicles to downtown Covington. This is also the only route that emergency vehicles can use during periods of high water to get to some areas of the city.

The current condition of the bridge has required that it be posted at 62kN (7 tons). The structure has a condition rating of 5 (fair condition with all primary elements experiencing only minor section loss). Inspections have shown that the existing W10x33 stringers supporting the deck of the bridge are no longer sufficient for meeting American Association of State Highway and Transportation Officials (AASHTO) deflection requirements. Additionally and of primary concern, the reinforced concrete (RC) deck is severely deteriorated and several large pieces of it fell from the structure onto the railroad tracks in February 2001. This prompted the Virginia Department of Transportation (VDOT) to close the bridge to make repairs. Based on the condition of the deck and superstructure, VDOT had determined that the Hawthorne Street

Bridge is a candidate for rehabilitation or replacement. However, replacement has been ruled out because of the historical significance of the bridge and alignment challenges at each approach.

Consequently the focus shifted towards finding a rehabilitation alternative. The alternative selected was replacing the bridge superstructure with a new deck/beam/girder system. The aging beams and girders will be replaced with new steel sections and the existing, deteriorating reinforced concrete bridge deck will be replaced with a fiber reinforced polymer (FRP) composite bridge deck system. Replacement of the existing reinforced concrete bridge deck with an FRP composite bridge deck system was decided upon for several reasons. The inherent advantages of FRP composites over conventional materials (in this case reinforced concrete) are higher strength to weight ratio (proposed FRP deck will be three times lighter than the existing reinforced concrete deck), rapid installation, resistance to corrosion, improved durability, and potentially lower life-cycle costs (decreased maintenance costs). The most important characteristic of the proposed rehabilitation is the reduction in dead load which will allow for an increased posting and use of the bridge by emergency vehicles.

The objective of this program is to implement a lightweight FRP bridge deck system in the Hawthorne St. Bridge, which will permit the posting to be raised so that emergency vehicles can pass. A secondary, but equally important feature of this program is to advance an FRP deck system from Strongwell Corp. with a target price range of $430-485/m^2 ($40-45/ft^2). The deck is made of 152x152x9.5 mm (6×6×3/8 in.) pultruded box beams and two skin plates 6.35 &12.7 mm (¼ and ½ in.) thick respectively. The plates and tubes are adhesively bonded to each other (Figure 2). The deck weighs less than 1.2 kN/m^2 (25lb/sq.ft) including wearing surface. The FRP deck manufactured by Strongwell Corporation of Bristol, VA will be shipped to the bridge site as full width 6.7 m (22 ft) panels that are about 2.13 m (7 ft) long in the direction of traffic.
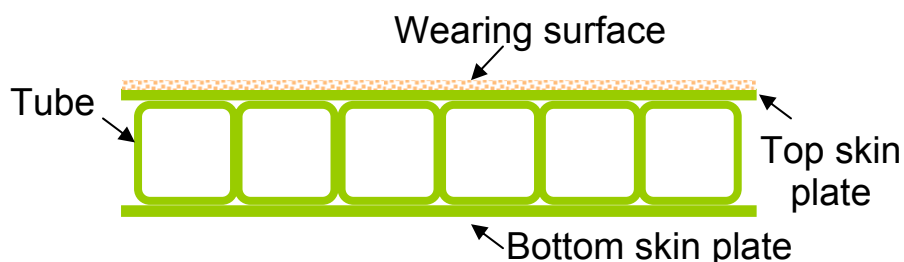
Figure 5.2 Cross section of cellular structure of FRP deck

It is important to mention that extensive research has been carried out at Virginia Tech over the past ten years on cellular FRP deck panels manufactured by Strongwell Corporation

(Hayes et al. 2000; Temeles 2001; Coleman 2002; Zhou et al. 2005) . The authors have also significantly extended previous work (Link 2003) on panel-to-panel connection to successful implementation of adhesive bonding method. In Hawthorne Street Bridge, the connection of the panels will be accomplished using a full length, adhesively bonded tongue and groove splice. However, the current analysis will not discuss panel-to-panel connection, and will be limited to performance of the deck and superstructure.

There have been an increasing number of research efforts reported on FRP composite deck and its application in rehabilitation or replacement of deteriorated bridges. While most of the researches were focused on testing of representative deck panels and subsequent field test, there are actually not many studies reported investigation of a large scale structure at the laboratory. To insure proper construction, serviceability, and strength of the FRP deck, a two-bay section of the bridge was constructed in the Structures Laboratory at Virginia Tech. The results of the extensive construction and testing of the bridge section have been documented in this paper. The authors also believe this paper is the first to report full scale structural response of FRP deck made of pultruded tube and plate assembly (manufactured by Strongwell Corporation).

5.2 Test Plan

In order to explore the viability of using the proposed FRP deck, it is necessary to develop an extensive test plan to investigate structural response under service load conditions and examine failure mode. For this purpose, the major steps are to construct the superstructure simulating the two bay section of the real bridge and then come up with probable loading conditions that the bridge might experience in the real application.

5.2.1 Building the Superstructure

The steel frame mock-up of the Hawthorne Street Bridge superstructure consists of two bays, which are 4.88 m (16 ft.) and 4.57 m (15 ft.) in length in the direction of traffic (Figure 5.3).
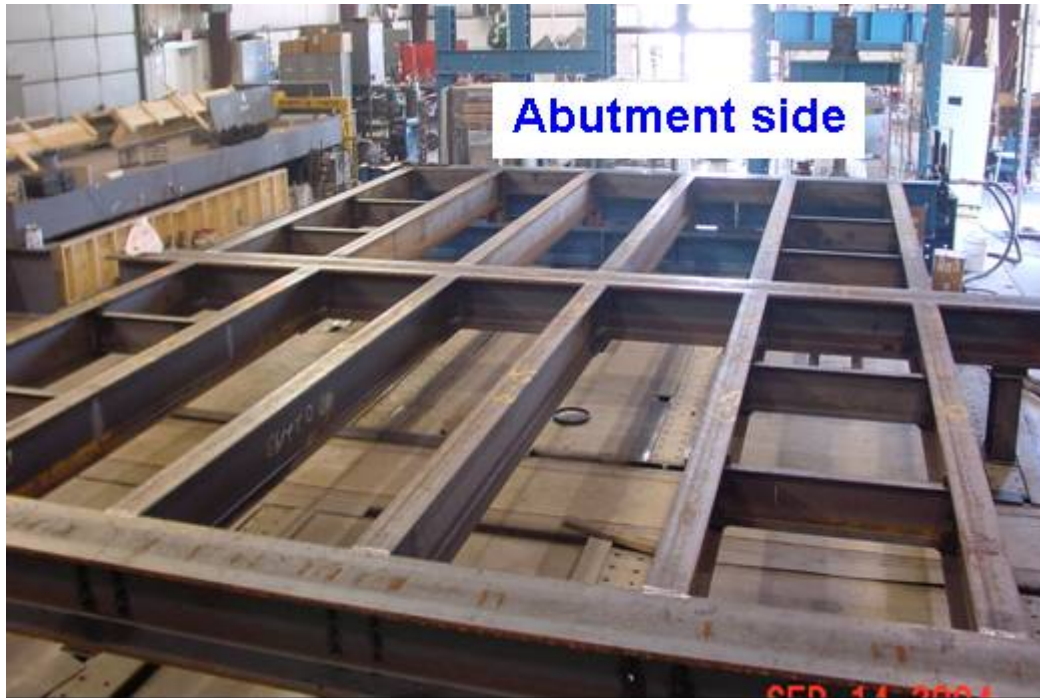
Figure 5.3 FRP deck superstructure built in the lab to mimic real structure

Each bay has six wide-flange W14x34 stringers with a transverse spacing of 1.22 m (4 ft) on-center. Diaphragm members, consisting of C10x15.3 steel sections, are bolted to the stringers through connector plates. Two W14x120 floor beams are supported by four pedestals that simulate the hangers in the through-truss bridge. All steel member sizes and dimensions mimic the actual ones in the Hawthorne Street Bridge superstructure. Neoprene pads are used between floor beams and pedestals to avoid direct contact of steel and to allow some movement at floor beam ends. Stringers and floor beams are joined together using moment resisting connections. A W21x132 beam is used to simulate the concrete abutment and five end diaphragms (C10x30) are placed to avoid free edge effect of the FRP deck. All Stringers at the abutment rest on the bearings anchored on the abutment.

FRP deck panels are adhesively bonded together to form the complete deck system and placed on the superstructure. The detail description of deck panel-to-panel bonding and their analyses are not included in this paper. Deck panels are connected to stringers with a number of deck-to-stringer connections and these connections are not intended to develop any composite action. The deck-to-girder connections are intended to resist the forces from braking of vehicles on the bridge deck and from uplift. The preliminary design, created by VDOT, attaches the panels using a bolt through the bottom flange of the deck with a clip to the side of the steel

stringer top flange. A photograph of the deck-to-girder connector is shown in Figure 5.4. A nut, bearing plate and steel sleeve are welded together as a connector. Then the connector is pushed along the tube to drop into the hole pre-drilled through the bottom plate and the bottom face sheet of the tube. Finally a 3/4 in. bolt is installed which screws into the matched nut of the connector from underneath the deck system. The bolted connections are spaced at 1.22 m (4ft) along the traffic direction for each stringer.
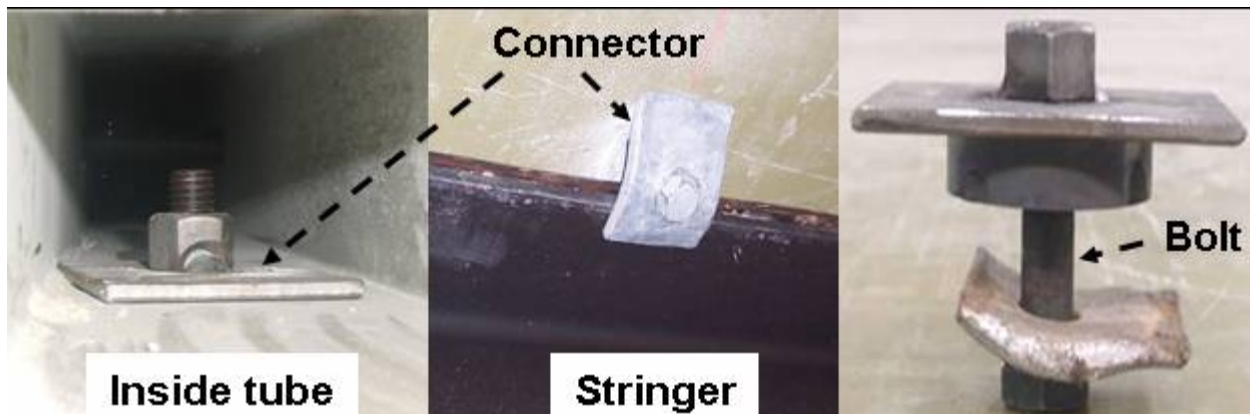
Figure 5.4 Deck-to-girder connector used in Hawthorne Street Bridge

5.2.2   Loading Plan

The HL-93 design truck dimensions and loads [AASHTO 2004] are used for evaluating the performance of FRP deck system under service load conditions. According to AASHTO specifications, this is a tire load of 71.2 kN (16 kips) with a dynamic load allowance of 33%, which yields a load of 94.8 kN (21.3 kips). Five different loading plans for service load level of 45 kips per axle (HS 20) are shown in Figure 5.5. Loading plans 1 to 4 are single truck cases and plan 5 is the symmetric case with double trucks representing the full lane loading scenario. Since a wheel is located at mid-span between two stringers, loading plans 1, 2, and 4 are the critical cases for flexure of FRP transverse to traffic. On the other hand, plan 3 is the case where truck straddling on stringer 3.
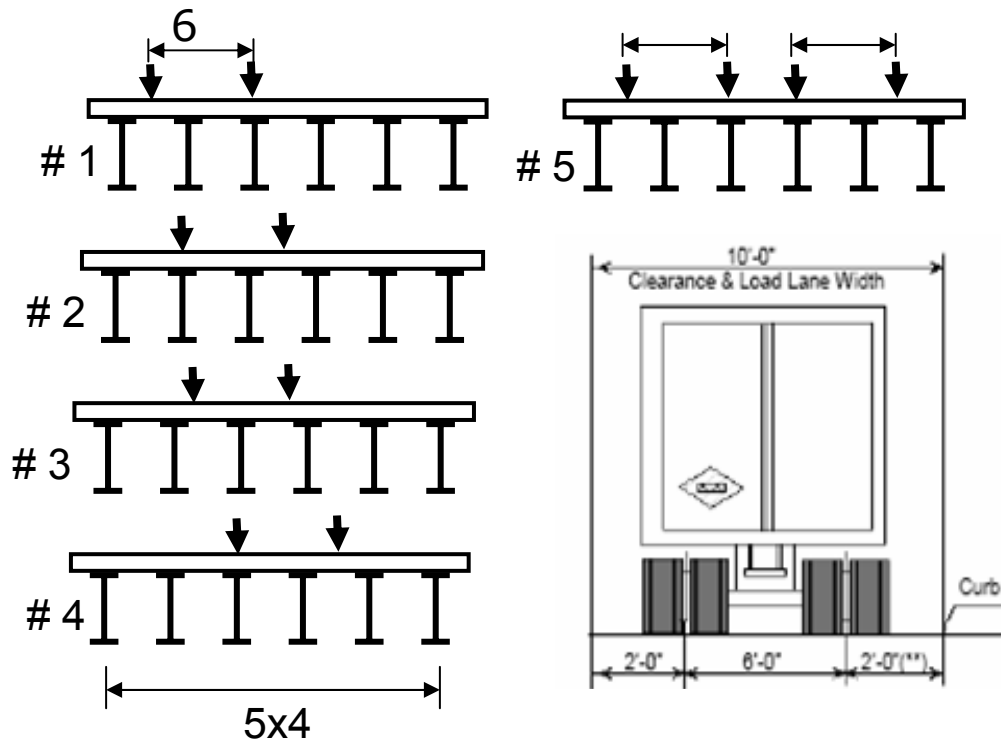
Figure 5.5 Loading plans for service load test (#1- 4 single truck, #5 double truck)

Most of the researches in the literature used rectangular steel pad for loading which may not be representative of actual stress contour as the bridge is likely to experience from vehicle loading. A special loading patch has been prepared by a quarter of a tire half-filled with silicone rubber to mimic the cushioning effect of a real pneumatic tire. This will minimize local stress concentrations around the edge of a standard rectangular steel patch.

5.3 Service Load Test

Service load tests are conducted along two maximum bending moment locations on each bay of the deck at a distance 0.43*L1 (location-A) from abutment and 0.5*L2 from Floor Beam #2 (location-B) as shown in Figure 5.6. All five loading plans are followed for both location A and B.
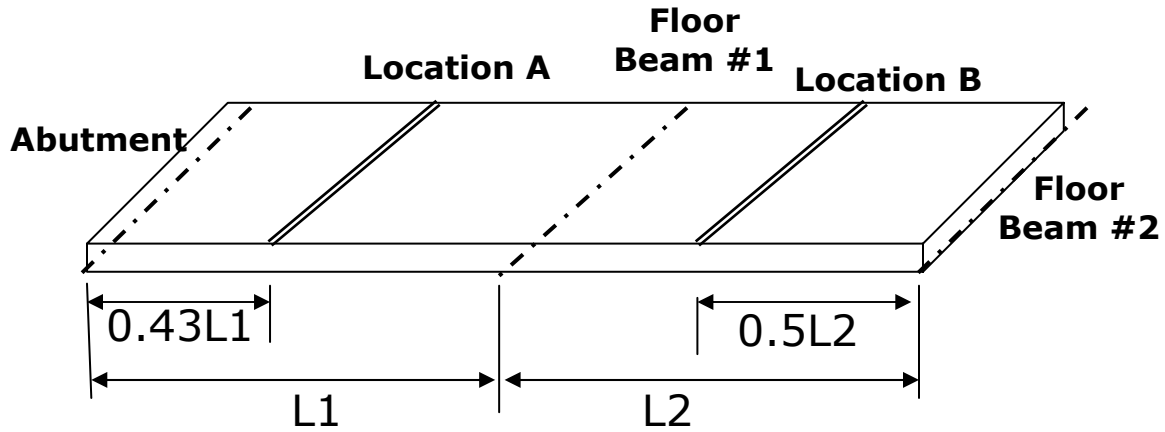
Figure 5.6 Loading locations (A and B) for service load test

The major objectives of this service load test are to study response of the deck to ensure that it operates within linear elastic range at the intended load level, look for damage if any, find the load distribution factors to get an idea of load transfer from deck to structure, and verify if there is any composite action although the bridge is not designed for composite action.

5.3.1 Test Setup and Instrumentation

A real time photograph of the test setup is shown in Figure 5.7. The load is applied using hydraulic actuators through a spreader beam acting on the loading tire patches. The position of the spreader beam along with the tire patches is varied through the width of the deck (along Location-A and Location-B) for different the loading plans.

Figure 5.7 Experimental Set-up for service load test

Deck

■ Transverse strain gage
▭ Longitudinal strain gage

Stringer ● Wire pot (displacement transducer)
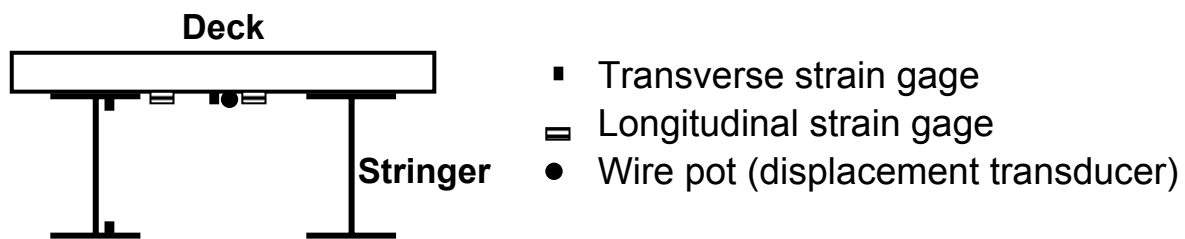
Figure 5.8 Instrumentation on stringer and deck at location-A & location-B

An overview of the instrumentation plan to investigate the performance of FRP deck during service load tests is shown in Figure 5.8. For consistency throughout the discussion, all references to "longitudinal" and "transverse" are given with respect to the bridge deck orientation; thus, "longitudinal" implies parallel to the pultruded tube direction of the FRP deck system and the "transverse" direction refers to the traffic flow direction (perpendicular to the tube axis or Pultrusion direction).

As shown in Figure 5.8, different strain and displacement measuring gages are installed on both the deck and stringers to quantify deformation under service load conditions. These gages are positioned with two distinct objectives in mind. One set is intended for monitoring the response of the deck and therefore those gages are attached to the deck at mid span. At mid span, two strain gages are positioned in mutually perpendicular orientation to measure longitudinal and transverse strain of the deck. Also a wire pot (displacement transducer) is used to record span

73

deflection. The other set of gages are placed on stringers for measuring the response of the superstructure. In this case, strain gages are attached to both top and bottom flange of the stringer. These strain measurements will help understand transfer of load from deck to structure and existence of composite action. The entire instrumentation pattern is repeated at each span to provide strain distribution pattern for the structural assembly.

5.3.2   Finite Element Model of Deck and Superstructure

A three dimensional model (33ft by 22 ft) of the two-bay bridge super structure and the cellular FRP deck system is developed using ANSYS. This model is generated using ANSYS programmer's design language (APDL) coding to allow automatic mesh generation and parametric studies. The stringers and floor beams are modeled using elastic shell element (shell 63). The cellular structure of the deck is modeled with non-linear shell element (shell 91) capable of large deformation analysis. The interface between deck and superstructure is constraint only in vertical direction such that there is no composite action developed. Some of the structural details (such as bearing pad at supports and diaphragms connecting exterior to interior stringers) are left out in the model and more focus is given on capturing response of the FRP deck itself. A representative plot of the model is shown in figure 5.9. The mesh density is biased near the loading area compared to far away from loading area in order to minimize model size (number or nodes and elements). A special program is written in ANSYS APDL to input conformable pressure profile of simulated tire patch loading. A profile load is moved to different locations for different loading cases. Results of FEA simulation is discussed along with experimental results in later sections.
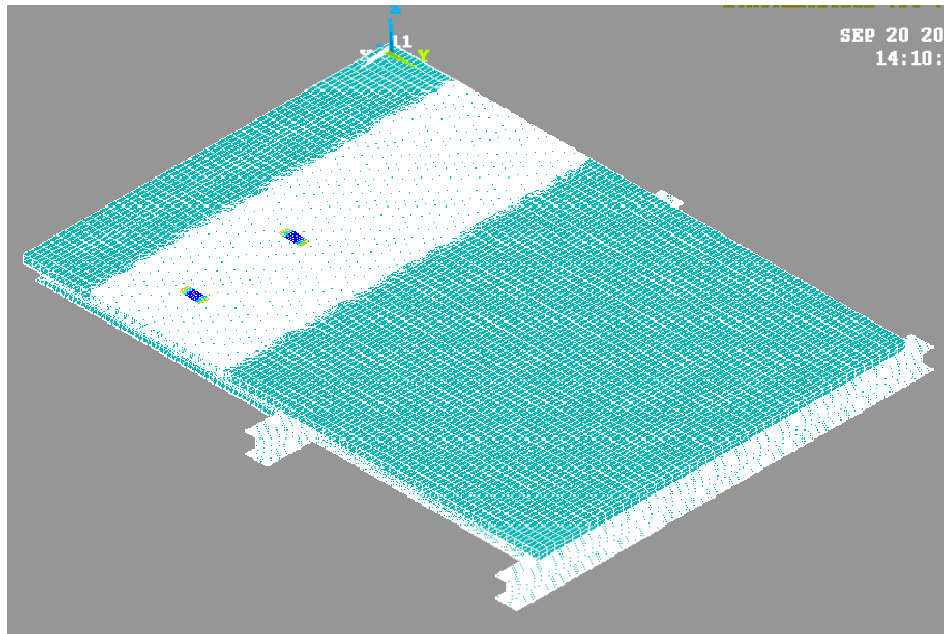
Figure 5.9 Two-bay model of deck with superstructure under tire patch loading

5.3.3 Results of Service Load Test

At each test location, load is applied up to the service load level at a quasi-static speed and unloaded gradually. Load, deflection, and strains are continuously recorded during each test using a data acquisition system. For a particular loading plan, tests are run at least three times and the response is found to be fairly repetitive. From service load test, the response of the deck and superstructure is observed to be linear. All the test locations are able to resist the service tire patch load without any indication of damage. Detail interpretation of the experimental results is discussed in the following sections.

5.3.4 Response of FRP Deck

Span deflection and strain data showed a linear behavior up to the service load level of 195 kN per axle (HS-20). The strain and deflection data corresponding to HL-93 loading are shown in Table-5.1. The FRP deck showed small relative deflection (maximum 3.11 mm) which means the deck has sufficient stiffness at service load level. At a particular test location, test plan was repeated at least three times to check for variability of recorded data and the average values are tabulated in Table 5.1.

Table 5.1 Strain & deflection data of service load test (22kips per axle)

Test Location	Loading Plan	Max. Strain transverse to traffic	Max Strain along traffic	Max. Span Deflection inch	Span/ Deflection	Relative deflection of deck at mid-span	Relative deflection of deck FEA
Loc-A	1	770	178	0.295	649	0.081	0.079
	2	837	461	0.337	569	0.093	0.076
	3	395	300	0.342	561	N/A	
	4	732	380	0.312	614	0.073	0.095
	5	843	384	0.373	513	0.095	0.090
Loc-B	1	774	605	0.340	529	0.099	0.087
	2	864	623	0.318	451	0.105	0.087
	3	360	490	0.223	805	N/A	
	4	875	541	0.397	453	0.11	0.088
	5	812	600	0.427	420	0.102	0.0867
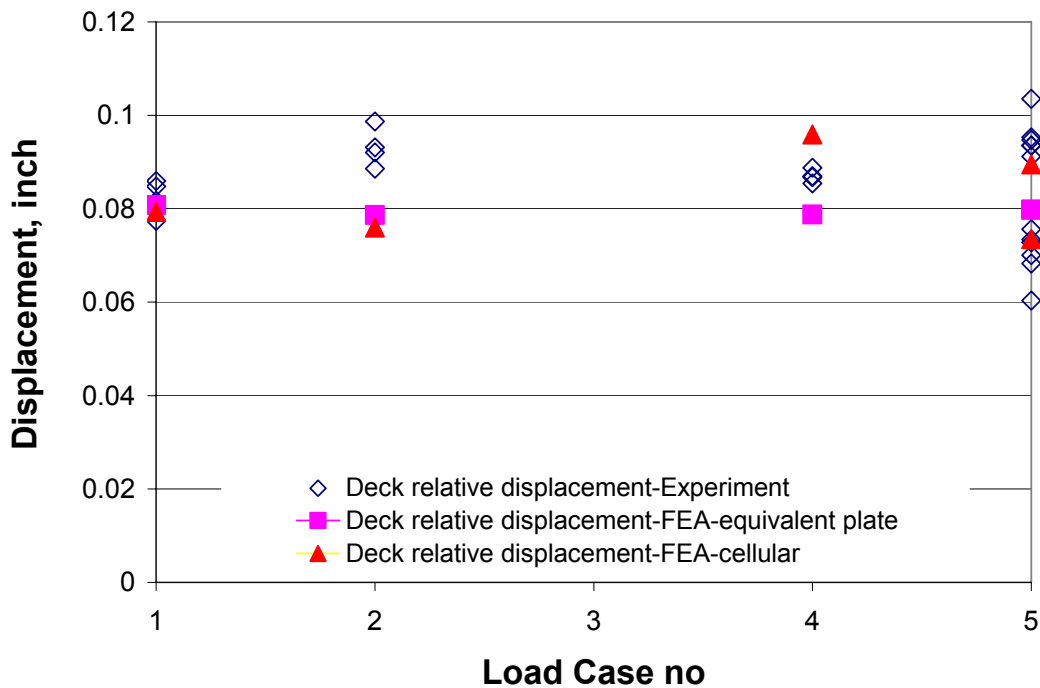
Figure 5.10 Relative deflection of deck at Location-A

A representative plot of deck relative displacement for different load cases at Location-A is shown in figure 5.10. The global displacement behavior can be predicted with reasonable accuracy using both equivalent plate model (with more detail on structure but less on deck) and

76

cellular model (with more detail on deck but less on structure). Therefore, it is advantageous to model the cellular structure of the deck by sacrificing some of the structural details (to reduce model size) because more information can be extracted about the behavior of FRP deck.

In the literature, researchers have argued that a direct application of L/800 criteria to advanced composite materials is not recommended without understanding the dynamic response of the component. Proper deflection limitation (an equivalent L/span) imposed on composite bridge components should be derived from human tolerance on static deflection or dynamic motion due to vehicular traffic (Demitz 2003). Many researchers have suggested L/400 as deflection criteria for FRP deck system (Demitz 2003; Zhang and Cai 2007). The proposed FRP deck system provided acceptable span/deflection ratios considering that there is no standard for FRP deck in AASHTO guidelines. It is also noteworthy that longitudinal or fiber direction strain (transverse to traffic direction) is higher than transverse strain (along the traffic direction). The magnitude of transverse strain is not significantly high (maximum 623 microstrain) and it can be stated that FRP deck is safe at this strain level.

5.3.5 Load Distribution Factors (DF)

Load distribution factors (DF) is reported in literature as one of the indicators of load transfer phenomena within the deck and superstructure. These factors are also dependent on whether the bridge is designed for composite action or not [Zhang and Cai 2007] and calculated from the observed strains assuming that the global deformation of the bridge under service load occur within its elastic limit. At each gage location, the distribution factor, DF is calculated as:

$$DF_{jth\ stringer} = \frac{Strain\ of\ jth\ Stringer}{\sum\limits_{stringers} Strain} \times No.\ of\ Truck$$

Although distribution factors are provided in the AASHTO Standard Specification for various combinations of bridge deck and girder types, none of them are reported for FRP bridge deck systems. For this reason, finding load distribution factors for such FRP deck system is very important. A representative plot of the distribution factors for loading plan #5 at two different locations (A & B) are shown in Figure 5.9.For design purposes, maximum value of distribution factor is important. Maximum values of DF at location-A is 0.472 and at location-B is 0.437. Finite Element predictions are in reasonable agreement with experimental observations for all the

loading cases and only double truck case is shown in figure 5.9. This suggests that FEA simulation can be used for design purposes to predict load distribution factor for FRP composite deck before constructing the superstructure.
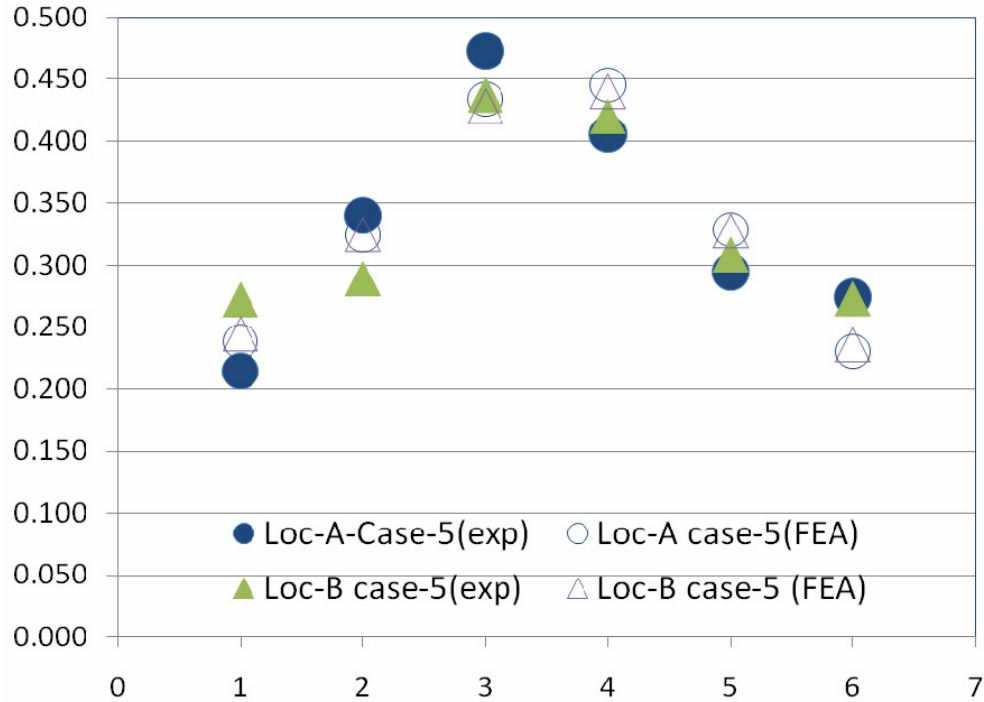
Figure 5.11 Load distribution factors for Loc-A& B for double truck case

The distribution factors calculated based on the test data have shown that the deck is capable of providing sufficient stiffness to distribute load to stringers not just directly adjacent to the truck. This can be clearly observed from load distribution plot for loading plan 5 (double truck case) where load is transferred from deck to all stringers. For reference, the AASHTO distribution factor based on AASHTO LRFD Bridge Design Specification for a concrete deck of similar thickness is determined to be 0.468 for the double truck loading, which is very close to the test results of in FRP deck. However, the calculation of AASHTO LRFD distribution factor of a concrete deck is based on the assumption of composite action and is not applicable in this case. AASHTO load distribution factors for the category of glued laminated wood panels on steel stringers also show good agreement with test results. Design value of DF for interior stringers is 0.457 is 3% smaller than critical value of 0.472 at Location A and 5% larger than 0.437 at Location B as obtained from experiments. This indicates that the FRP deck can provide longitudinal stiffness similar to a laminated timber deck. Also as a simplified method,

appropriate conservative design distribution factor may be found using level rule (DF=0.5) by assuming no load transfer across an interior stringer (deck is hinged at each stringer).

5.3.6 Composite Action

Degree of composite action between deck and stringer (if any) was investigated by calculating live load neutral axis for each stringer based on strain measurement. As described previously, strain gages are mounted on each stringer supporting the FRP deck to determine neutral axis of the deck-floor-beam system. If there is no composite action between the floor-beam and the deck, neutral axis of the deck-floor-beam system should coincide with the neutral axis of the floor-beam. In this situation, gages at top and bottom flange of stringers should provide strains of same magnitude with opposite signs (positive for tension, and negative for compression). If there is composite action between deck and girder, the neutral axis will either shift up or down depending on the magnitude of top or bottom flange strain. If the top flange strain is always higher, the neutral axis will shift up and vice versa.
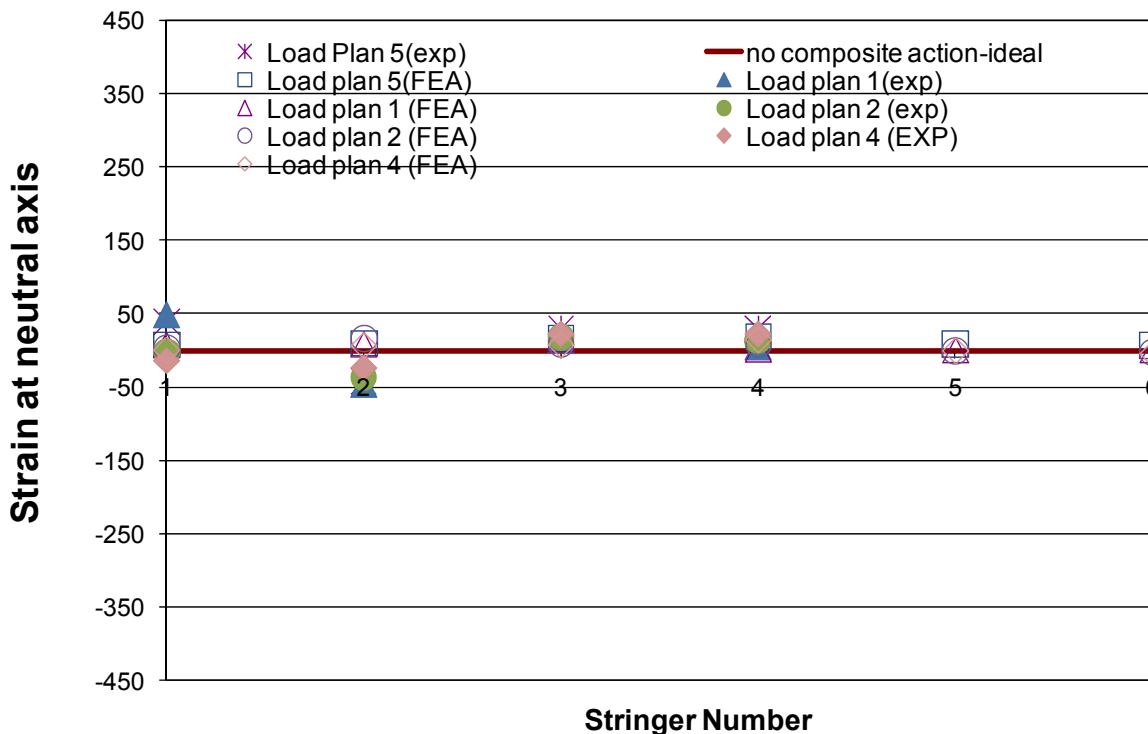
Figure 5.12 Strain at Neutral axis with FRP deck added to structure

The experimental results show that the strains in bottom and top flanges are reasonably close except for the sign (as expected). There is no trend of top or bottom strain reading being always higher or lower as shown in Figure 5.12. Hence the variation of strain data is considered as scatter within recorded data. Also, finite element analysis verifies that there is no composite action as per design and modeling assumption. Therefore, it can be stated that the neutral axis of the girder is unchanged with the addition of the FRP deck and no composite action exists between the deck and the floor-beams.

5.3.7   Test over Floor Beam for Negative Moment

A series of service load tests are carried out across the floor beam where there is possibility of negative moment. Although loading plan is same as it has been for previous service load tests on Location-A and Location-B, the arrangement of tire patch is different. Four tire patch system called "military tandem loading" configuration has been used as shown in Figure 5.13. This tandem loading represents a single truck scenario and therefore all the single truck loading plans 1 to 4 are repeated (Figure 5.5).
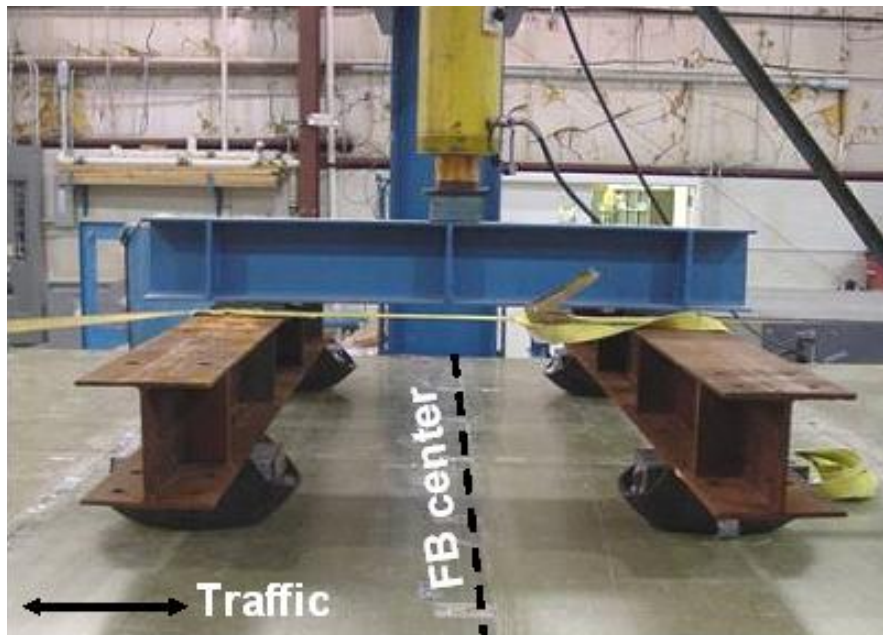
Figure 5.13 Loading configuration for test over floor beam

The deck is loaded to 311.38 kN (70 kips) which is distributed to 77.84 kN (17.5 kips) at each tire patch. Strain gages were mounted on the top surface of the deck right along the center line of the floor beam. From test results it is found that the maximum tensile strains are 62, 52, 62, and 56 microstrain for loading plans 1, 2, 3, and 4 respectively. The strain gages on the top surface of

the deck experienced very low tensile strain (maximum 62 microstrain) under tandem load straddling over the floor beam. Therefore the proposed FRP deck is safe in this respect.

5.3.8 Uplift Test of FRP Deck

There is possibility of uplifting of the deck at the free edge near the abutment and also over the stringers due to poor deck-to-girder connection. To measure uplift near abutment, a LVDT is placed on top of the deck and deck is loaded both near and away from the edge (at maximum bending moment location-B). There is no uplifting of the deck observed in either case. Similarly, in order to validate the effectiveness of the proposed deck-to-girder connectors, the FRP deck is loaded at span center between two end stringers and deck displacement at edge of the stringer is measured using LVDT. A representative photograph of uplift test near abutment and on stringers is shown in Figure 5.13. The test results show that deck-to-girder connectors are very effective in resisting any uplift of the deck over the stringers.

Figure 5.14 Uplift test at free edge for loading near or away from abutment

5.4 Failure Test

For failure test of the FRP deck, three loading configurations are considered based on the original loading plans of service load test. Two tire patches are used with center to center distance of about 279.4mm (11 inch) as shown in Figure 5.14.
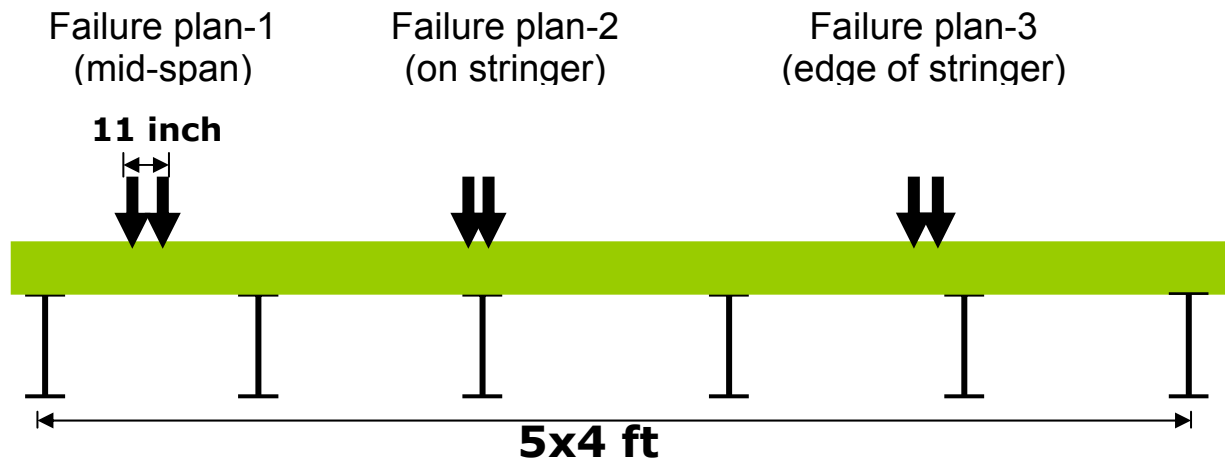
Figure 5.15 Loading configuration for Failure test

The instrumentation plan is somewhat similar to service load test. Two unidirectional strain gages are mounted at the mid-span location and they are oriented in mutually perpendicular directions (Longitudinal and transverse). Wire pots are placed to measure deflections of stringers and deck at span location. A real time photograph of the failure test is shown in Figure 5.15. The deck is loaded until initiation of failure and measurements are recorded in situ. Failure is detected by large variation in strain and displacement with increasing load. Also, there has been huge audible sound indicative of failure.

Figure 5.16 Failure test setup

5.4.1 Failure Test Results

Experimental results of failure test of FRP deck under three failure plans are summarized in Table 5.2. For the test results it is observed that loading at the span center (failure loading plan-1) is the worst case compared to other two scenarios where loading was at the edge and on top of the stringer. The failure initiated at 416 kN and the corresponding span deflection was 23.5 mm (relative deck displacement of 12.2 mm). Significantly high longitudinal (3920 microstrain) and transverse strain (2850 microstrain) are recorded at the bottom of the deck.

Table 5.2 Failure test results

Loading location	Failure load, kN (kips)	Longitudinal Strain microstrain	Transverse strain microstrain	Span deflection, mm (inch)	Relative deflection of deck, mm (inch)
Failure Plan-1	416 (93.5)	3916	2847	23.5 (0.925)	12.2 (0.48)
Failure Plan-2	711.7 (160)	N/A	N/A	45.2 (1.78)	14.2 (0.56)
Failure Plan-3	702.5 (157.93)	N/A	N/A	42.93 (1.69)	6.35 (0.25)

5.4.2 Failure Mode

Failure was observed to be localized under the loading patch and it was at bottom of top plate and top surface of the tube. It is believed that failure is due to high transverse strain because the composite lay-up is predominantly unidirectional and the laminate is weak in transverse direction. Due to cellular structure of the FRP deck, it is impossible to put strain gage inside the tube and therefore the actual strain at the failure location can not be measured. Strain gages are attached at the bottom of the deck which is not the failure location. Failure mode is found to be consistent in all three failure plans with failure of top plate and top surface of tube as shown in the Figure 5.17.
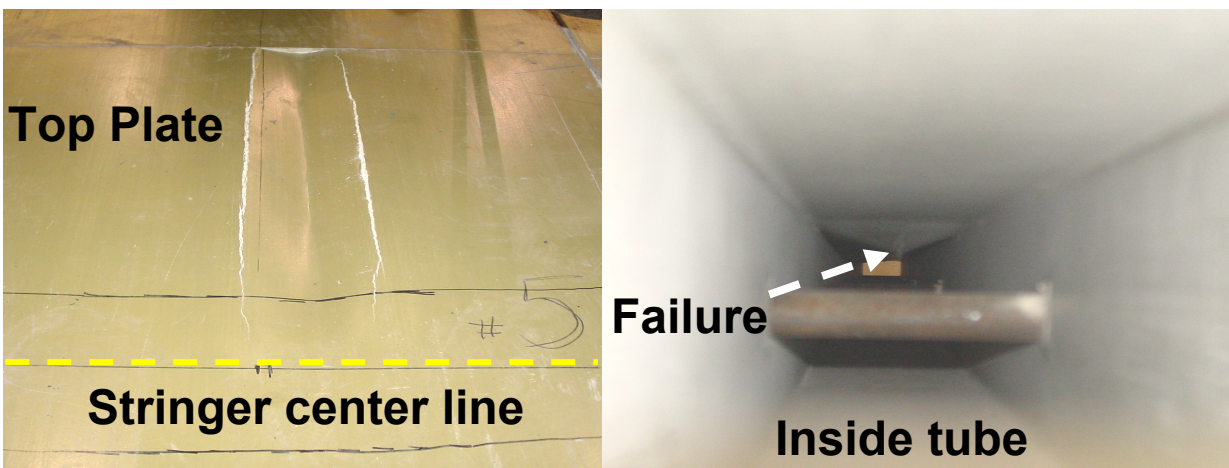
Figure 5.17 Failure mode of FRP deck

Using finite element model, failure analysis is carried out to investigate failure status of each component in cellular FRP deck and verified against experimental observations. Deflection and transverse strain are found to be significantly higher at top flange of the cellular structure than at the bottom surface of the deck. Eventually, failure was localized at top flange under the loading patch and this was consistent with experimental observations. It is found that FEA model accurately predicts the component failure status at 94kips load. Previous studies by Zhou (Zhou et al. 2005) could not predict failure accurately and found false failure prediction of bottom plate which did not happen during experiment. In this current model, we used simulated tire patch for experiment and corresponding profile load was applied. We believe this played a significant role in our accurate prediction compared to previous studies where uniform loading was applied in model but experiment was done by tire patch. We will explore the strength and failure mode analysis in detail in the next chapter.

Table 5.3 Failure status using finite element model

Loading location	Failure criteria	Top plate	Top flange	Bottom flange	Bottom plate
Failure Plan-1 load 416 kN (93.5kips)	Tsai-Wu	Failed	Failed	Safe	Safe
	Max-stress	Failed	Failed	Safe	Safe

5.5 Local Deformation Behavior of Cellular deck

To further explore the local response of the cellular FRP composite deck, a 3D finite element model of 5ft by 6ft deck panel is developed using ANSYS. The orthotropic deck is modeled using shell element (shell91) and supporting structure is modeled using shear deformable beam element (Beam189). To study the response of the deck alone, the supporting structure is anchored to the floor. The deck displacement is measured experimentally both at bottom and top span location within the cellular structure. From the displacement response (Figure 5.18 and Figure 5.19), it is clear that the deformation behavior is very localized under the loading area and displacement at the top flange of the tube can be as high as 20% or more compared to bottom displacement. Another notable feature is that the shape of displacement curves is different along traffic and transverse to traffic direction. In the transverse to traffic direction (pultrusion direction of tubes), the distribution is wider suggesting similar to plate bending behavior. However, in the traffic direction, the narrow distribution pattern is characteristic of cellular structure where load distribution is not uniform across the series of bonded tubes. On the other hand, stress and strain distribution patterns also demonstrate localized response with significantly higher values at the top compared to bottom span center. This suggests that global deformation analysis with equivalent orthotropic plate analysis is inadequate to capture critical response of the cellular FRP deck. Conventional design criteria based on global displacement is also need to be revised to incorporate local deformation characteristics and current approach of displacement specification (L/800) is not only insufficient but also misleading.
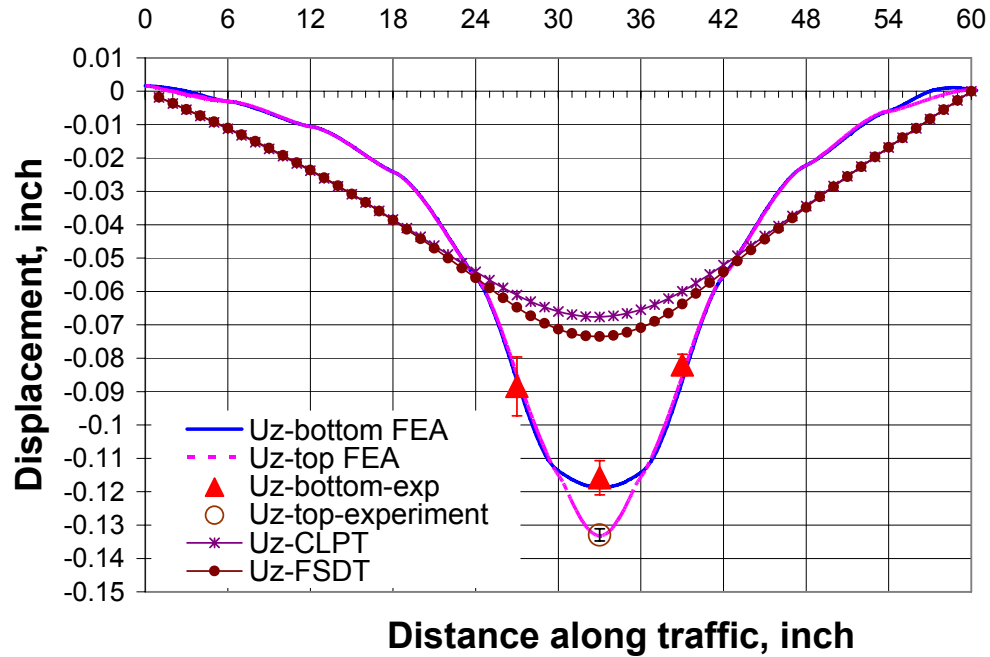
Figure 5.18 Local displacement behavior along traffic direction

(Vertical grid lines also represent web locations at 6 inch spacing)
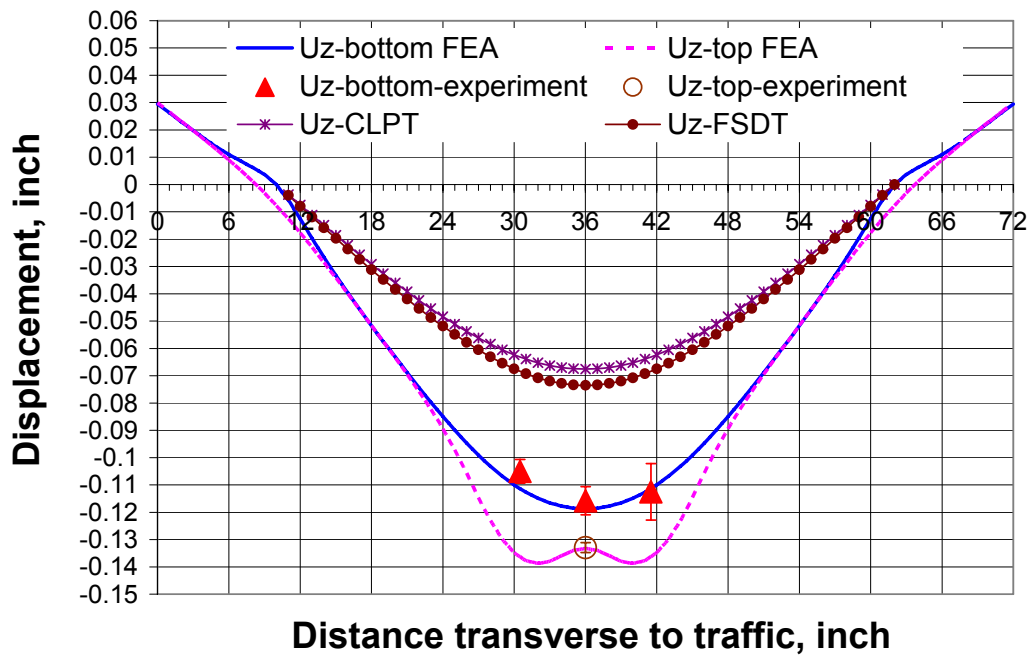
Figure 5.19 Displacement behavior along transverse to traffic direction
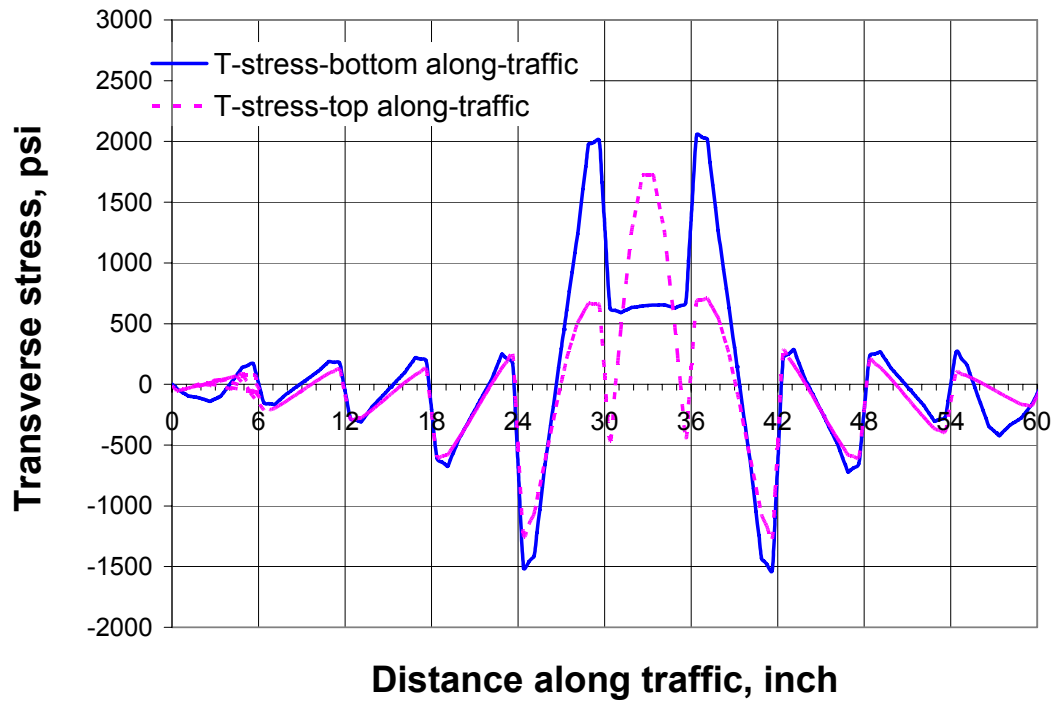
Figure 5.20 Local transverse stress distribution along traffic direction

(vertical grid lines also represent web locations at 6 inch spacing)
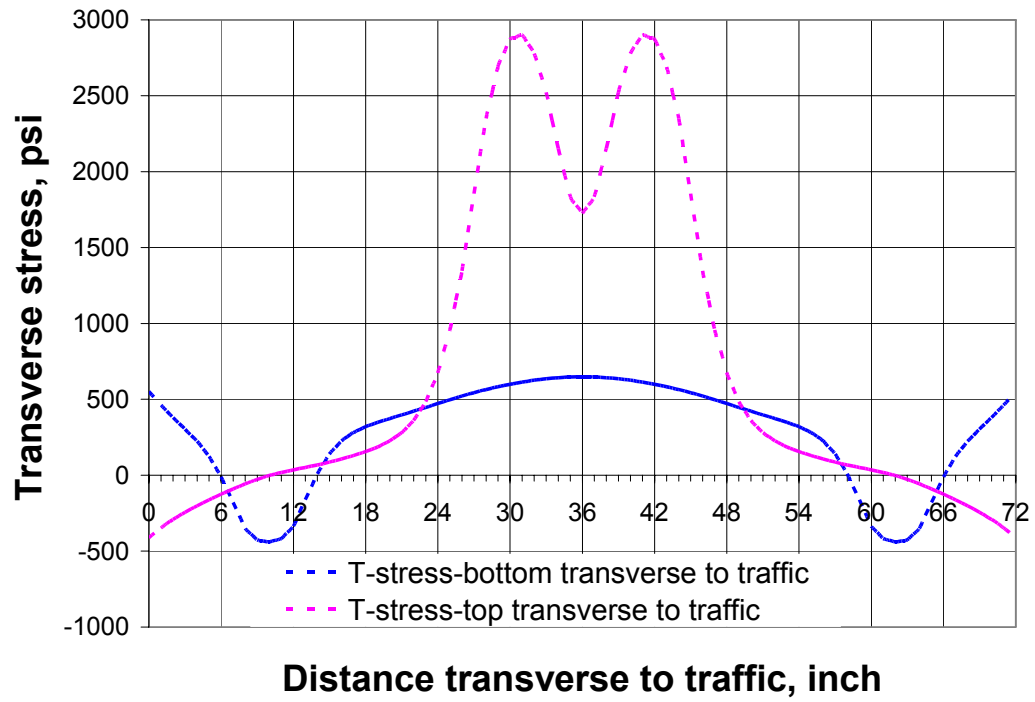
Figure 5.21 Local transverse stress distribution transverse to traffic direction
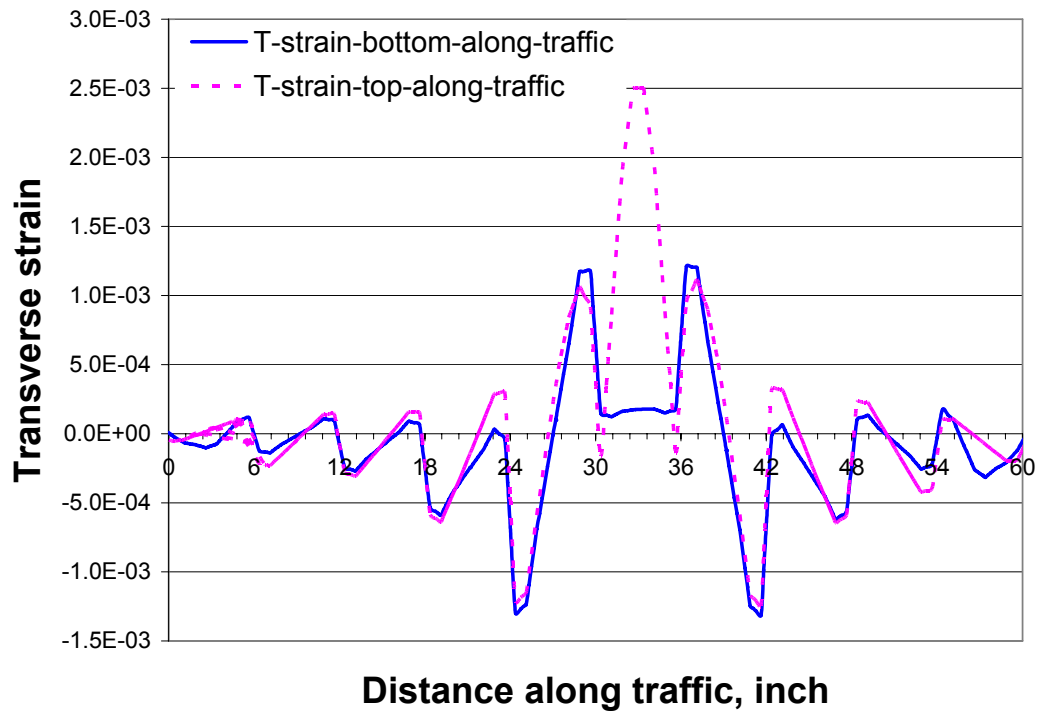
Figure 5.22 Local transverse strain distribution along traffic direction

(vertical grid lines also represent web locations at 6 inch spacing)
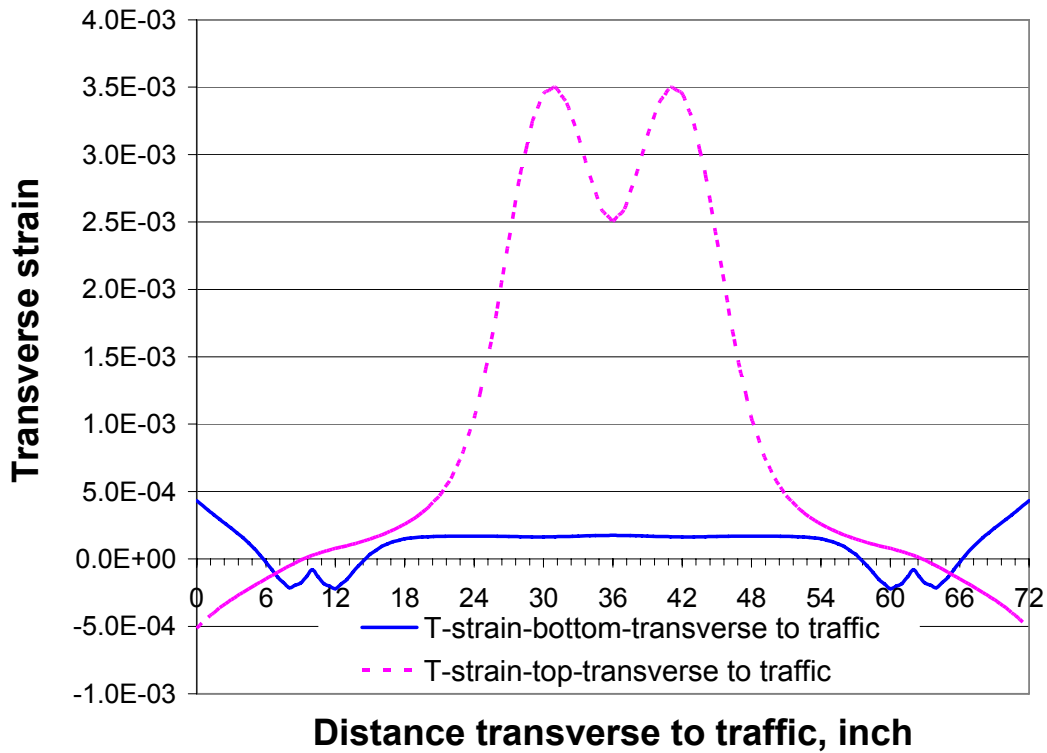
Figure 5.23 Local transverse strain distribution transverse to traffic direction

5.6 Conclusion

From experimental data it is observed that displacement and strain behavior of the deck are linear elastic under service load conditions. There is no evidence of initiation of damage at any location during service load test. Strains transverse to traffic (along fiber direction) are higher than strain values in the traffic direction. The small relative deflections between deck and stringer under service load show that the FRP deck system provides enough stiffness. It is also to be noted that no composite action between deck and stringers is observed consistent with design expectation. The deck-to-girder connection is very effective in resisting any uplift of the deck. The minimum failure load is approximately five times the service load and this indicates that the proposed FRP deck system from Strongwell Corporation is safe at the intended service load level. Local deformation analysis of cellular FRP composite deck provided vital information about variation of structural response (displacement, stress, strain) within the cellular geometry. Displacement and stress at top flange of cellular structure can be much higher compared to bottom span and therefore, design criteria based on global displacement alone is insufficient to characterize FRP composite deck. The difference in response of FRP composite deck compared

to conventional decks (concrete and steel) due to relative stiffness effect and geometry effect under conformable contact interaction should be considered for realistic design criteria development.

Acknowledgement

Chapter 6:   Strength and Fatigue Life Prediction

Failure mechanism and Fatigue life prediction of a cellular FRP composite bridge deck

[13] Prasun K. Majumdar, [14]John J. Lesko, [15]Thomas E. Cousins, [16]Zihong Liu

Abstract

Long term performance of fiber reinforced polymer (FRP) composite bridge deck is dependent on progressive damage in the materials (due to change in the internal stress state and material state) and still a subject of considerable interest as there is lack of understanding of the underlying mechanisms. Determination of strength and failure mode under actual service conditions plays a pivotal role for predicting possible damage initiation areas and eventually life of the bridge deck. In this research, a systematic approach to investigate the strength characteristics such as failure mode and failure sequence (first ply failure and ultimate failure) of a cellular FRP deck is presented. For the cellular deck system made of pultruded shapes, transverse tension (off-axis failure) is found to be the likely failure mode and corresponding critical elements which will control durability of the deck are identified. Stress analysis of FRP bridge deck is carried out using finite element model developed by ANSYS and failure function is expressed as function of stiffness degradation in the sub-critical element. Based on residual strength approach, a simplified framework is presented to predict the fatigue life of the cellular FRP composite bridge deck. The proposed framework only needs experimental data at the coupon level and the stress analysis at the structural level can take into account local effects due to conformable contact interaction between loading patch and FRP deck. Material response from local deformation analysis and fatigue analysis provide useful information which may help develop design criteria for FRP deck.

[13]Corresponding author. Graduate Research Assistant, Department of Engineering Science & Mechanics, 106 Norris Hall, Virginia Tech, Blacksburg, VA 24061, USA. Tel.:540-449-2282; Fax: 540-231-9187 Email: pkm2004@vt.edu

[14]Professor, Department of Engineering Science & Mechanics, 106 Norris Hall , Virginia Tech, Blacksburg, VA 24061, USA. Email: jlesko@vt.edu

[15]Professor, Department of Civil & Environmental Engineering, Virginia Tech, Blacksburg, VA 24061, USA. Email: tcousins@vt.edu

[16] Graduate Student, Department of Civil & Environmental Engineering, 200 Patton Hall, Virginia Tech, Blacksburg, VA 24061, USA. Email: lzh@vt.edu

6.1 Introduction

Fiber reinforced polymer (FRP) composites are increasingly being used in infrastructure applications such as bridge decks. However, there is lack of effort in understanding strength and failure mechanisms in FRP composite bridge decks under realistic service conditions. It has been observed that type of loading method controls the failure mode of cellular FRP decks made of pultruded shapes and use of conventional loading method is unrealistic. This may provide misleading information about damage accumulation areas for further strength and durability predictions. That research proposed a new simulated tire patch for loading on FRP deck which is likely to mimic the load effects produced by actual truck tire. Therefore, in this current study we will explore strength, failure mode and fatigue life of FRP composite bridge deck under simulated tire patch loading.

During failure test of large structural components such as FRP composite bridge deck, it is often difficult to pin-point failure due to inability to position sensors in exact failure locations (inaccessibility or lack of anticipation), lack of visibility of damage areas and apparently simultaneous (with their sequence unknown) failure at multiple locations. Common practices have been to rely upon audible noise, visible crack or large change in material response (such as load vs. displacement or strain behavior). This often gives a gross approximation of ultimate failure of the deck and design engineer takes care of the uncertainty with large factor of safety. However, the issue becomes critical when one considers long term performance of the composite structures as there is not much information available about the potential damage initiation areas and their effect on overall performance as the damage propagates. For composite materials with directional properties and complex stress state, it is also quite challenging to even define and characterize failure phenomenon. We will consider appearance of any visible damage as indicator of failure during experiment and in our ply level FEA analysis, failure of the 0-degree layer in the pultruded composite will be considered as the ultimate failure point of the structure. The failure mode and corresponding failure initiation areas will be identified for subsequent life prediction analysis.

Most durability studies have been limited to coupon-level testing, and the development of life prediction for actual bridge deck structure based on the kinetics of damage mechanisms in coupon specimen is very limited. In this current study, we will use the "critical element

93

approach" (Reifsnider 1986; Reifsnider and Gao 1991; Reifsnider et al. 2000; Case 2002) to predict fatigue life based on residual strength and stiffness degradation information. Details of strength, failure analysis and life prediction methodologies will be discussed in the following sections.

6.2 Fatigue Life Prediction Methodology

In the residual strength approach, fatigue failure is assumed to occur when the residual or remaining strength is equal to the applied stress. In particular, Reifsnider postulated that remaining strength can be used as a measure of the damage and that remaining strength is an internal state variable. The remaining strength will depend upon the load level and number of fatigue cycles (or time). In general, the reduction in strength can be non-linear, so that the sequence of damage events can affect the length of life. The ability of this approach to capture such path-dependence is a distinct advantage over linear models such as Miner's rule popularly used for conventional materials (metals).

In critical element approach, the remaining strength of "critical element" governs the life of the entire structure. Degradation and eventual failure of the sub-critical elements serves only to redistribute the stress to the critical elements, eventually causing ultimate failure of the structure. Thus, the keys to the critical element approach are to identify the critical element(s), to determine the fatigue performance of the critical elements, and to identify and quantify the damage mechanisms and their kinetics in the sub-critical elements. Appropriate failure functions must be selected to model the sub-critical damage mechanisms and to calculate the remaining strength in the critical element(s).

Using a non-linear rate equation to describe the damage processes, Case has derived a strength evolution integral which has been tested extensively for a variety of problems and materials (Case 2002). This equation has the form:

$$Fr = 1 - \left[\int_0^n \left(\left(1 - Fa \right)^{\frac{1}{j}} \right) \frac{dn}{N} \right]^j$$

94

Here, Fr is the normalized remaining strength, Fa is the applied stress (or more generally, the failure function such as maximum stress, Tsai-Hill, etc.), and j is considered to be a material constant (The value of j is determined empirically).

The equation reduces to $Fr = 1 - (1 - Fa)\left[\dfrac{n}{N}\right]^{j}$ for constant amplitude and

$$Fr = 1 - \left[\sum_{i=1}^{n-steps}\left((1-Fa_i)^{\frac{1}{j}}\right)*\frac{\Delta n_i}{N_i}\right]^{j}$$ for variable amplitude loading.

As damage occurs in the sub-critical elements, the stress level in the critical element increases, and Fa increases with time or cycles. To apply the strength evolution integral to predict fatigue life, the following information is required: 1) the fatigue S-N curve for the critical element, 2) the stiffness changes in the sub-critical elements with cycles, and 3) the value of the j parameter. These input parameters are typically found by performing coupon level fatigue testing. However, the first step is to identify critical element from strength and failure analysis.

6.3 Experimental Observation of Failure Locations

Figure 6.1 Failure Test setup for 5ft by 6 ft specimen

Failure tests conducted on 33 ft by 22 ft large pultruded FRP deck system on beam-stringer super structure (described in previous chapter) and also 5 by 6 ft deck panels (Fig. 6.1) showed

consistent failure locations. We will use 5 by 6 panel strength test data along with FEA correlation to explore failure sequence and identify first failure initiation point which will define the critical element for further fatigue life prediction studies.
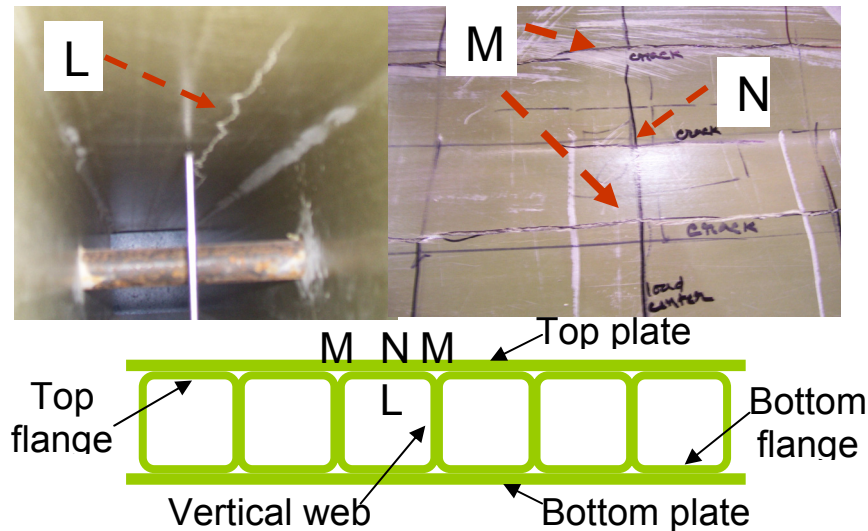

Figure 6.2 Failure locations in a cellular FRP deck under tire patch loading

A representative diagram of failure locations in a cellular FRP deck is shown in Fig. 6.2. Location-L is span center inside the cellular structure (top flange of the pultruded tube section) just under the loading patch, Location-M is the top surface of the deck along the vertical web locations and Location-N is the span location at the top of the deck under the loading patch. A displacement transducer (LVDT) is placed to monitor response at location-L but no sensor could be placed at location-M and location-N since those are directly under the loading patch. Pictures were taken at frequent intervals to monitor first initiation of failure at location-L. A representative plot of Load vs. displacement (top flange location-L) behavior is shown in Fig. 6.3. From the response, it is clear that first change in material response (deviation from linear behavior) occurs at around 72 kips and this is believed to be initiation of first crack. From the real time photographs taken also confirms that crack appears at location-X (bottom surface of top flange of tube) at around 74-76kips. The crack extends in the fiber direction of pultruded tube and this is characteristic of a transverse tension failure. The load vs. displacement behavior also indicates failure at around 100-106 kips where audible noise was heard. Upon unloading, it is observed that failure occurred at Location-M (tensile failure of top plate along vertical web locations) and location-N (compression failure of top plate at span center). In order to further verify the first failure location, a separate test panel was loaded until crack appears at location-L

and then unloaded. Upon removal of loading patch, it is observed that no failure at location-M and location-N. This confirms that Location-L is the point of initiation of first failure and other two failure locations are secondary failures depending on damage progression as the loading continued.
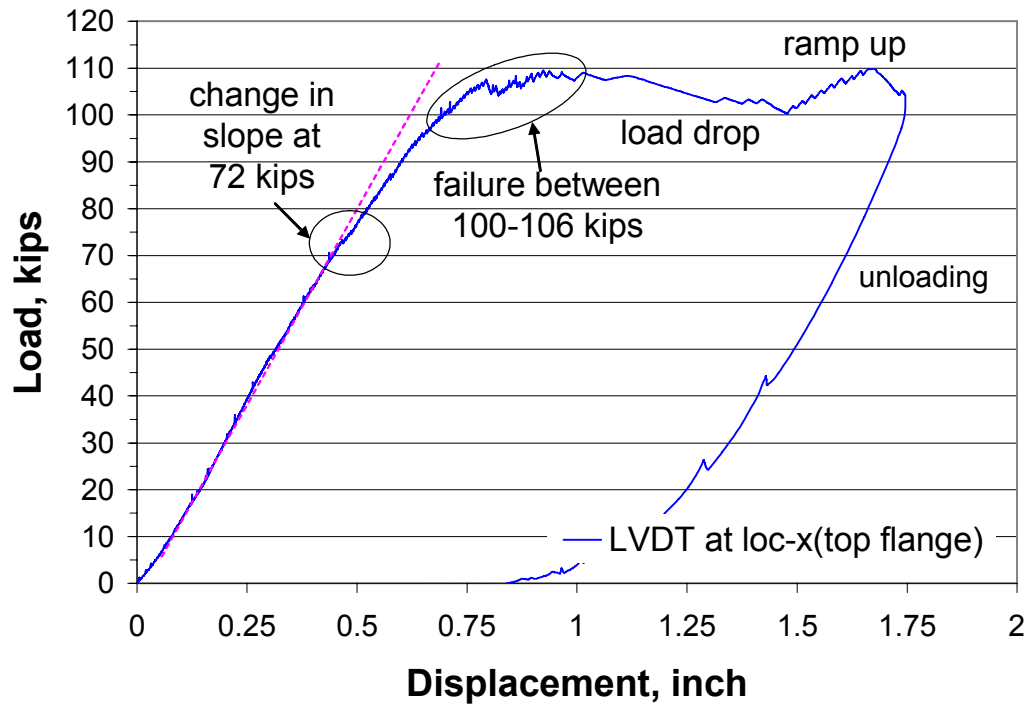
Figure 6.3 Load vs. displacement behavior at top flange (location-L in Figure 6.2)

6.3.1   FEA Ply Level Failure Analysis

A 3D finite element model is developed using ANSYS to predict first ply failure and ultimate failure. The model used layered nonlinear shell element (shell91 capable of large deformation) for deck and shear deformable beam element (beam189) for supporting structure.
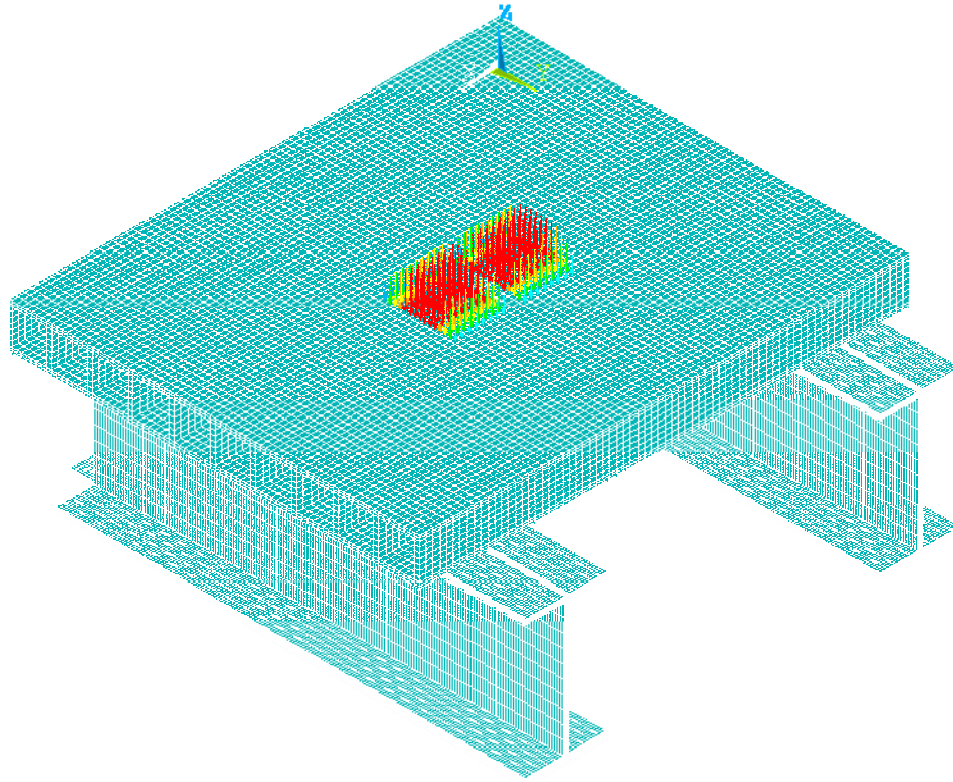
Figure 6.4 FEA model of deck panel for failure analysis

The pultruded FRP deck consists primarily of three types of layers (A-glass CSM, E-glass CSM and E-glass roving) arranged in different lay-up sequence for plate and tube section. Exact lay-up sequence is obtained through personal contact with manufacturer (not disclosed in this work). Properties of each layer were estimated using micromechanics equations of laminated composites (Mallick 1993; Hyer 1998) and strength data is taken from Strongwell design manual (reports conservative value). For prediction of strength, both maximum stress and Tsai-Wu criterion are considered. FEA prediction of the initiation of failure is compared with experimental observations and they are in reasonable agreement (Table 6.1).

From above failure analysis, it is found that the E-glass roving layer at the bottom of the top flange of the tube (Location-L in Figure 6.2) controls the failure of the structure and this layer will be considered as the critical element for fatigue life prediction.

Table 6.1 Prediction of initiation of failure (critical element)

Load (kips)	First ply-failure (CSM layer at Location-X)	Failure of critical element (0-deg E-glass roving at Location-X)	Failure at location-Y	Failure at location-Z
EXP		74 (first visible crack)	100-106	100-106
FEA (Max stress)	54.16	71.46		
FEA (Tsai-Wu)	50.34	65.8		

6.4 Determination of Input Parameters for Fatigue Life Prediction

We will need to determine few parameters to be used as input for the life prediction methodology described earlier. From failure analysis, it is found that transverse tension is the first failure mode for the cellular FRP composite bridge deck. Therefore, transverse tension strength and fatigue tests are carried out on 3/8 and 1/8 inch plate samples with R-ratio of 10 at frequency of 10 Hz.
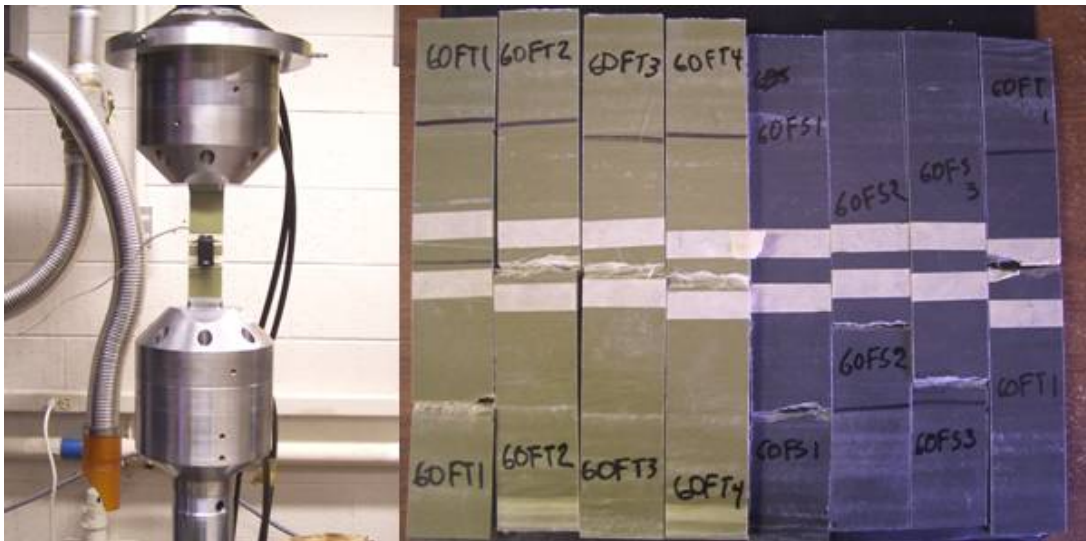
Figure 6.5 Transverse tension fatigue test with plate samples

Each specimen is subjected to cyclic loading until failure and response of material such as displacement and strain behavior are recorded in real-time. A representative picture of test setup and failed specimens is shown in figure 6.5.

6.4.1 Estimated Life from S-N Plot

Fatigue strength is determined at different applied load levels and the corresponding data is presented in popular strength vs. No of cycles plot in Fig. 6.6 (S-N diagram). A least square curve fit to this data gives a relationship for estimating life of the coupon specimen as a function of applied stress level.

$$Log(N) = aLog(Fa) + Log\ b \quad or \quad N = b(Fa)^a$$

The curve fitting constant parameters are a= -9.02 and b= 9.634.
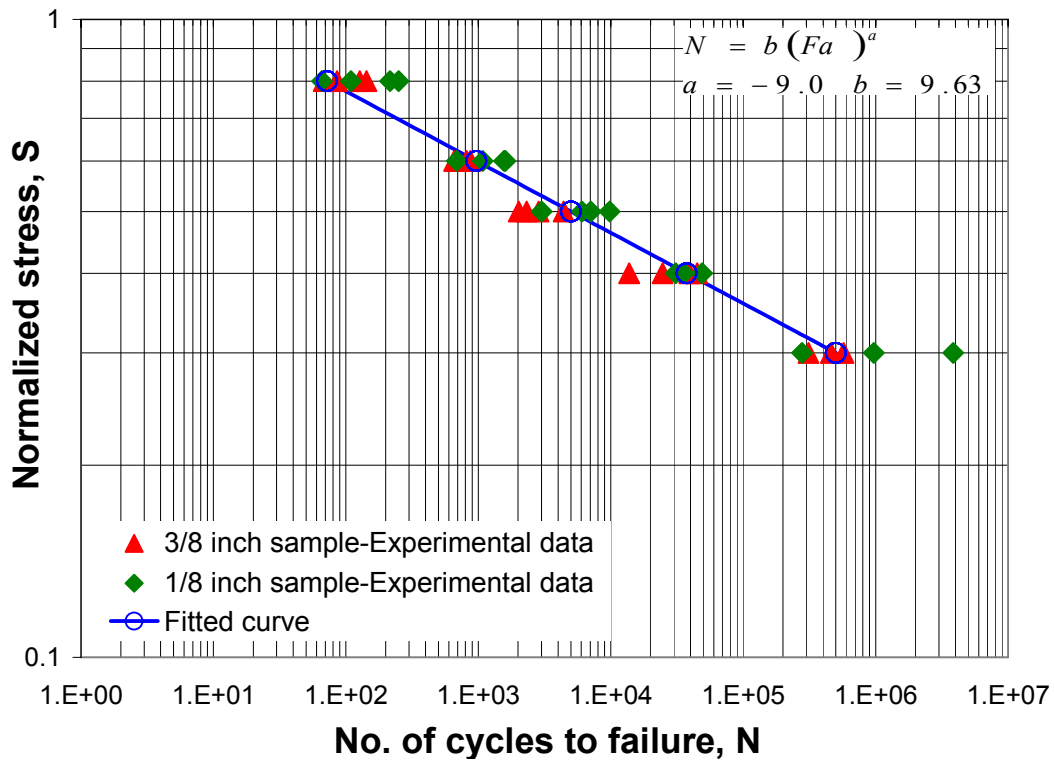
Figure 6.6 S-N data from coupon level fatigue test

6.4.2 Determination of j Value from Residual Strength Data

Residual strength is determined at different life intervals (25%, 50% and 75% of life) and corresponding data is plotted in Figure 6.7. The experimental data is compared with predicted residual strength determined using constant amplitude expression:

$$Fr = 1 - (1 - Fa)\left[\frac{n}{N}\right]^j$$

The value of parameter, j is determined (j=1.7652) such that sum of error squared is minimized.
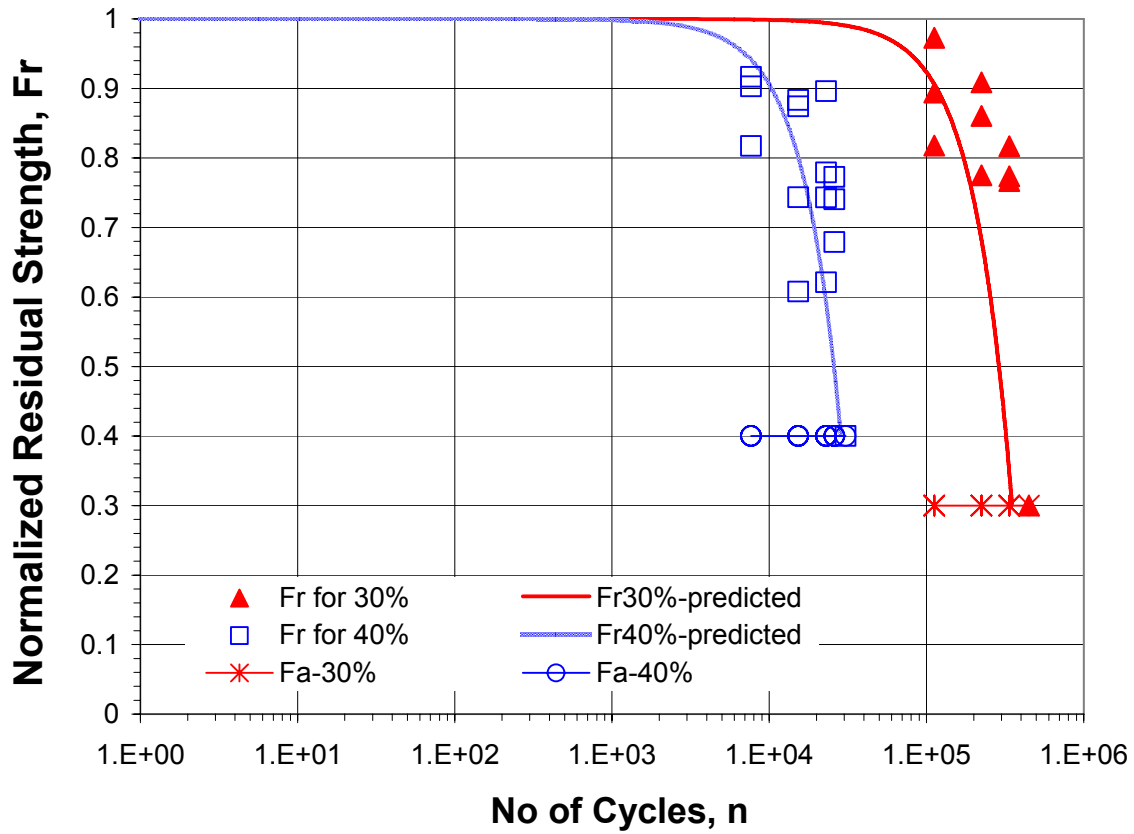
Figure 6.7 Variation of Residual strength with no of cycles

6.4.3 Off-Axis Stiffness Degradation Model

Transverse stiffness reduction with number of fatigue cycles is also determined experimentally at different stress levels (Fig. 6.8). The curves show three regions of damage which are typically observed in FRP composites. During initial region-I , there is a sharp drop in stiffness due to matrix cracking, region-II demonstrates growth of matrix crack and delamination, and finally in region-III, there is interactions of various damage causing sudden death.
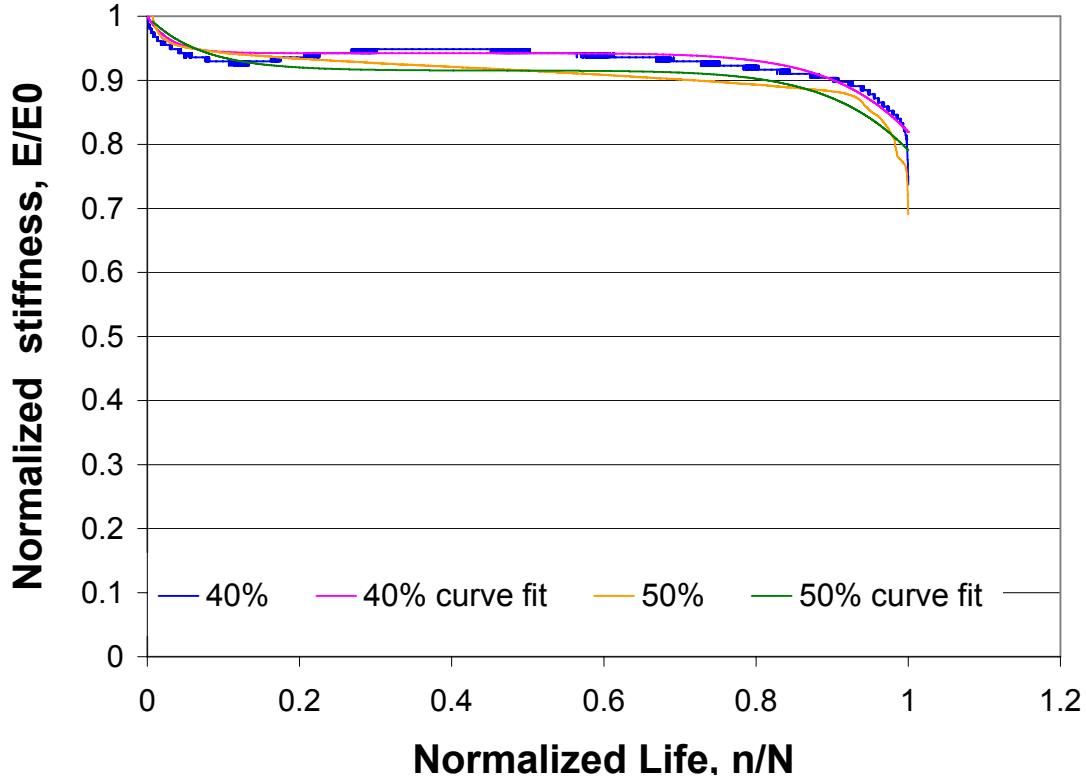
Figure 6.8 Normalized off-axis stiffness degradation from coupon test

The data also shows stress level dependence and therefore, it is fitted with an exponential series so that it can be extrapolated to other stress levels.

$$\hat{E} = (\hat{E}1 - \hat{E}2)\, Exp\left[-\left(\frac{\hat{n}}{N_1}\right)^{m1}\right] + \hat{E}2\ Exp\left[-\left(\frac{\hat{n}}{N_2}\right)^{m2}\right]$$

The curve fitting parameters can be determined from experimental data. The hat ($^$) symbol denotes normalized quantities. Thus, E-hat is the normalized stiffness, which is a function of the normalized life (n-hat) .The first stiffness parameter E1-hat   is the initial normalized stiffness and is therefore equal to 1. The second stiffness parameter   is a normalized stiffness plateau that might exist in a cross-ply laminate and roughly describes the stiffness at half-life (n/N-fail = 0.5) for the quasi-isotropic laminates. The parameters N1 and N2 roughly correspond to the normalized lives at the transition from one region to another. Finally, m1 and m2 are parameters which describe the shape or breadth of the transitions. For this study, we consider parameters N2=1.2, m1=1, m2=10.76(average) so that they become independent of

stress level. However, parameters N1 and E2-hat are dependent on stress level (Fig 6.9 and 6.10) and are found by curve fitting to experimental data. The expressions are:

E2-hat=1-0.0637*(Fa)-0.2065*(Fa)^2

N1= 0.0011*e$^{(8.3699*Fa)}$.

Now the projected curves for stiffness degradation at lower stress level are found and shown in figure 6.11.
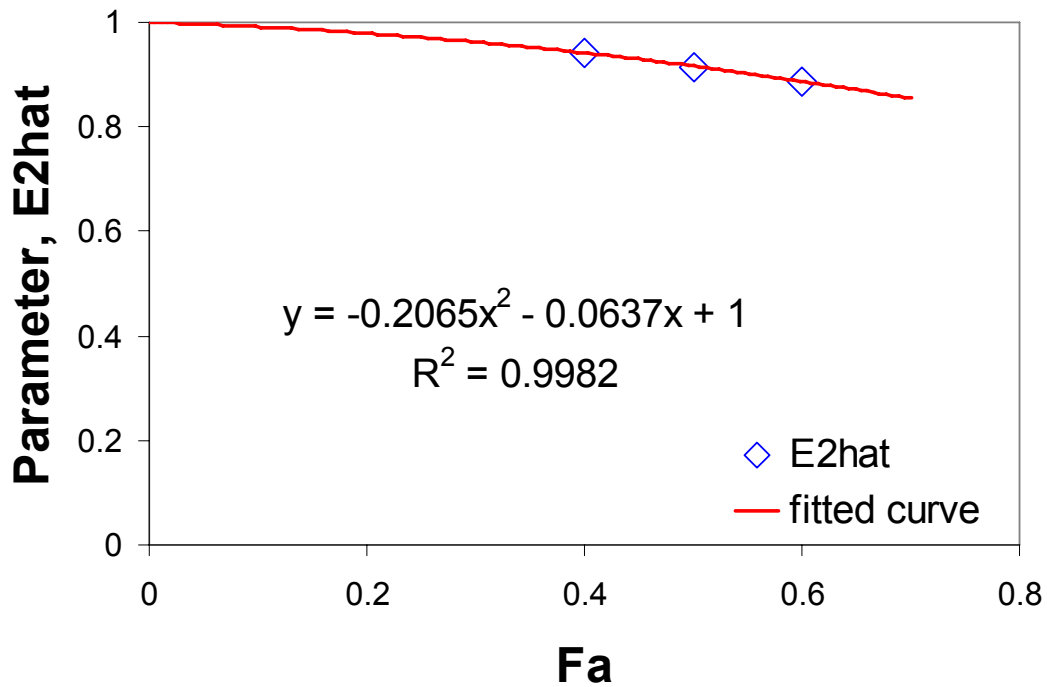
Figure 6.9 Determination of curve fit parameter E2hat

$$y = 0.0011e^{8.3699x}$$
$$R^2 = 0.9999$$

◇ N1
— fitted curve
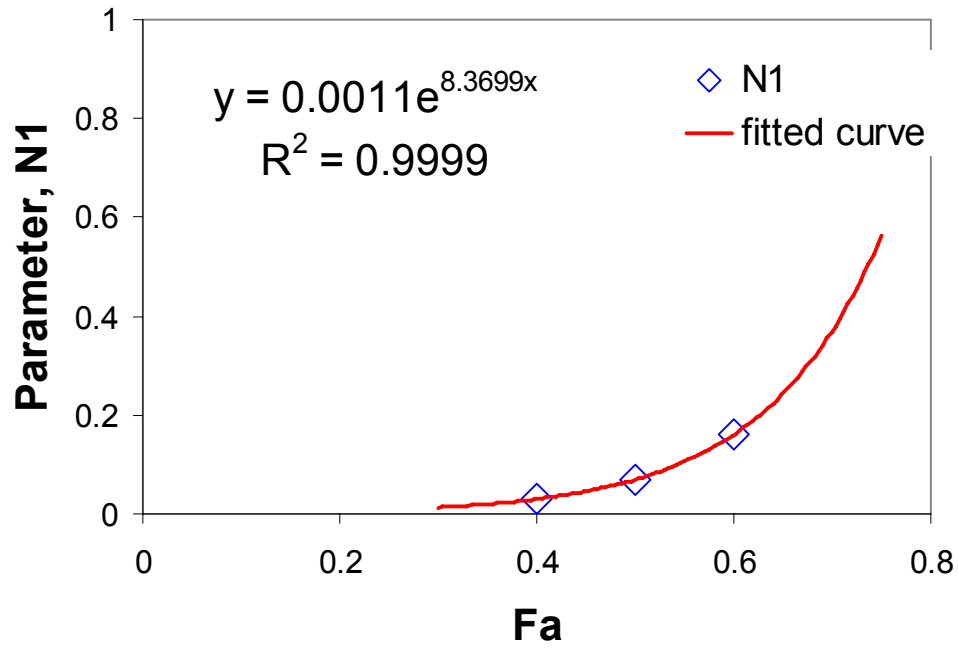
Figure 6.10 Determination of curve fit parameter N1

Decreasing Fa

◆ Fa=0.2 ■ Fa=0.3 ▲ Fa=0.4 ✕ Fa=0.5 ✳ Fa=0.6 ● Fa=0.7
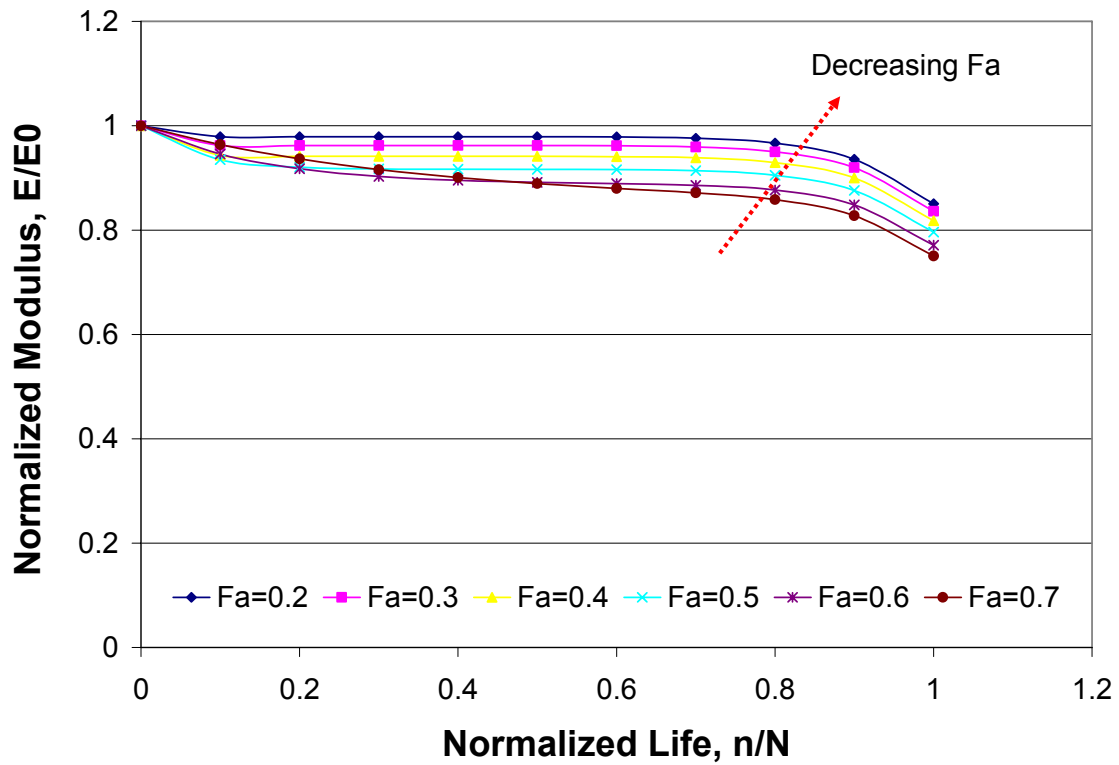
Figure 6.11 Prediction of stiffness degradation at different load level

6.4.4 Failure Function

Stress analysis of FRP deck under simulated tire patch loading is performed using FEA model generated by ANSYS. Using parametric variables, the stress re-distribution within the critical elements (0-deg layers in top flange of tube) is monitored as a function of change in transverse stiffness of sub-critical elements (CSM layers in top flange of tube).

The variation in stress state is plotted in Figure 6.12 and can be expressed as:

$$\sigma_2^{0^0\,ply}\left(\frac{E_2}{E_2^{\,0}}\right) = \left(4.8816*\left(\frac{E_2}{E_2^{\,0}}\right)^2 - 35.923*\left(\frac{E_2}{E_2^{\,0}}\right) + 234.35\right)\frac{Total\;load\,(kips)}{2}$$

The above expression is valid for load per tire less than 30 kips and for load per tire more than 30 kips, use

$$\sigma_2^{0^0\,ply}\left(\frac{E_2}{E_2^{\,0}}\right) = \left(4.2521\left(\frac{E_2}{E_2^{\,0}}\right)^2 - 30.919\left(\frac{E_2}{E_2^{\,0}}\right) + 198.95\right)\frac{Total\;load\,(kips)}{2}$$

Using maximum stress criterion, the failure function is written as $Fa(n) = \dfrac{\sigma_2^{0^0\,ply}(n)}{Y_t}$.

$$y = 4.8816x^2 - 35.923x + 234.35$$
$$R^2 = 1$$
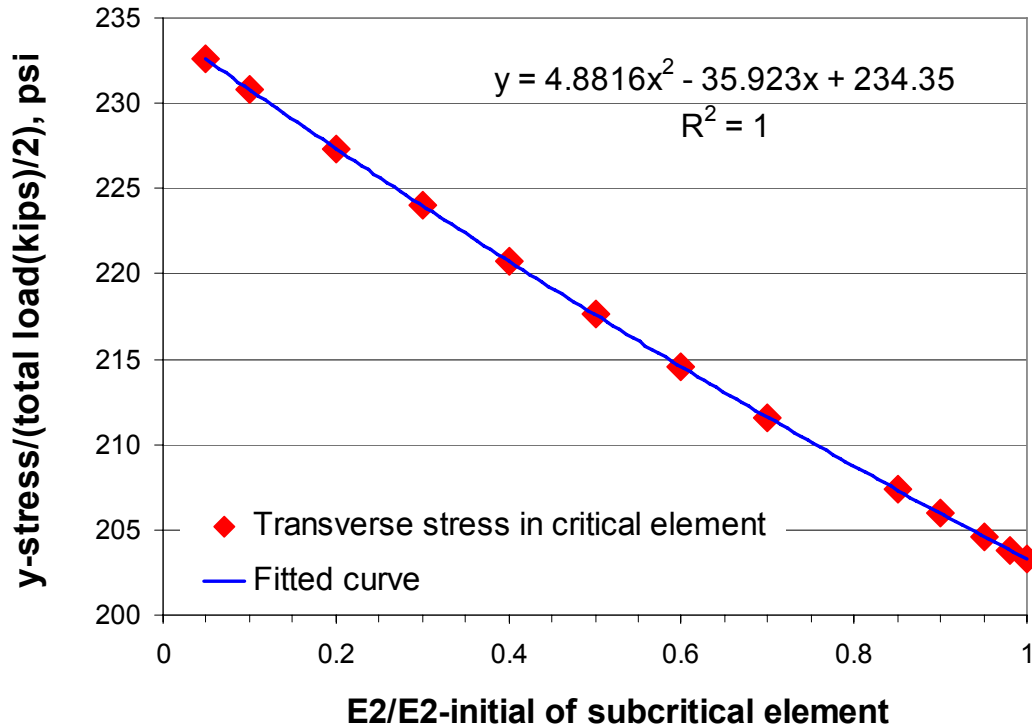
Figure 6.12 Transverse stress in critical element as a function of stiffness degradation in sub-critical element

6.5   Simplified Framework for Life Prediction of Bridge Deck

We now have all the input required to predict the life of the cellular FRP bridge deck. The framework is flexible in the sense that one can easily accommodate changes in geometry, materials and loading by changing the stress vs. stiffness degradation analysis using FEA. A flow diagram of the simplified methodology is shown in Figure 6.13:
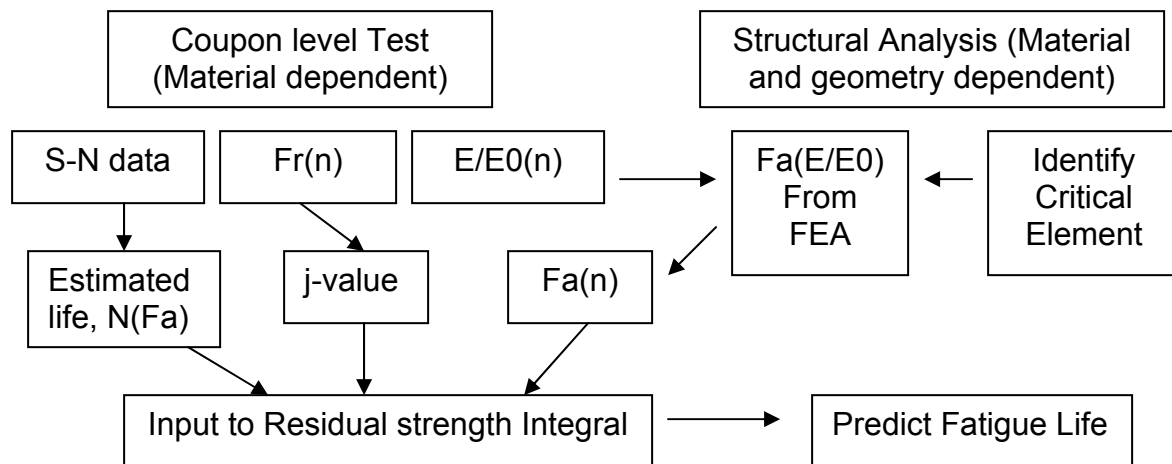
Figure 6.13 Simplified life prediction framework for FRP deck
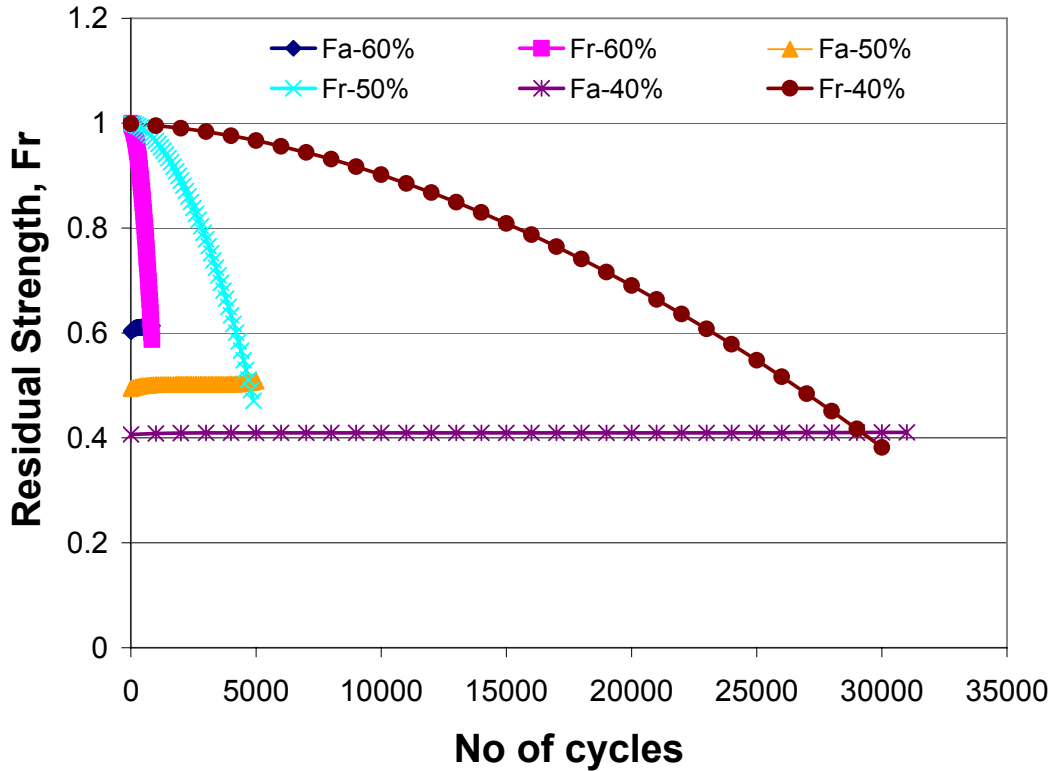
Figure 6.14 Residual strength of FRP deck

Using the above mentioned methodology, residual strength (Fr) and failure function (Fa) can be plotted as a function of number of cycles. Failure is identified where Fr equals Fa. A representative plot of predicted residual strength of FRP bridge deck is shown in Figure 6.14. The advantage of this simplified framework is that it requires little or no experiment at the structural level and minimum experiment at coupon level is sufficient to get model parameters. Also, coupon level analysis is independent of structural geometry (only constituent material dependent) and structural level analysis can be easily varied to accommodate different geometry. Since residual strength calculation is uncoupled from structural stress analysis, it reduces level of complexity in automating the calculation and can be done even using a simple spreadsheet.

6.5.1 Fatigue Experiment on FRP Deck Panel

It is often difficult to do structural level fatigue test with FRP composite deck system due to limited availability of good specimens and amount of time involved. We obtained several deck panels (5 ft by 6 ft) for fatigue testing by cutting pieces from 33 ft by 22 ft deck system tested in our lab. Our validation consisted of limited number of actual deck samples (Total four) deemed

to be of good quality. One of the salient features of this fatigue test is the use of simulated tire patch for loading (Figure 6.15) which produces conformable contact like real truck tire. To the best of our knowledge, there is no other research that reported the use of simulated tire patch for fatigue test on any bridge deck

The S-N curve for this experimental fatigue data is compared with predicted life curve from residual strength based methodology described earlier (Figure 6.16). There is reasonable agreement between experiment and prediction. The prediction appears more conservative because crack initiation was identified by visual inspection of real-time photographs during experiment but actual failure may have initiated earlier.

Figure 6.15 Fatigue test on FRP deck using simulated tire patch
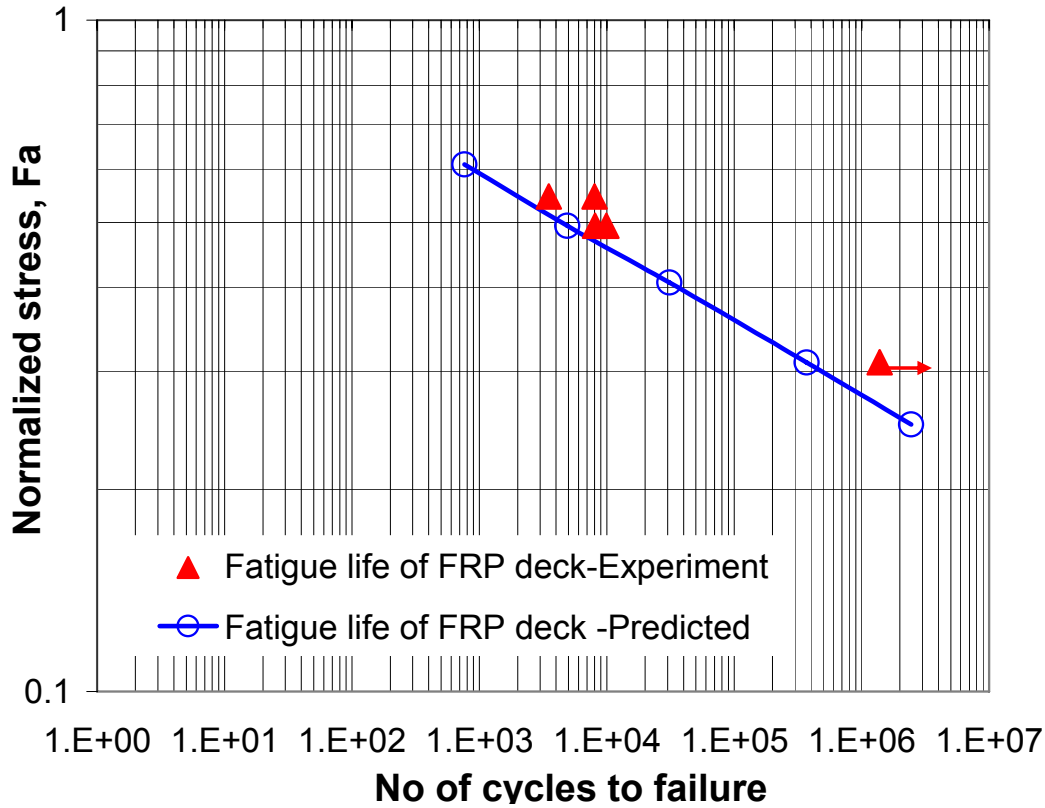
Figure 6.16 Predicted Life of FRP bridge deck

6.6 Conclusion

Failure analysis of cellular FRP deck under simulated tire patch loading was performed using finite element model developed by ANSYS. Transverse tension was identified as failure mode both experimentally and using ply-level failure analysis. First crack was observed at the bottom of the top flange of tube and this is characteristic of localized effect of simulated tire patch on cellular FRP deck. A simplified framework is presented for fatigue life prediction of FRP composite bridge deck with little or no experiment needed at the structural level. The "critical element method" utilizes damage kinetics from coupon level data and integrates with stress analysis at structural level to predict fatigue life based on residual strength approach. Predicted life is compared with fatigue test data obtained from fatigue test on FRP deck panels using simulated tire patch. There is reasonable agreement between predicted value of life and experimental observations. Fatigue tests on FRP deck also confirmed transverse tension failure mode at the same location as predicted from failure analysis. This proposed simplified

framework can be used as a design tool to study geometry effects and only need to reevaluate the stress analysis which is uncoupled from life prediction.

Acknowledgement

Chapter 7: Conclusions and Recommendations

7.1 Contribution to Bridge Deck Research

The following is a list of accomplishments from this dissertation research:

7.1.1 Observations

- The contact pressure distribution of real truck loading is non-uniform with more concentration near the center of the contact area, in direct contrast to the conventional steel patch loading that produces stress concentration near edges. Due to the localization of load under the tire, conventional uniform patch loading is not suitable for performance evaluation of FRP composite deck systems with cellular geometry and relatively low modulus as compare to concrete decks.

- There are significant differences in response of FRP deck compared to conventional decks due to relative stiffness and geometry effect. The stress, strain and displacement response of the cellular FRP deck is highly localized and shows significant variation within the cellular geometry. Design criteria based on global deformation is insufficient to characterize such cellular FRP composite deck.

- New design criteria needs to be developed particularly for FRP deck and local deformation behavior due to conformable contact interaction should be considered. Fatigue performance could also be integrated into the design criteria such that allowable stresses (at designed load level) contribute to value of strength level below desired fatigue life.

- For FRP deck manufactured by pultruded shapes, transverse tension is identified as the failure mode and failure initiation occur at the top flange of the tube directly under the loading patch.

- Adhesive bonding is promising for joining FRP composite bridge deck panels. It is observed that efficient design of joint (such as incorporating scarf geometry) can improve performance of the bridge deck panel. However, care should be taken to ensure quality of the joint (avoiding dry areas and proper fit of components).

- Identification of failure mode is critical for predicting fatigue life of the bridge deck. Nonlinear models such as residual strength based critical element approach can be used for life prediction of bridge deck. The model can work with minimum experimental data at the

coupon level and stress analysis from FEA model of the structure can be integrated into life prediction calculation. No structural level testing is required for the model to work and can only be used for validation purposes.

7.1.2 Specific Contributions

- A new simulated tire patch is proposed for loading on FRP deck and the load distribution are characterized by contact area studies using pressure sensitive sensors and 3D contact analysis using finite element method. The proposed profile can be a useful design tool for performance evaluation of cellular FRP deck.

- An efficient adhesive joint configuration with scarf geometry is proposed for joining cellular FRP deck and it is tested at structural level for desired performance.

- After extensive performance testing (laboratory and field) and analysis, a low cost pultruded FRP composite deck system has been successfully installed to rehabilitate a historically significant Hawthorne Street bridge in Covington, Virginia. This is the first installation of a FRP composite bridge deck in Virginia and the new deck provided benefit of increasing live load rating of the bridge. Such cellular FRP composite deck system made of pultruded tube and plates can be a viable alternative to conventional bridge decks.

- Failure mode of the cellular FRP deck is identified as transverse tension (off-axis failure) as opposed to significant amount of confusing literature about punching shear as typical failure mode. No other research work could characterize the conformable contact interaction behavior between tire patch and FRP deck, and therefore could not identify realistic failure mode which is critical for durability studies.

- A simplified residual strength based life prediction methodology has been proposed for application to FRP composite bridge decks and the proposed framework takes into account stress analysis with conformable tire patch loading.

7.2 Recommendation for Future Research

- More in depth analysis of adhesive joint for structural application is required with particular attention to environmental effects on joint performance.

- Since classical plate theories can not capture deformation behavior of cellular FRP composite bridge deck, new theories need to be developed to fully understand response of FRP bridge

deck. It is likely that folded plate theory and theories on stiffened plates might be able to represent deformation behavior of such cellular FRP deck.

- The fatigue life prediction methodology proposed in this work can be extended and further validated with more structural level testing. Parametric study can be carried out on material and geometry based on fatigue performance, and can be correlated to develop design criteria.

References

AASHTO-LRFD (1998). Design Specifications (Second edition). Washington, D.C.

AASHTO (1996). Standard Specifications for Highway Bridges. Washington, D.C.

Abdel Wahab, M. M., I. A. Ashcroft, et al. (2004). "Finite element prediction of fatigue crack propagation lifetime in composite bonded joints." Composites Part A: Applied Science and Manufacturing 35(2): 213-222.

Adams RD, C. J., Wake WC. (1997). Structural Adhesive Joints in Engineering. London, Chapman & Hall.

Al-Qadi, I. L., A. Loulizi, et al. (2002). "Pavement response to dual tires and new wide-base tires at same tire pressure." Transportation Research Record(1806): 38-47.

Alagusundaramoorthy, P., I. E. Harik, et al. (2006). "Structural behavior of FRP composite bridge deck panels." Journal of Bridge Engineering 11(4): 384-393.

Alampalli, S. (2000). Modal analysis of a fiber-reinforced polymer composite highway bridge, San Antonio, TX, USA, Society of Photo-Optical Instrumentation Engineers, Bellingham, WA, USA.

Alampalli, S. (2006). "Field performance of an FRP slab bridge." Composite Structures 72(4): 494-502.

Alampalli, S. and J. Kunin (2002). "Rehabilitation and field testing of an FRP bridge deck on a truss bridge." Composite Structures 57(1-4): 373-375.

Alampalli, S. and J. Kunin (2003). "Load testing of an FRP bridge deck on a truss bridge." Applied Composite Materials 10(2): 85-102.

Aluri, S., C. Jinka, et al. (2005). "Dynamic response of three fiber reinforced polymer composite bridges." Journal of Bridge Engineering 10(6): 722-730.

Anon (2001). "FRP decks help control corrosion." Better Roads 71(5): 46.

ANSYS. "ANSYS INC." from http://www.ansys.com

Aref, A. J., S. Alampalli, et al. (2005). "Performance of a fiber reinforced polymer web core skew bridge superstructure. Part I: Field testing and finite element simulations." Composite Structures 69(4): 491-499.

Aref, A. J., S. Alampalli, et al. (2005). "Performance of a fiber reinforced polymer web core skew bridge superstructure. Part II: Failure modes and parametric study." Composite Structures 69(4): 500-509.

ASCE Emerging Materials for Civil Infrastructure-State of the Art Review., American Society of Civil Engineers

Atadero, R., L. Lee, et al. (2005). "Consideration of material variability in reliability analysis of FRP strengthened bridge decks." Composite Structures 70(4): 430-443.

Bakis, C. E., L. C. Bank, et al. (2002). "Fiber-reinforced polymer composites for construction - State-of-the-art review." Journal of Composites for Construction 6(2): 73-87.

Ballinger, C. A. (1992). Advanced composites in the construction industry, Anaheim, CA, USA, Publ by SAMPE, Covina, CA, USA.

Bank, L. (2005). "Fiber-reinforced grid system provides bridge with 75-year life." Advanced Materials and Processes 163(8): 23-24.

Berbinau, P., C. Soutis, et al. (1999). "Effect of off-axis ply orientation on 0[degree sign]-fibre microbuckling." Composites Part A: Applied Science and Manufacturing 30(10): 1197-1207.

BLAB, R. (1999). Introducing Improved Loading Assumptions into Analytical Pavement Models Based on Measured Contact Stresses of Tires. International Conference on Accelerated Pavement Testing. Reno, NV.

Bogdanovich, A. E. and I. Kizhakkethara (1999). "Three-dimensional finite element analysis of double-lap composite adhesive bonded joint using submodeling approach." Composites Part B:Engineering 30(6): 537-551.

Bogdanovich, A. E. and S. P. Yushanov (1999). "Progressive failure analysis of adhesive bonded joints with laminated composite adherends." Journal of Reinforced Plastics and Composites 18(18): 1689-1707.

Boyd, S. W., J. M. Dulieu-Barton, et al. (2006). "Stress analysis of finger joints in pultruded GRP materials." International Journal of Adhesion and Adhesives 26(7): 498-510.

Boyd, S. W., I. E. Winkle, et al. (2004). "Bonded butt joints in pultruded GRP panels--an experimental study." International Journal of Adhesion and Adhesives 24(3): 263-275.

Brinson, H. F. and J. W. Grant (1986). "Mechanical properties for durability predictions of FRP bonded joint." Composite Structures 6(1-3): 107-121.

Busel, J. P. (2002). "Engineered FRP bridge decks- solutions for the future." SAMPE Journal 38(5): 46-48.

Busel, J. P. and J. D. Lockwood (2000). Engineered FRP products in civil engineering, Boston, MA, Soc. for the Advancement of Material and Process Engineering.

Case, S. W., and Reifsnider, K. L. (2002). Damage Tolerance and Durability of Material Systems. New Tork, John Wiley & Sons, Inc.

Chan, T. H. T., Z. X. Li, et al. (2001). "Fatigue analysis and life prediction of bridges with structural health monitoring data -- Part II: application." International Journal of Fatigue 23(1): 55-64.

Chen, D. and S. Cheng (1989). Stress distribution in plane scarf and butt joints, San Diego, CA, USA, Publ by American Soc of Mechanical Engineers (ASME), New York, NY, USA.

Chiewanichakorn, M., A. J. Aref, et al. (2007). "Dynamic and fatigue response of a truss bridge with fiber reinforced polymer deck." International Journal of Fatigue 29(8): 1475-1489.

Coleman, J. T. (2002). Continuation of Field and Laboratory Tests of a Proposed Bridge Deck Panel Fabricated from Pultruded Fiber-Reinforced Polymer Components. Blacksburg, VA, Virginia Polytechnic Institute and State University. MS.

Coogler K, H. K., Wan B, Rizos DC, Petrou MF. (2005). "Critical Evaluation of Strain Measurements in Glass Fiber-Reinforced Polymer Bridge Decks." Journal of Bridge Engineering 10(6): 704-712.

Datta, P. K., S.-C. Kwon, et al. (2002). Fatigue Studies of FRP Composite Decks at-30°C and 50°C, Kitakyushu, Japan, International Society of Offshore and Polar Engineers, Cupertino, CA 95015-0189, United States.

Davalos, J. F., P. Qiao, et al. (2001). "Modeling and characterization of fiber-reinforced plastic honeycomb sandwich panels for highway bridge applications." Composite Structures 52(3-4): 441-452.

Davey, S. W., G. M. Van Erp, et al. (2001). "Fibre composite bridge decks -- an alternative approach." Composites Part A: Applied Science and Manufacturing 32(9): 1339-1343.

De Beer, M. (1996). "Measurement of tire/pavement interface stresses under moving wheel loads." Heavy Vehicle Systems , Special series, International journal of vehicle design Vol 3(Nos 1-4): 97-115.

de Beer, M. (1996). "Measurement of tyre/pavement interface stresses under moving wheel loads." Heavy Vehicle Systems 3(1-4): 97-115.

De Beer, M., E. M. Sadzik, et al. (2005). <u>Tyre-pavement contact stress patterns from the test tyres of the Gautrans Heavy Vehicle Simulator (HVS) MK IV+</u>, Pretoria, South Africa, Document Transformation Technologies cc., Irene, 0062, South Africa.

Demitz, J. R., Mertz, D. R., and Gillespie, J. W. (2003). "Deflection Requirements for Bridges Constructed with Advanced Composite Materials." <u>Journal of bridge engineering</u> 8(2): 73-83.

Djiauw, L. K. and D. G. Fesko (1979). "FATIGUE LIFE PREDICTION IN FRP BY ACOUSTIC EMISSION ANALYSIS." <u>Institute of Physics Conference Series</u>: 79-83.

Du, J., F. T. Salmon, et al. (2004). "Modeling of cohesive failure processes in structural adhesive bonded joints." <u>Journal of Adhesion Science and Technology</u> 18(3): 287-99.

Faraji, A. (2005). <u>Elastic and elastoplastic contact analysis: using boundary elements and mathematical programming</u>. Southampton, WIT Press.

Fernando, E. G., D. Musani, et al. (2006). Evaluation of Effects of Tire Size and Inflation Pressure on Tire Contact Stresses and Pavement Response. FHWA/TX-06/0-4361-1, United States: 288p.

FHWA Corrosion costs and preventative strategies in the United States. <u>(FHWA-RD-01-156)</u>, http://www.corrosioncost.com.

FHWA/USDOT (2005). TSAR 2005. <u>Transportation Statistics Annual Report, Federal Highway Administration and United States Department of Transportation</u>

Fischer-Cripps, A. C. (2000). <u>Introduction to contact mechanics</u>. New York :, Springer.

GangaRao, H. V. S. and A. Vali (1990). "Truck-tire steel grid deck contact pressure distributions." <u>Journal of Structural Engineering</u> 116(3): 791-808.

Gladwell, G. M. L. (1980). <u>Contact problems in the classical theory of elasticity</u>. Alphen aan den Rijn, The Netherlands ; Germantown, Md., Sijthoff & Noordhoff.

Gleich, D. M., M. J. L. Van Tooren, et al. (2000). "Shear and peel stress analysis of an adhesively bonded scarf joint." <u>Journal of Adhesion Science and Technology</u> 14(6): 879-893.

Goland, M. and E. Reissner (1943). <u>Stresses in cemented joints</u>, American Society of Mechanical Engineers (ASME), New York, NY, United States.

Gunnion, A. J. and I. Herszberg (2006). "Parametric study of scarf joints in composite structures." <u>Composite Structures</u> 75(1-4): 364-376.

Harik, I., P. Alagusundaramoorthy, et al. (1999). "Static testing on FRP bridge deck panels." International SAMPE Symposium and Exhibition (Proceedings) 44(pt 2): 1643-1654.

Harries, K. (2006). "FRP bridge decks-A maturing technology." Journal of Bridge Engineering 11(4): 382.

Hart-Smith, L. J. (2002). "Adhesive bonding of composite structures - Progress to date and some remaining challenges." Journal of Composites Technology and Research 24(3): 133-151.

Hayes, M. D., D. Ohanehi, et al. (2000). "Performance of tube and plate fiberglass composite bridge deck." Journal of Composites for Construction 4(2): 48-55.

He, Y. and A. J. Aref (2003). "An optimization design procedure for fiber reinforced polymer web-core sandwich bridge deck systems." Composite Structures 60(2): 183-195.

Hildebrand, M. (1994). "Non-linear analysis and optimization of adhesively bonded single lap joints between fibre-reinforced plastics and metals." International Journal of Adhesion and Adhesives 14(4): 261-267.

Hollaway, L. C. (2003). "The evolution of and the way forward for advanced polymer composites in the civil infrastructure." Construction and Building Materials 17(6-7): 365-378.

Hong, T. and M. Hastak (2007). "Simulation study on construction process of FRP bridge deck panels." Automation in Construction 16(5): 620-631.

Huston, R. J. (1994). "Fatigue life prediction in composites." International Journal of Pressure Vessels and Piping 59(1-3): 131-140.

Hyer, M. W. (1998). Stress ANalysis of Fiber-Reinforced Composite Materials, The McGraw-Hill Companies, Inc.

Iyer, S. L. and R. Bharil (2005). Appropriate applications of FRP deck on bridges, Long Beach, CA, United States, Soc. for the Advancement of Material and Process Engineering, Covina, CA 91724-3748, United States.

Johnson, K. L. (1985). Contact mechanics. Cambridge [Cambridgeshire] ; New York, Cambridge University Press.

Karbhari, V. M. (2004). "Fiber reinforced composite bridge systems--transition from the laboratory to the field." Composite Structures 66(1-4): 5-16.

Karbhari, V. M., J. W. Chin, et al. (2003). "Durability gap analysis for fiber-reinforced polymer composites in civil infrastructure." Journal of Composites for Construction 7(3): 238-247.

Karbhari, V. M., J. W. Chin, et al. (2000). "Critical gaps in durability data for FRP composites in civil infrastructure." International SAMPE Symposium and Exhibition (Proceedings) 45 (I): 549-563.

Kawai, M. (2004). "A phenomenological model for off-axis fatigue behavior of unidirectional polymer matrix composites under different stress ratios." Composites Part A: Applied Science and Manufacturing 35(7-8): 955-963.

Kawai, M., A. Hachinohe, et al. (2001). "Off-axis fatigue behaviour and its damage mechanics modelling for unidirectional fibre-metal hybrid composite: GLARE 2." Composites Part A: Applied Science and Manufacturing 32(1): 13-23.

Kawai, M. and T. Taniguchi (2006). "Off-axis fatigue behavior of plain weave carbon/epoxy fabric laminates at room and high temperatures and its mechanical modeling." Composites Part A: Applied Science and Manufacturing 37(2): 243-256.

Kawai, M., S. Yajima, et al. (2001). "High-temperature off-axis fatigue behaviour of unidirectional carbon-fibre-reinforced composites with different resin matrices." Composites Science and Technology 61(9): 1285-1302.

Keller, T. and H. Gurtler (2005). "Quasi-static and fatigue performance of a cellular FRP bridge deck adhesively bonded to steel girders." Composite Structures 70(4): 484-496.

Keller, T., T. Tirelli, et al. (2005). "Tensile fatigue performance of pultruded glass fiber reinforced polymer profiles." Composite Structures 68(2): 235-245.

Keller, T. and T. Vallee (2005). "Adhesively bonded lap joints from pultruded GFRP profiles. Part I: stress-strain analysis and failure modes." Composites Part B: Engineering 36(4): 331-340.

Keller, T. and T. Vallee (2005). "Adhesively bonded lap joints from pultruded GFRP profiles. Part II: joint strength prediction." Composites Part B: Engineering 36(4): 341-350.

Keller, T. and T. Vallee (2006). "Adhesively bonded lap joints from pultruded GFRP profiles. Part III: Effects of chamfers." Composites Part B (Engineering) 37(4-5): 328-36.

Kim, O.-K., C. A. Bell, et al. (1989). "Effect of increased truck tire pressure on asphalt concrete pavement." Journal of Transportation Engineering 115(4): 329-350.

Knippers, J. and M. Gabler (2006). New design concepts for advanced composite bridges the Friedberg bridge in Germany, Budapest, Hungary, ETH Honggerberg.

Kumar, P., K. Chandrashekhara, et al. (2004). "Structural performance of a FRP bridge deck." Construction and Building Materials 18(1): 35-47.

Laursen, T. A. (2002). Computational contact and impact mechanics : fundamentals of modeling interfacial phenomena in nonlinear finite element analysis. Berlin, Springer.

Li, Z. X., T. H. T. Chan, et al. (2001). "Fatigue analysis and life prediction of bridges with structural health monitoring data -- Part I: methodology and strategy." International Journal of Fatigue 23(1): 45-53.

Liao, K., C. R. Schultheisz, et al. (1999). "Long-term environmental fatigue of pultruded glass-fiber-reinforced composites under flexural loading." International Journal of Fatigue 21(5): 485-495.

Link, C. T. (2003). Development of Panel-to-Panel Connection for use with a Pultruded Fiber-Reinforced-Polymer Bridge Deck System. Civil & Environmental Engineering. Blacksburg, Virginia Polytechnic Institute & State University. MS.

Liu, Y. and S. Mahadevan (2007). "A unified multiaxial fatigue damage model for isotropic and anisotropic materials." International Journal of Fatigue 29(2): 347-359.

Luke, S., L. Canning, et al. (2002). "Advanced composite bridge decking system - Project ASSET." Structural Engineering International: Journal of the International Association for Bridge and Structural Engineering (IABSE) 12(2): 76-79.

Majumdar, P. K., Liu, Z.,Lesko, J.J.,Cousins, T.E. (2007). Evaluation of FRP Composite Deck for Bridge Rehabilitation. SAMPE 2007. Baltimore, Maryland.

Mallick, P. K. (1993). Fiber-Reinforced Composites. New York, Marcel Dekker, Inc.

Marshek, K. M., H. H. Chen, et al. (1986). EFFECT OF TRUCK TIRE INFLATION PRESSURE AND AXLE LOAD ON FLEXIBLE AND RIGID PAVEMENT PERFORMANCE: 14-21.

Matthews, F. L., P. F. Kilty, et al. (1982). "REVIEW OF THE STRENGTH OF JOINTS IN FIBRE-REINFORCED PLASTICS - 2. ADHESIVELY BONDED JOINTS." Composites 13(1): 29-37.

McBagonluri, F., K. Garcia, et al. (2000). "Characterization of fatigue and combined environment on durability performance of glass/vinyl ester composite for infrastructure applications." International Journal of Fatigue 22(1): 53-64.

Momenkhani, K. and S. Sarkani (2006). "A new method for predicting the fatigue life of fiber-reinforced plastic laminates." Journal of Composite Materials 40(21): 1971-1982.

Moses, J., Harries, K., Earls, C., and Yulismana, W. (2006). "Evaluation of effective width and distribution factors for GFRP bridge deck supported on steel girders." Journal of Bridge Engineering 11(4): 401-409.

Mu, B., H.-C. Wu, et al. (2006). "FEA of complex bridge system with FRP composite deck." Journal of Composites for Construction 10(1): 79-86.

Myers, L. A. R., R ; Ruth, B E; Drakos, C (1999). "Measurement of Contact Stresses for Different Truck Tire Types To Evaluate Their Influence on Near-Surface Cracking and Rutting." Transportation Research Record(1655): 175-184.

Objois, A., J. Assih, et al. (2005). "Theoretical method to predict the first microcracks in a scarf joint." Journal of Adhesion 81(9): 893-909.

Pandita, S. D., G. Huysmans, et al. (2001). "Tensile fatigue behaviour of glass plain-weave fabric composites in on- and off-axis directions." Composites Part A: Applied Science and Manufacturing 32(10): 1533-1539.

Park, K.-T., S.-H. Kim, et al. (2005). "Pilot test on a developed GFRP bridge deck." Composite Structures 70(1): 48-59.

Philippidis, T. P. and V. A. Passipoularidis "Residual strength after fatigue in composites: Theory vs. experiment." International Journal of Fatigue In Press, Corrected Proof.

Philippidis, T. P. and A. P. Vassilopoulos (1999). "Fatigue of composite laminates under off-axis loading." International Journal of Fatigue 21(3): 253-262.

Pickett, A. K. and L. Hollaway (1985). "The analysis of elastic-plastic adhesive stress in bonded lap joints in FRP structures." Composite Structures 4(2): 135-160.

Pickett, A. K. and L. Hollaway (1985). "The analysis of elastic adhesive stresses in bonded lap joints in FRP structures." Composite Structures 3(1): 55-79.

Plumtree, A. and G. X. Cheng (1999). "A fatigue damage parameter for off-axis unidirectional fibre-reinforced composites." International Journal of Fatigue 21(8): 849-856.

Plumtree, A. and L. Shi (2002). "Fatigue damage evolution in off-axis unidirectional CFRP." International Journal of Fatigue 24(2-4): 155-159.

Pottinger, M. G. (1992). "Three-dimensional contact patch stress field of solid and pneumatic tires." Tire Science & Technology 20(1): 3-32.

Pottinger, M. G. and J. E. McIntyre, III (1999). "Effect of suspension alignment and modest cornering on the footprint behavior of performance tires and heavy duty radial tires." Tire Science and Technology 27(3): 128-160.

Prachasaree, W., H. V. S. GangaRao, et al. (2007). "Theoretical and experimental analysis of FRP bridge deck under cold temperatures." International Journal of Materials and Product Technology 28(1-2): 103-121.

Prozzi, J. A. and R. Luo (2005). "Quantification of the joint effect of wheel load and tire inflation pressure on pavement response." Transportation Research Record(1919): 134-141.

Qiao, P., J. F. Davalos, et al. (2000). "A systematic analysis and design approach for single-span FRP deck/stringer bridges." Composites Part B: Engineering 31(6-7): 593-609.

Quaresimin, M. and M. Ricotta (2006). "Life prediction of bonded joints in composite materials." International Journal of Fatigue 28(10): 1166-1176.

Quaresimin, M. and M. Ricotta (2006). "Stress intensity factors and strain energy release rates in single lap bonded joints in composite materials." Composites Science and Technology 66(5): 647-656.

Reddy, J. N. (1997). Mechanics of Laminated Composite Plates and Shells:Theory and Analysis. Ne York, CRC Press LLC.

Reddy, J. N. (1999). Theory and Analysis of Elastic Plates. Philadelphia, Taylor & Francis.

Reifsnider, K., S. Case, et al. (2000). "The mechanics of composite strength evolution." Composites Science and Technology 60(12-13): 2539-2546.

Reifsnider, K. L. (1986). "The critical element model: A modeling philosophy." Engineering Fracture Mechanics 25(5-6): 739-749.

Reifsnider, K. L. and Z. Gao (1991). "A micromechanics model for composites under fatigue loading." International Journal of Fatigue 13(2): 149-156.

Reising, R. M. W., B. M. Shahrooz, et al. (2004). "Performance comparison of four fiber-reinforced polymer deck panels." Journal of Composites for Construction 8(3): 265-274.

Reising, R. M. W., B. M. Shahrooz, et al. (2004). "Close look at construction issues and performance of four fiber-reinforced polymer composite bridge decks." Journal of Composites for Construction 8(1): 33-42.

Renton, J. W. and J. R. Vinson (1975). "On the behavior of bonded joints in composite material structures." Engineering Fracture Mechanics 7(1): 41-52.

Salim, H. A., M. Barker, et al. (2006). "Approximate series solution for analysis of FRP composite highway bridges." Journal of Composites for Construction 10(4): 357-366.

Salim, H. A., J. E. Davalos, et al. (1997). "Analysis and design of fiber reinforced plastic composite deck-and-stringer bridges." Composite Structures 38(1-4): 295-307.

Sebaaly, P. and N. Tabatabaee (1989). Effect of tire pressure and type on response of flexible pavement: 115-127.

Sebaaly, P. E. (1992). Pavement damage as related to tires, pressures, axle loads, and configurations, Santa Barbara, CA, USA, Publ by ASTM, Philadelphia, PA, USA.

Shahrooz, B. M., A. R. Neumann, et al. (2007). "Durability of FRP composite bridge decks - Construction and temperature effects." International Journal of Materials and Product Technology 28(1-2): 66-88.

Shen, Y., M. Xu, et al. (2002). "Finite element analysis of FRP tube assemblies for bridge decks." Advanced Composite Materials: The Official Journal of the Japan Society of Composite Materials 11(2): 151-169.

Shokrieh, M. M. and F. Taheri-Behrooz (2006). "A unified fatigue life model based on energy method." Composite Structures 75(1-4): 444-450.

Soon, S.-C., A. Drescher, et al. (2004). "Tire-induced surface stresses in flexible pavements." Transportation Research Record(1896): 170-176.

SPI. "Sensor Products Inc." from http://www.pressurex.com

Strongwell. "Strongwell Corporation." from www.strongwell.com.

Temeles, A. B. (2001). Field and Laboratory Tests of a Proposed Bridge Deck Panel Fabricated from Pultruded Fiber-Reinforced Polymer Components. Blacksburg, Virginia., Virginia Polytechnic Institute and State University. MS.

Tielking, J. T. and M. A. Abraham (1994). Measurement of truck tire footprint pressures, National Research Council, Washington, DC, USA: 92-99.

Tielking, J. T. and F. L. Roberts (1987). "TIRE CONTACT PRESSURE AND ITS EFFECT ON PAVEMENT STRAIN." Journal of Transportation Engineering 113(1): 56-71.

Turner, M. K., Harries, K. A., Petrou, M. F., and Rizos, D. (2004). "In situ structural evaluation of a GFRP bridge deck system." Composite Structures 65(2): 157-165.

Vallee, T., J. R. Correia, et al. (2006). "Probabilistic strength prediction for double lap joints composed of pultruded GFRP profiles - Part II: Strength prediction." Composites Science and Technology 66(13): 1915-1930.

Vallee, T., J. R. Correia, et al. (2006). "Probabilistic strength prediction for double lap joints composed of pultruded GFRP profiles part I: Experimental and numerical investigations." Composites Science and Technology 66(13): 1903-1914.

Varvani-Farahani, A., H. Haftchenari, et al. (2007). "An energy-based fatigue damage parameter for off-axis unidirectional FRP composites." Composite Structures 79(3): 381-389.

Volkersen, O. (1965). "Research on theory of cemented joints

Recherches sur la theorie des assemblages colles." Construction Metallique(4): 3-13.

Wah, T. (1976). "PLANE STRESS ANALYSIS OF A SCARF JOINT." International Journal of Solids and Structures 12(7): 491-500.

Wan, B., D. C. Rizos, et al. (2005). "Computer simulations and parametric studies of GFRP bridge deck systems." Composite Structures 69(1): 103-115.

Wang, F. and R. Machemehl (2006). Predicting Truck Tire Pressure Effects Upon Pavement Performance, Center for Transportation Research ,University of Texas at Austin, USA: 158.

Wang, F. and R. B. Machemehl (2005). Analysis of effects of truck tire pressure on flexible pavements, Toronto, ON, Canada, Canadian Society for Civil Engineering, Montreal, H3H 2R9, Canada.

Wang, F. and R. B. Machemehl (2006). "Mechanistic-empirical study of effects of truck tire pressure on pavement: Measured tire-pavement contact stress data." Transportation Research Record(1947): 136-145.

Williams, B., E. Shehata, et al. (2003). "Filament-wound glass fiber reinforced polymer bridge deck modules." Journal of Composites for Construction 7(3): 266-273.

Wriggers, P. (2006). Computational contact mechanics. Berlin ; New York :, Springer.

Wu, H.-C., K. Warnemuende, et al. (2003). Strategic Sensor Locations of FRP Bridge Decks, San Diego, CA, United States, The International Society for Optical Engineering.

Yue, Z. Q. and O. J. Svec (1995). "Effects of tire-pavement contact pressure distributions on the response of asphalt concrete pavements." Canadian Journal of Civil Engineering 22(5): 849-860.

Zetterberg, T., B. T. Astrom, et al. (2001). "On design of joints between composite profiles for bridge deck applications." Composite Structures 51(1): 83-91.

Zhang, Y. and C. S. Cai (2007). "Load distribution and dynamic response of multi-girder bridges with FRP decks." Engineering Structures 29(8): 1676-1689.

Zhang, Y., C. S. Cai, et al. (2006). Vehicle load-induced dynamic performance of FRP slab bridges, St. Louis, MO, United States, American Society of Civil Engineers, Reston, VA 20191-4400, United States.

Zhang, Y., C. S. Cai, et al. (2006). "Vehicle-induced dynamic performance of FRP versus concrete slab bridge." Journal of Bridge Engineering 11(4): 410-419.

Zhou, A. (2002). Stiffness and Strength of Fiber Reinforced Polymer Composite Bridge Deck Systems Enginerring Science & Mechanics. Blacksburg, VA, Virginia Polytechnic Institute & State University. PhD.

Zhou, A., J. T. Coleman, et al. (2005). "Laboratory and field performance of cellular fiber-reinforced polymer composite bridge deck systems." Journal of Composites for Construction 9(5): 458-467.

Zhou, A. and T. Keller (2005). "Joining techniques for fiber reinforced polymer composite bridge deck systems." Composite Structures 69(3): 336-345.